FACULDADE DE ENGENHARIA DA UNIVERSIDADE DO PORTO

A study on roll forming modelling in Abaqus

João Bernardo Galvão Gomes

Mestrado Integrado em Engenharia Mecânica

Supervisors:
Dr. Thomas Dietl
Prof. Dr. Abel D. Santos
M.Sc. Miguel Pereira

October 19, 2020

A study on roll forming modelling in Abaqus

João Bernardo Galvão Gomes

Mestrado Integrado em Engenharia Mecânica

October 19, 2020

Abstract

Roll forming is a metal forming process that consists in submitting a sheet metal strip to continuous bending by forcing it through multiple rolls, until a profile with the desired cross section is obtained. Manufacturing parts through roll forming can be extremely advantageous for large production series as its production rates are generally substantially higher than other processes meant to manufacture similar components. Nevertheless the rolls design and manufacturing, combined with the roll mill assembly, take time, meaning that any downtime is very costly. It is then crucial to have a method of verifying the viability of the roll forming project, in order to detect and eliminate defects even before the manufacturing of the tools.

Throughout this dissertation, it is intended to ascertain the viability of Abaqus as a reliable finite element analysis tool through the construction of a sturdy and reliable model and subsequent result comparison with a reference roll forming simulation FEA package: COPRA® FEA RF. This FEA package was chosen as the reference, as it is the industrial standard FEA package for roll forming simulations. In order to do that, several parameters were studied and discussed, so as to evaluate the adequate definitions to setup the aforementioned models.

A model was developed in Abaqus in order to obtain results that reflect a realistic roll forming process. The parameters deemed relevant to use as comparing factors between the two FEA packages were the equivalent plastic strain, longitudinal strain, equivalent stress, sheet thickness, cross sectional geometry after springback and computational time. Some modelling simplifications were considered, such as foregoing friction and roll rotation, as they were deemed nonessential for the scope of this research. A chapter was dedicated to a preliminary study on the element technology used by Abaqus, as the element choice is fundamental for any sheet metal forming simulation.

Another inherent challenge facing the scope of this thesis lies on the difficulty to compare the results of both FEA packages, as the post-processing of tensor values is generally particular to every software. As such, a post-processing tool was developed as a solution to effectively compare tensor values between the two FEA packages and to analyse the obtained results.

It was finally concluded that the considered Abaqus model with an incompatible modes element and simulated in an explicit solver, yields similar results to the ones obtained with COPRA ®FEA RF, for simple models and in less time for the same number of elements, when considering a single layer of elements over the thickness. However, by refining the mesh of the sheet metal, the total simulation time of Abaqus/Explicit surpasses the one taken by COPRA ®FEA RF. The lack of complexity of the profile geometry and the simplifications made for the development of the final model, contributed to the success of the simulations carried out in Abaqus/Explicit using the C3D8I element. Nevertheless, the explicit solver has some drawbacks that can hinder the success of a roll forming finite element analysis, making the simulation more unpredictable and less robust.

Furthermore, the models in which the reduced integration element was incorporated – subsequently simulated with Abaqus/Explicit – yielded unsatisfactory results for the developed roll forming model when comparing to COPRA ®FEA RF and to the usage of the C3D8I element. Finally, the developed models were not successfully simulated using Abaqus/Standard nor when using shell elements in Abaqus/Explicit.

Keywords: Roll Forming, Numerical Simulation, Abaqus/Explicit, Abaqus/Standard, COPRA® FEA RF, Finite Element Analysis

Resumo

Perfilagem a frio é um processo de conformação plástica de chapas metálicas de produção em massa. Consiste em submeter uma chapa metálica a dobragem contínua, ao conduzi-la por uma linha de fabrico composta por rolos que por deformação plástica levarão à obtenção de um perfil com a secção desejada. Um dos atributos mais apelativos deste processo de fabrico reside na possibilidade de produção em massa de perfis metálicos, dado que a cadência de produção associada a este processo de fabrico é significativamente mais elevada do que outros processos destinados a obter componentes semelhantes. No entanto, o *design* dos rolos e o seu fabrico, associado ao tempo de *setup* das linhas de montagem, leva a que o custo do tempo de inatividade seja elevado. O desenvolvimento de métodos de validação da viabilidade do projeto de perfilagem a frio torna-se assim essencial, de maneira a detetar e eliminar eventuais defeitos de produção antes do fabrico das ferramentas.

Ao longo desta dissertação, pretende-se averiguar a viabilidade do Abaqus como uma ferramenta de análise por elementos finitos através da construção e do desenvolvimento de um modelo de perfilagem a frio robusto e da posterior comparação com os resultados obtidos com o COPRA® FEA RF. Este programa de análise por elementos finitos foi escolhido como referência dado que é considerado o *standard* industrial para simulação de processos de perfilagem a frio. De modo a estabelecer uma comparação válida, foram estudados e discutidos vários parâmetros com o objetivo de avaliar e determinar as definições corretas para o desenvolvimento de um modelo de perfilagem adequado.

Foi desenvolvido um modelo no código de elementos finitos Abaqus de maneira a obter resultados que representem um processo real de perfilagem a frio. Os parâmetros tidos como relevantes para usar como base de comparação entre os dois códigos de elementos finitos foram a deformação plástica equivalente, deformação longitudinal, tensão equivalente, espessura da chapa metálica, geometria da secção obtida e tempo de simulação. Foram consideradas algumas simplificações no modelo desenvolvido, como abicar de fricção e rotação dos rolos, dado que estes parâmetros foram contemplados como não essenciais para o foco desta dissertação. Dedicou-se também um capítulo ao estudo da tecnologia dos elementos usados disponíveis na biblioteca do Abaqus, dado que a escolha do elemento é essencial ao simular processos de conformação plástica.

Outro desafio inerente ao foco desta tese reside na dificuldade em comparar os resultados obtidos por dois códigos de elementos finitos distintos, visto que o pós-processamento dos valores dos pontos de integração é geralmente particular a cada programa. Como tal, uma ferramenta de pós-processamento de resultados foi desenvolvida, de maneira a poder analisar os mesmos usando um método comum de extrapolação de resultados.

Foi finalmente concluído que o modelo desenvolvido com o elemento de modos incompatíveis e simulado com o Abaqus/Explicit, gerou resultados similares aos que foram obtidos com o COPRA® FEA RF, em menos tempo e para o mesmo número de elementos ao considerar uma única camada de elementos através da espessura da chapa metálica. No entanto, ao refinar malha na direção da espessura da chapa, o tempo de simulação do Abaqus/Explicit acaba por exceder o

tempo tomado pelo COPRA® FEA RF. A falta de complexidade associada à geometria do perfil e as simplificações efetuadas no sentido de facilitar o desenvolvimento do modelo de perfilagem contribuíram para o sucesso das simulações levadas a cabo pelo Abaqus/Explicit ao usar o elemento C3D8I. No entanto, o *solver* explícito apresentou algumas limitações que poderão prejudicar futuras simulações de processos de perfilagem, na medida em que as simulações poderão ser imprevisíveis e pouco robustas. No caso dos elementos de integração reduzida – subsequentemente simulados em Abaqus/Explicit – os resultados obtidos foram insatisfatórios quando comparados com os resultados do COPRA® FEA RF e do Abaqus/Explicit com elementos C3D8I. Finalmente, os modelos de perfilagem desenvolvidos com o Abaqus/Standard não foram corretamente simulados, nem tão pouco os modelos desenvolvidos com elementos casca e simulados em Abaqus/Explicit.

Palavras-Chave: Perfilagem a Frio, Simulação Numérica, Abaqus/Explicit, Abaqus/Standard, COPRA® FEA RF, Análise por Elementos Finitos

Acknowledgements

I would like to express my gratitude to everyone that took part in the development of this dissertation. To everyone at data M Sheet Metal Solutions for the opportunity to develop my Master's dissertation and for the wonderful experience. A special word of appreciation to Dipl.-Ing. Albert Sedlmaier for the support during an extremely atypical context and for providing the necessary tools to work from home when needed.

I would like to extend my gratitude to my supervisor in Porto, Prof. Dr. Abel D. Santos for the availability, guidance and encouragement provided throughout this dissertation.

I would like to thank my supervisor at data M, Dr. Thomas Dietl, for his guidance, for the invaluable help, input and lessons provided throughout the entire project as well as for his unwavering patience. To M.Sc. Miguel Pereira for all the invaluable help, patience and support he provided from day one, up until the end of the project. To ir. Andre Abee and to Dipl.-Ing. Johann Harraßer for helping me develop the models used in this dissertation and for the theoretical insights provided throughout. Finally, to Viviane Bauer, to Mattias Wimmer and to Bhargav Sama for the friendship and conviviality.

I would also like to leave a word of gratitude to Dr. Nuno Rebelo for his availability to contribute to the progress of this thesis. His invaluable input, backed by his extensive experience in roll forming simulation, was highly appreciated.

Finally, I would like to thank my family and friends that stayed by my side throughout my academic journey. I will always be grateful for your relentless support and unwavering encouragement. Thank you.

João Galvão Gomes

"You don't have to see the whole staircase,
just take the first step."

Martin Luther King Jr.

Contents

List of Figures

List of Tables

Abbreviations

Abaqus Variables

ALLAE	Artificial Energy for Hourglass Control (Abaqus history variable)
ALLDC	Energy Associated with Distortion Control (Abaqus history variable)
ALLDMD	Energy Dissipated by Damage (Abaqus history variable)
ALLFC	Fluid Cavity Energy (Abaqus history variable)
ALLIE	Internal Energy (Abaqus history variable)
ALLKE	Kinetic Energy (Abaqus history variable)
ALLPD	Plastic Deformation Energy (Abaqus history variable)
ALLSE	Recoverable Strain Energy (Abaqus history variable)
C3D20	Quadratic Three-Dimensional Fully Integrated Solid Brick Element
C3D8	Linear Three-Dimensional Fully Integrated Solid Brick Element
C3D8I	Linear Three-Dimensional Fully Integrated Solid Brick Element with Incompatible Modes
C3D8R	Linear Three-Dimensional Solid Brick Element with Reduced Integration
EHC	Enhanced Hourglass Control
PEEQ	Equivalent Plastic Strain (Abaqus field variable)
PEMAG	Plastic Strain Magnitude (Abaqus field variable)
RSHC	Relaxed Stiffness Hourglass Control
S4R	Linear Shell Element with Reduced Integration
TSHC	Total Stiffness Hourglass Control
U	Total Displacements (Abaqus field variable)
UR	Rotational Displacements (Abaqus field variable)
UT	Translation Displacements (Abaqus field variable)

General Abbreviations

CAD	Computer-Aided Design
CAE	Computer-Aided Engineering
CFL	Courant-Friedrichs-Lewy (Rule)
EAS	Enhanced Assumed Strains
FEA	Finite Element Analysis
FEM	Finite Element Method
GUI	Graphic User Interface
HSS	High Strength Steel

Chapter 1

Introduction

This dissertation was written under the scope of a six months long internship in data M Sheet Metal Solutions GmbH as part of a long lasting cooperation between the company and FEUP. This introductory chapter is aimed to present the company, the main underlying problems surrounding the subject of this work, the context in which it is inserted and the structure of the thesis itself.

1.1 data M Sheet Metal Solutions GmbH

data M Sheet Metal Solution GmbH is an independent software and engineering company that specialises in the sheet metal forming industry, namely in roll forming processes. The company's headquarters are located in Oberlaindern, 40km to the south of the city of Munich.

Figure 1.1: Location of data M Sheet Metal Solutions GmbH, near Munich, and logo.

The company was first founded by Dipl. -Ing. Albert Sedlmaier and Dipl. -Ing. Stefan Freitag and soon developed several sheet metal forming software programmes, with a special focus in roll forming processes and roll design.

They are known for their expertise in the field, having ultimately developed COPRA® RF – a roll design tool that simplifies the modelling of the forming tools.

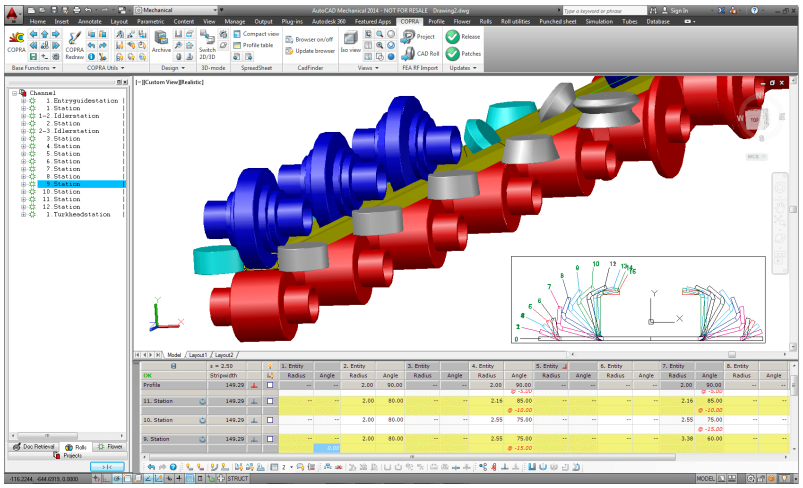

Figure 1.2: COPRA® RF's graphic user interface [data M Software India, 2020].

Later, the company developed simulation solutions based on the finite difference method. In 2000, data M developed COPRA® FEA RF – an FEA package specially designed for roll forming processes. It is a software that successfully established itself in the market as a reference product, assisting engineers in roll forming projects throughout the world.

Nowadays the company is focused in further software and roll forming machine development, conception of roll forming lines as well as consulting services, having partners throughout the world and participating in numerous international projects. data M also dedicates itself to user training, in order to increase the knowledge of FEA applied to roll forming.

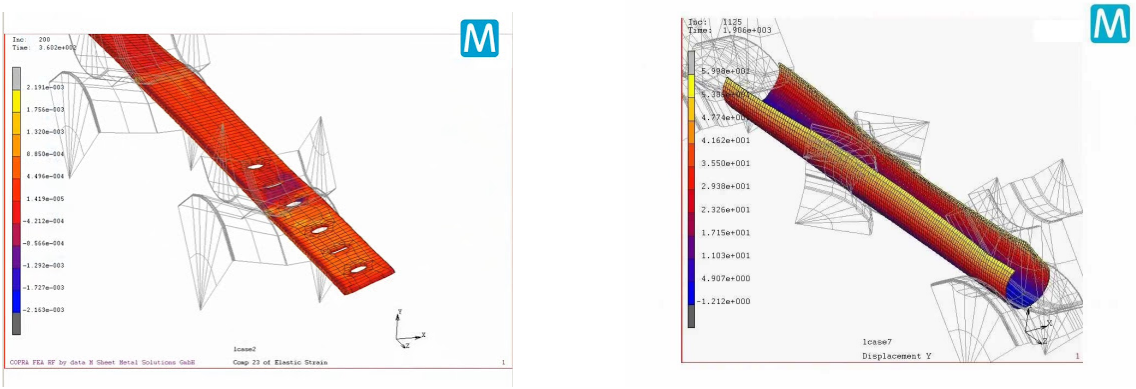

(a) Roll forming of a perforated sheet metal.

(b) Roll forming of a tubular section.

Figure 1.3: Visualisation module of COPRA® FEA RF's user interface, where the countour plots and sectioned rolls of two distinct roll forming simulations can be observed [dataM Sheet Metal Solutions, 2020].

1.2 Abaqus - Simulia™ by Dassault Systèmes®

Abaqus is an FEA package developed in 1978 by Dr. David Hibbitt, Dr. Bengt Karlsson, and Dr. Paul Sorensen. The software has been a part of Dassault Systèmes' portfolio after being acquired by the company in 2005 [Huang, 2005], under the brand Simulia™.

It consists in an all-purpose FEA package, with applications in the automotive, industrial and aerospace industries, among many others.

It counts with several integrated modules, from which three can be highlighted:

- Abaqus/CAE (standing for Complete Abaqus Environment) provides a complete modelling and result analysis interface between the user and software.
- Abaqus/Standard is meant to be used to simulate static, quasi-static/transient and thermal models and relies on an implicit solver to carry them out.
- Abaqus/Explicit is typically used for dynamical and fast-paced models and/or highly non-linear static or transient models, relying for that purpose on an explicit solver.

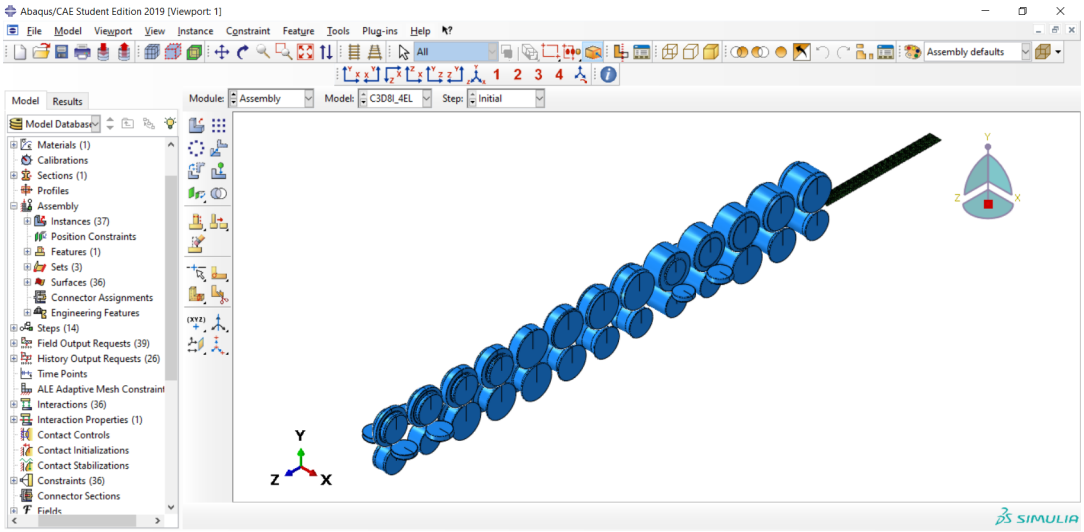

Figure 1.4: Abaqus' user interface applied to a roll forming model.

1.3 Project Context and Motivation

Roll forming is a sheet metal bending process that relies on roll stations to gradually form a strip of metal into a profile with a predefined cross section. Roll forming has applications across a wide number of industries, as illustrated by figures 1.5, 1.6 and 1.7.

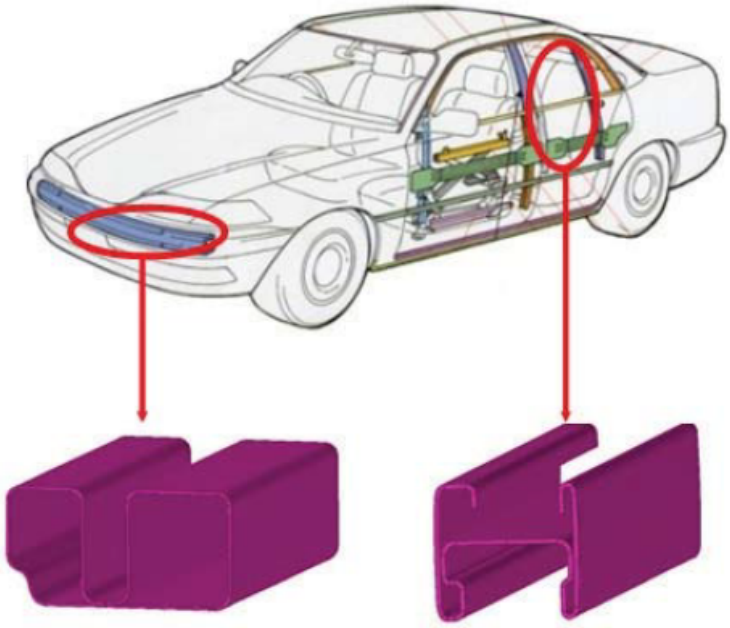

Figure 1.5: Example of two possible applications of roll formed structures in the automotive industry (bumper reinforcement on the left picture and a car door frame on the right) [data M Sheet Metal Solutions GmbH, 2014].

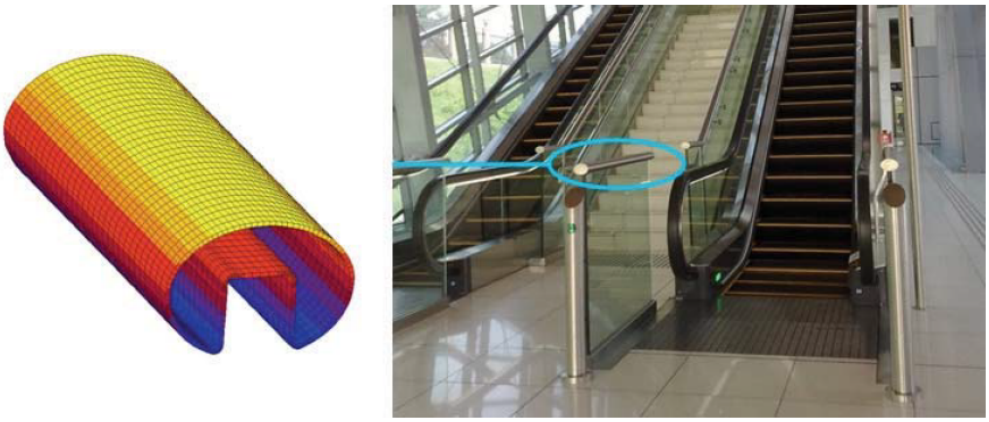

Figure 1.6: Example of an application of a roll formed structure in the construction industry (hand rail) [data M Sheet Metal Solutions GmbH, 2014].

Roll forming is known for being a process with a low manufacturing lead time, resulting in a fast output of parts. As such, the interest for this sort of fast-paced manufacturing processes has grown overtime, leading to new advances surrounding this technology, such as 3D roll forming that allows profiles with a variable cross-section to be obtained [Sedlmaier and Dietl, 2018].

Roll forming is, however, a costly process as the rolls have to be custom designed for the project at hand. With that in mind, and as it will be established in the subsequent chapters,

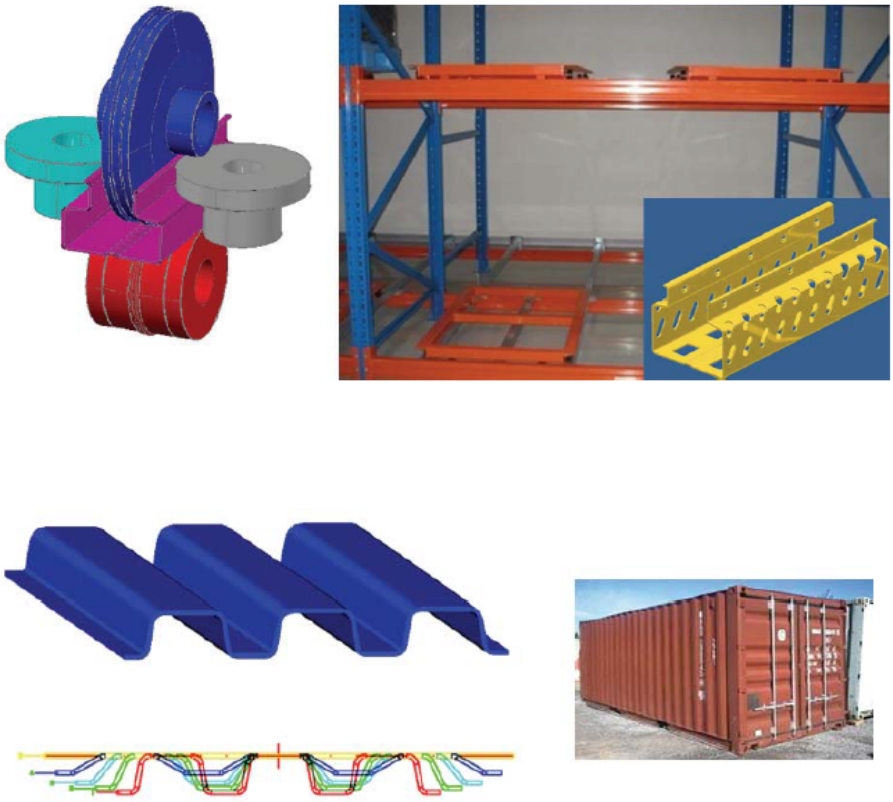

Figure 1.7: Example of an application of a roll formed structure in the oil and gas industry (pressure armours for flexible risers) [data M Sheet Metal Solutions GmbH, 2014].

this process benefits greatly from finite element analysis. Simulating a roll forming operation avoids roll design errors by detecting them and helps to investigate and optimise the process [Abee and Sedlmaier, 2010].

The main goal of this dissertation consists in modelling a functional roll forming process in Abaqus, simulating it with different elements, and establishing a valid set of criteria that allows the comparison of the obtained results in Abaqus with the ones obtained in COPRA® FEA RF [dataM Sheet Metal Solutions, 2020]. As a reference FEA package that is well established in the roll forming simulation market, the results obtained with COPRA® FEA RF will be the reference point to which all evaluation parameters will be judged.

However, the assumption that the direct comparison of results obtained by two different FEA packages is a valid approach is an inherent problem within both industrial and academical contexts, as the post-processing of simulations often varies from an FEA package to another. As part of the scope of this dissertation, the correct approach to compare results yielded by two distinct FEA packages will be approached in subsequent chapters.

To summarise, the scope of this work can be divided in three major points:

- Modelling a functional roll forming process in Abaqus.

- Devise an adequate way to compare the results obtained with Abaqus with the ones obtained in COPRA® FEA RF.
- Carrying out the simulation with different settings and analysing the results by selecting a set of relevant evaluation criteria.

1.4 Structure of the Thesis

The thesis will be structured as follows:

- Chapter 1, the current chapter, provides an introduction and motivation behind this work.
- Chapter 2 is dedicated to review some essential concepts regarding roll forming and investigate the state of the art of modelling and simulating roll forming processes.
- Chapter 3 is dedicated to exploring the different steps towards modelling a roll forming process. It is also a chapter that analyses the pros and cons of every choice made throughout the construction of the aforementioned models.
- Chapter 4 is dedicated to understanding the behaviour of different elements in order to understand their behaviour when subjected to basic loads. The goal is to understand if every considered element is suited for a roll forming simulation and if any preliminary conclusions can be taken.
- Chapter 5 is dedicated to the definition of the evaluation criteria and how to assess it, as well as to the model description, taking into account the conclusions brought by chapters 3 and 4.
- Chapter 6 is aimed at presenting the results of the simulated roll forming processes using the model described in chapter 5.
- Finally, chapter 7 is dedicated to providing the conclusions and observations gathered along this dissertation, as well as some final remarks and considerations about possible future work.

Chapter 2

Literature Review

Throughout this chapter, essential concepts for the construction of a robust roll forming model are approached. In the first section, the roll forming process is described in terms of its general layout and in terms of the acting forces and interactions between contact bodies throughout the operation. Furthermore, concepts like the deformation of the sheet metal, the design of the tools and the importance of finite element analysis for the validation of any roll forming problem will also be addressed. Subsequently, a second section is dedicated to explore what was done in the field of roll forming simulation by finite element analysis. In order to setup a functional and effective roll forming model, it is necessary to determine what was done in the sheet metal forming field (especially in the roll forming area) by previous investigators and set a solid theoretical foundation for the dissertation.

2.1 Roll Forming Process

2.1.1 Process Overview

The roll forming process consists in forcing a strip of sheet metal through a set of contoured rolls, in order to progressively shape it into a profile with a predesignated cross-section geometry. This process has been gradually increasing its industrial demand due to the numerous advantages it brings when correctly implemented:

- high manufacturing rate;
- possibility to create bends with a low bending radius;
- allows the forming of complex cross-section geometries;
- can be used to form high strength steel sheet metal without preheating processes.

Roll forming is described by Halmos [Halmos, 2006] as a process that allows:

> "to form sheet metal strip along straight, longitudinal, parallel bend lines with multiple pairs of contoured rolls without changing the thickness of the material at room temperature".

However, this description is incomplete since the process can be changed to meet a project's requirements. For instance, flexible roll forming allows the creation of profiles with a variable cross section along the length of the sheet metal [Gülçeken et al., 2007].

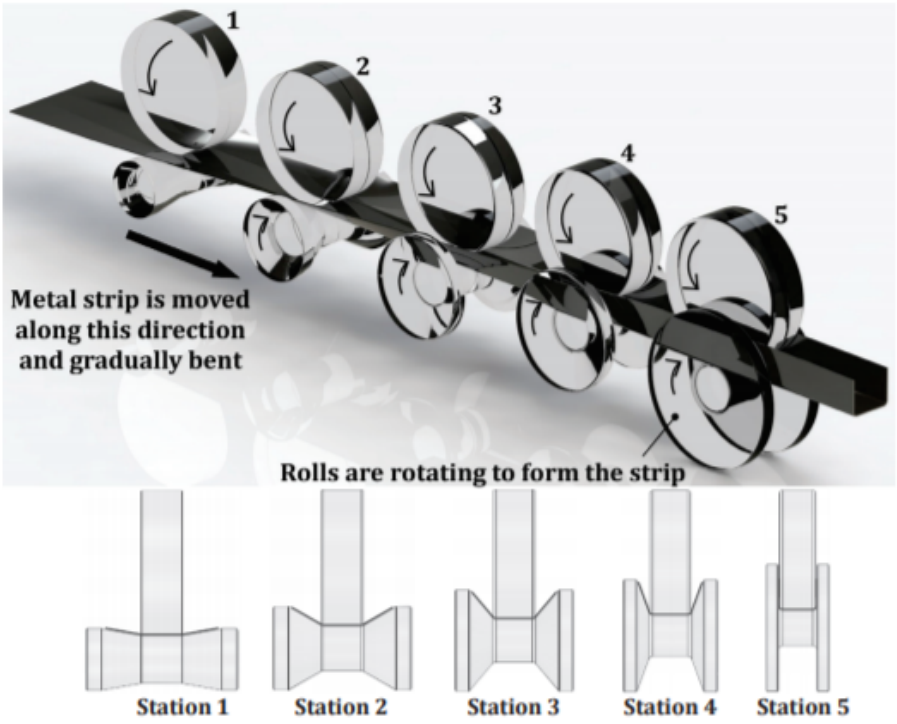

Figure 2.1: Gradual bending of sheet metal strip into a U-channel profile [Abvabi, 2014].

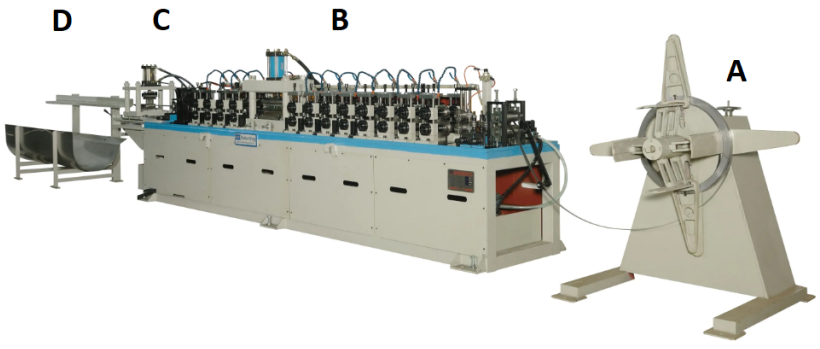

Figure 2.2: Example of a roll forming machine; A: decoiler feeding a coil of sheet metal to the roll forming machine, B: roll forming line where the metal forming will take place, C: cutting station where the parts are separated from the coil, D: station where the parts are collected [Roller King Enterprise Co., 2020].

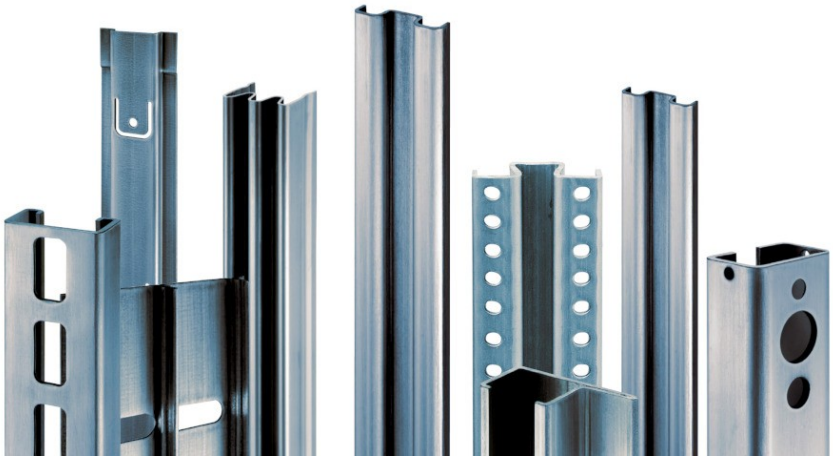

Figure 2.3: Example of different roll formed profiles [Voestalpine, 2019a].

Furthermore, the process does not have to occur at room temperature as in-line heating of the sheet metal is also an operation that can occur, depending on the adopted materials and the specifications of the project [Figueiredo, 2016]. Finally, secondary operations in the roll forming line can also take place, altering the shape of the bend lines [Halmos, 2006].

These secondary operations can dramatically change the geometry of the final product; they consist in:

- straightening of the final product;
- bend-line geometry altering operations such as swooping or bending;
- material removal operations such as punching or perforating;
- bonding operations such as welding, soldering, brazing and adhesive bonding;
- other operations such as embossing or drawing, among many other possibilities.

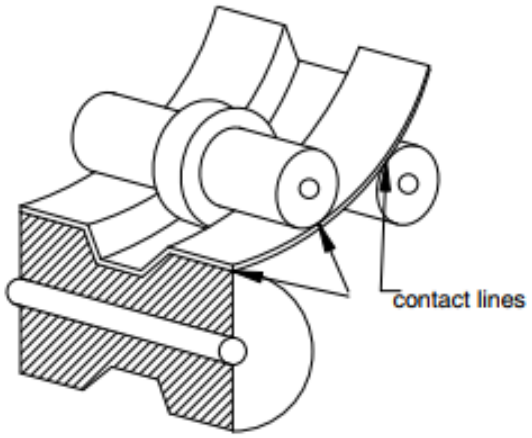

Figure 2.4: In-line curving operation [Halmos, 2006].

These secondary operations are important as the applications of the profiles often require additional features. For instance, Ni et al. [Ni et al., 1991] simulated sweeping or curving operations, necessary for the manufacturing of some parts for the automotive industry (e.g. bumpers). Some application required punched profiles which can be done in-line (e.g. metal storage units, car seat rails, among others [data M Sheet Metal Solutions GmbH, 2014]).

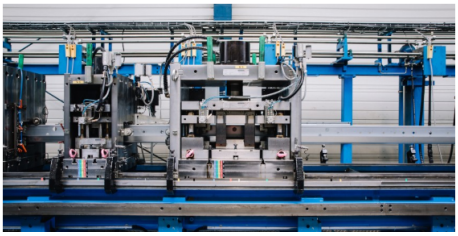

(a) in-line press brake punching.

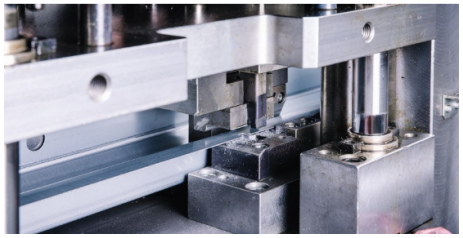

(b) Detail of the in-line punching operation.

Figure 2.5: In-line punching operation [Voestalpine, 2019b]

Figure 2.6: Example of punched profiles [Voestalpine, 2019b].

Despite the visual simplicity of the process, roll forming is an incredibly complex process in terms of sheet metal deformation; even though the metal forming is mostly carried out by transversal bending that occurs inside the rolls, some plastic deformation happens between stations [Lindgren, 2007].

In a roll formed profile there are three main areas:

- The web of the profile, that contains the vertical guide plane.
- The bending areas, area of the sheet metal that will be submitted to bending.
- The flanges, limited by the bending areas, that are the areas that will basculate in order to form a profile geometry.

2.1.2 Roll Design

The roll design is a crucial step in every roll forming process since the rolls have to be customised to the project in hand. As such, it is of the utmost importance to design and validate the roll forming project to minimise the likelihood of obtaining defective parts. The first step of roll design is to define the section orientation and the number of passes through the different roll stations until the final product is obtained; an overestimation of the number of rolls will increase the cost of the project and an underestimation might lead to defects in the final product (as pointed out in section 2.1.5).

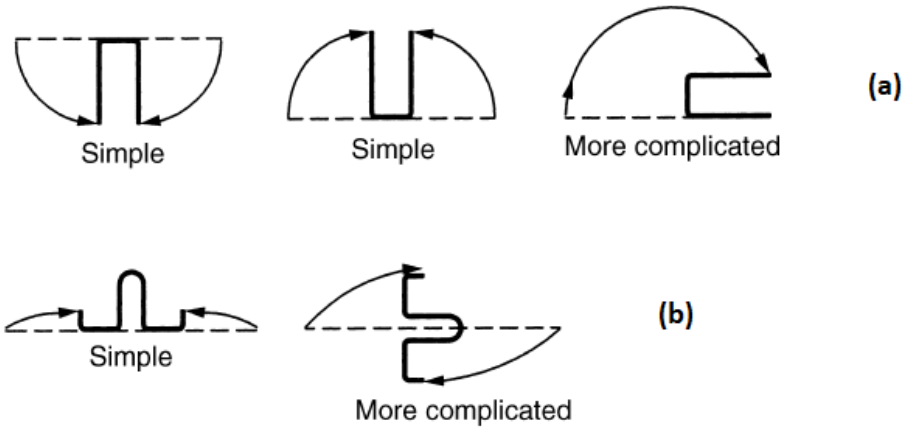

Figure 2.7: The simplicity of the forming process often dictates the section orientation; the illustrated example concerns (a) a profile with two bending zones (U-profile) (b) a more complex profile with six bending zones [Halmos, 2006].

The main goal of roll design is to reduce the number of passes all the while preserving the quality of the final product, which means that it can be an extremely iterative process. There are a great number of considerations when designing the rolls, defining the inter-station distance and determining the number of passes.

The rolls have to be designed in order to not exceed a maximum bending angle threshold; a large bending initial angle can lead to local strip edge buckling. This particular defect, explored in depth in section 2.1.5, aggravates throughout the forming if any buckling has occurred in the first roll station [Tehrani et al., 2006].

Reducing the inter-station distance affects the longitudinal and shear strains in the sheet metal's strip edge, as they are increased significantly [Paralikas et al., 2008]. An excessive compressive strain in the strip edge can lead to defects in the final product [Najafabadi et al., 2019].

Finally, a reduced number of passes, intrinsically related to the consecutive roll angles, can also lead to defective final products [Halmos, 2006]. There are a few empirical guidelines to estimate these parameters but ultimately, the responsibility lies with the roll designer.

The different geometries of the sheet metal's cross-section at each pass compose the flower diagram. This diagram consists in a superimposed or split pattern that enables the observation of the geometrical progression of the sheet metal, the number of passes and the selected vertical guide planes throughout the roll forming process. It is a schematic way of illustrating a roll forming process for its quick analysis. Figure 2.8 illustrates this concept, applied to a profile with twelve bending zones.

After defining the aforementioned parameters, the roll design can effectively start.

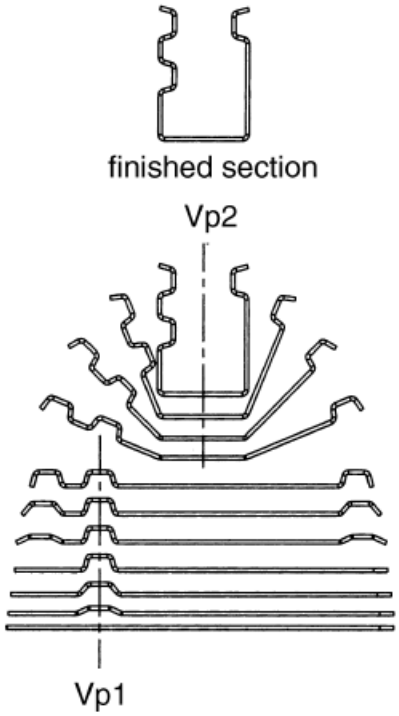

Figure 2.8: Split flower pattern for an asymmetrical cross-section, with a depiction of the two distinct vertical planes (Vp) [Halmos, 2006].

2.1.3 Fundamentals of Sheet Metal Bending

In a roll forming process, the final product is obtained through gradual sheet metal bending. As such, its principles will be analysed.

Bending is a metal forming process in which sheet metal is bent to form angles through the application of a force.

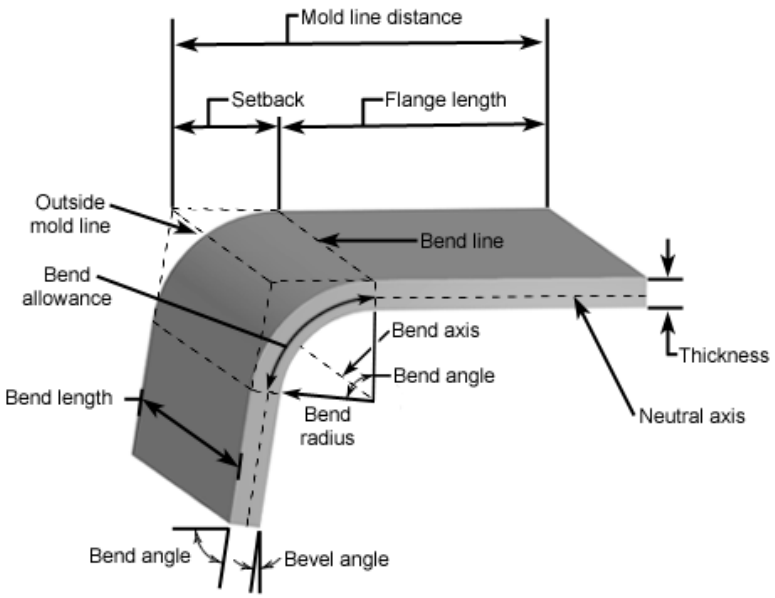

Figure 2.9: Example of a bending process and the concepts inherent to the sheet metal forming process [CustomPartNet, 2009].

While some of these concepts are secondary when it comes to roll forming processes, other are extremely important. The neutral axis is an example of a concept that is inherently fundamental to every sheet metal forming process. It is defined as a region of the sheet metal in which no material contraction or tension occurs; as such its length remains constant throughout the process; it is extremely useful to calculate the original dimensions of the sheet metal in order to obtain a final product through metal forming processes [Pacheco, 2019].

The neutral axis can be considered the line that separates the material that goes into compression from the one that undergoes tension, as illustrated by figure 2.10.

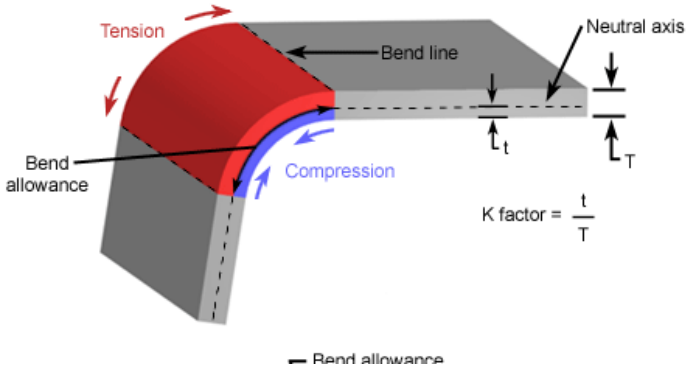

Figure 2.10: Behaviour of the material and neutral axis throughout a sheet metal bending process [CustomPartNet, 2009].

The duality in the behaviour of the material around the neutral axis, leads to its approximation to the inner part of the bending area.

2.1.4 Deformation of the Sheet Metal in Roll Forming

Roll forming consists in an extremely complex process, as forming occurs not only in the rolls but also between stations [Lindgren, 2009]. As such, it is important to understand the causes of this behaviour, in order to correctly model the plasticity behaviour of the selected material.

Throughout the roll forming process the sheet metal will be subjected to plastic deformation. The most prominent type of plastic deformation will be the transversal bending, as this will allow the sheet metal to be formed into the final product.

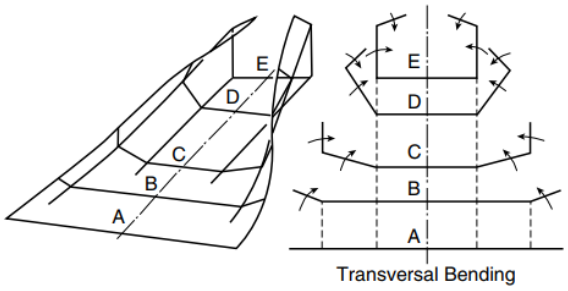

Figure 2.11: Flower diagram depicting the transversal bending of the sheet metal throughout each roll forming pass [Halmos, 2006].

However, there is a great number of other deformations that will influence the quality of the final product. Those are referred to as redundant deformations and consist in secondary material movement such as longitudinal elongation/shrinkage and bending as well as transversal elongation/shrinkage.

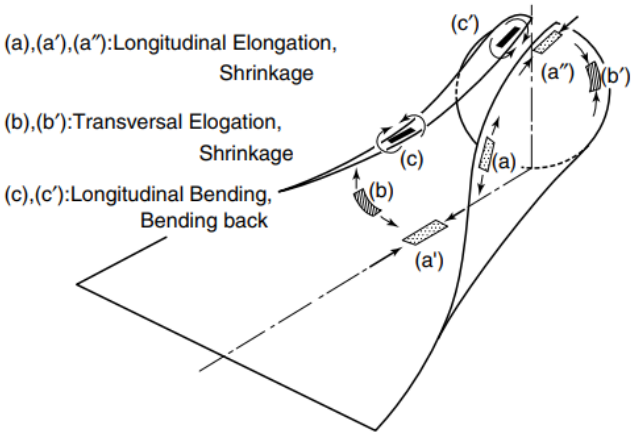

Figure 2.12: Redundant deformations of the sheet metal throughout the roll forming process [Halmos, 2006].

Sometimes shear stresses in the metal strip can lead to combinations of multiple of these phenomenons, causing simultaneously elongation and shrinkage in different points of the sheet metal.

2.1.5 Defects

In case that excessive redundant deformation occurs throughout the roll forming process, defects can show up in the final product. These can include a vast array of problems, as shown in figure 2.13.

Safdarian and Moslemi Naeini (2014) [Safdarian and Naeini, 2014] studied (both experimentally and by finite element analysis) the correlation between the effects of several roll forming parameters and their influence in bowing defects and longitudinal strain in the sheet metal. Excessive longitudinal strain can lead to wrinkling, necking and fracture. They concluded that increasing the bending angle can lead to the introduction of both bowing defects and higher peak of longitudinal strain; the latter also decreases with the flange width, web width and with the increase in distance between consecutive roll stands. Finally, Safdarian and Moslemi Naeini also observed that the influence of roll stand speed and friction coefficient are negligible for the proposed conditions.

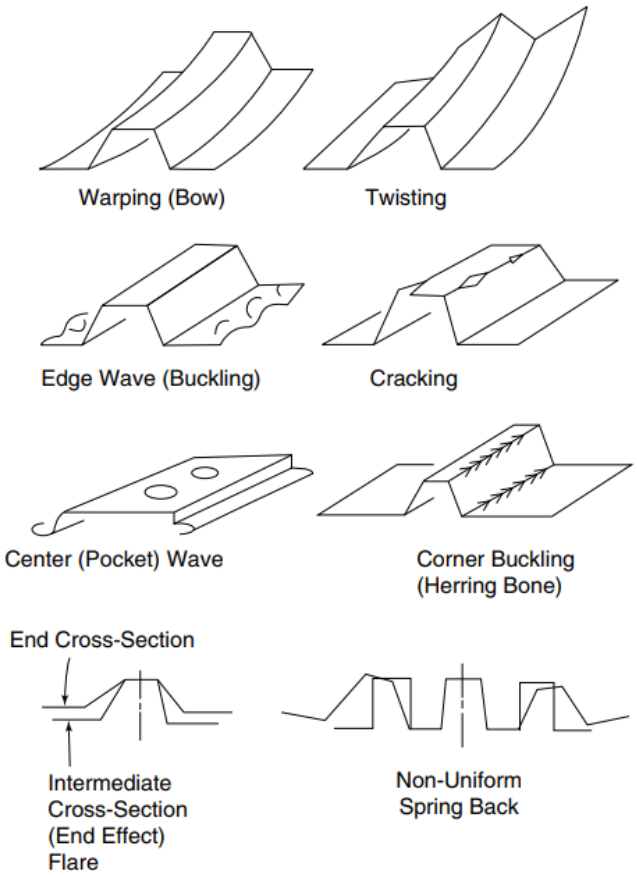

Figure 2.13: Examples of roll forming induced defects [Halmos, 2006].

These premises are important for FEA purposes as they enable to model a roll forming process forgoing the friction coefficient and setting the roll forming speed as a compromise between the respect of the quasi-static condition and the speed of the simulation (for the explicit solver where the simulations are time-dependant).

2.2 Finite Element Analyses of Roll Forming Processes

Before starting the process of modelling a roll forming process, it is important to ascertain what was made so far in FEA of roll forming processes, namely with Abaqus.

Rebelo et al. resorted to both implicit and explicit solver of Abaqus in order to simulate the roll forming process of a U-channel profile. One of the main drawn conclusions was that Abaqus/-Explicit is the preferred FEA solver for coarser meshes as the cost of the analysis increases in proportion with the size of the smallest element of the modelled mesh. As such, for simple models Abaqus/Explicit fares better than Abaqus/Standard in terms of CPU time [Rebelo et al., 1992].

The same conclusions were reached by Yin et al. as the authors managed to correctly simulate a roll forming process of a U-channel using reduced integration elements. Yin et al. modelled the process forgoing elements such as the rotation of the rolls, while accelerating the simulation through time scaling (i.e. applying a larger value of speed to the sheet metal), in order to save CPU time. However, the contact algorithm proved to be one of Abaqus/Explicit's shortcomings, as most of the CPU time was spent on contact enforcement [Yin Ji-long, 2005].

Hellborg also resorted to both Abaqus/Explicit and Abaqus/Standard to simulate a roll forming process of a U-channel. The author modelled two distinct sheet metal strips; one using S4R elements (shell elements) and the other one using C3D8R elements (reduced integration). The explicit simulation ran with shell elements yielded undesirable results, given that the springback was overestimated leading to an incorrect representation of the final geometry. The C3D8R element simulated with the explicit solver yielded satisfactory results, representing the geometry accurately when comparing the simulation results with the experimental work. However, none of the Abaqus/Standard simulations was completed, facing multiple convergence problems [Hellborg, 2007].

McClure and Li simulated a roll forming process with Abaqus and compared the result with experiments from Bhattacharrya and Smith [Bhattacharyya et al., 1984]. The authors modelled the process disregarding friction between the tools and rotation of the rolls, relying instead on a horizontal force to pull the material through the roll stations, simmilarly to what was made by Yin et al. The obtained membrane strain was similar to the experiments carried out by Bhattacharrya et al. [Lindgren, 2009].

Other authors such as Lindgren simulated roll forming processes using the implicit FEA package MSC Marc, yielding satisfying results in accordance to the theoretical context of his project. The author included friction and rotation of the rolls, increasing the complexity of the model, and despite the favourable results, the total simulation time was deemed too long for industrial use [Lindgren, 2005].

Fang et al. simulate a three-pass roll forming process to manufacture a truck wheel rim using Abaqus/Explicit and resorting to shell elements [Fang et al., 2015]. They also proposed a way of avoiding major kinematic effects on the final outcome of the simulation by considering the speed of the sheet metal as 1% of a stress propagation wave speed in steel. The outcome was a satisfactory result in terms of wall thickness, as the difference between experimental and simulated results was only as large as 7%.

Woo et al. also resorted to modelling the sheet metal with shell elements and subsequently simulating the process in Abaqus/Explicit [Woo et al., 2019]. However, they simulated flexible roll forming, which implies movement of the rolls, adding to the complexity of the simulation. They obtained a good correlation between the experimental results and the simulated ones in terms of longitudinal and edge wave bowing prediction.

Chapter 3

Roll Forming Modelling in Abaqus

This chapter is dedicated to explain the process which was used to simulate a roll forming process in Abaqus. There are several essential parameters to define that dictate the outcome of a simulation. It is crucial to understand and define correctly every aspect of a roll forming model – such as boundary conditions, contact definitions, among many others – hence the importance of understanding the core concepts inherent to both Abaqus and roll forming processes.

Throughout this chapter, a general approach to modelling a roll forming process is discussed. As it is expected, there are several ways of modelling it, as well as many considerations and simplifications that can be applied to the model. As such, this chapter is dedicated to explore the different possible choices that lead to a working and effective roll forming model.

In a first instance, the explicit and implicit solvers are analysed and compared, in terms of advantages and drawbacks in simulating roll forming processes. Subsequently, the different parameters for modelling the process are described in order to put into context the different choices taken throughout the construction of the model. Finally, the problem of comparing the different results obtained with Abaqus and COPRA® FEA RF is discussed, as the result extrapolation of the tensor values in the integration points to the nodes is not identical.

3.1 Implicit vs. Explicit Analysis

The first aspect to consider before starting to model a roll forming process is the type of solver used to carry out the simulation. Abaqus supports implicit and explicit solvers. The implicit solver is mostly used for linear problems such as structural loading analysis or dynamic transient or quasi-static problems such as metal forming processes. The explicit solver is mainly used to simulate dynamic and fast-paced events such as a crash analysis. However it is also used to simulate highly non-linear quasi-static and transient processes. Non-linearity can be caused by complex contact definition for instance, which is the case of roll forming problems.

Both solvers have characteristics that would play a positive role when simulating roll forming process as well as disadvantages. For instance, the implicit solver does not consider inertial forces, which is ideal for quasi-static problems, but takes longer to complete a roll forming simulation.

On the other hand, the explicit solver allows for a faster simulation but with inertial forces at play. It is then important to understand how to exploit the advantages of each solver while overcoming the challenges inherent to the disadvantages that they might bring.

3.1.1 Implicit Solver

The implicit solver is mainly used for smooth and quasi-static non-linear problems. This simulation method is time-independent which means that it will always solve the problem towards nodal static equilibrium. The equation 3.1 represents the equilibrium meant to achieve in the implicit method [Simulia, 2005b].

$$\sum^{N} \{F\} = 0, \tag{3.1}$$

where F represents the nodal force vector while N represents the number of degrees of freedom. The nodal load vector can then be correlated with the nodal displacements {u} – the unknown variables meant to be determined in an FEA implicit simulation – and the global stiffness matrix [K] [Dean, 2020]. Equation 3.2 illustrates the aforementioned relation.

$$[K]\{u\} = \{F\}, \tag{3.2}$$

To solve for {u}, one can manipulate equation 3.2 into equation 3.3. The implicit solver inverts the stiffness matrix in order to obtain the nodal displacements.

$$\{u\} = [K]^{-1}\{F\}, \tag{3.3}$$

In case of a linear problem, where [K] is a constant matrix, the problem can be solved in a single increment. However, the inversion of the stiffness matrix can become cumbersome if the model assumes a large dimension combined with a high non-linearity, as convergence has to be achieved through iteration. If the iteration returns a divergent solution, the increment time suffers a cutback; successive cutbacks will naturally lead to a very significant increase of computational time. Moreover, an under-constrained model will lead to singularities, which are the result of a non-existent determinant in the stiffness matrix [Dean, 2020].

It can then be concluded that an implicit simulation of a highly non-linear and inherently discontinuous process requires maximum attention to the model definition so that convergence is achieved at each increment.

3.1.2 Explicit Solver

The explicit solver is mainly used for fast-paced and dynamic processes, that usually occur in very short periods of time. However, the solver has been frequently used to successfully simulate quasi static processes as well [Harewood and McHugh, 2006]. An explicit simulation considers

inertial forces, which means that mass and time are extremely important factors to take into account. The nodal load equilibrium is therefore not static anymore because the d'Alembert forces have to be included in the equation [Seabra, 2004].

$$[M]\{\ddot{u}\} + [C]\{\dot{u}\} + [K]\{u\} = \{F\}, \quad \{F\} \approx \vec{0}, \tag{3.4}$$

where [M] represents the mass matrix, [C] the damping matrix and $\{\ddot{u}\}$, $\{\dot{u}\}$ and {u} represent the nodal accelerations, velocities and displacements respectively. As a quasi-static process, the loading vector {F} must be as close to zero as possible, meaning that inertial forces cannot exert a significant influence. According to the Abaqus manual, kinematic energy should not assume values larger than 5% of the internal energy, to respect the quasi-static condition [Simulia, 2019].

Equation 3.4 is solved by inverting the mass matrix, which is assumed as a diagonal matrix for simplicity purposes [Simulia, 2019]; the accelerations are then obtained and the velocities and displacements are subsequently calculated by the central difference rule [Mashayekhi, 2015]. Equation 3.5 represents the simplified mathematical relation that allows the calculation of the nodal accelerations. The nodal velocities and displacements are obtained using the central difference rule, represented by equations 3.6 and 3.7. The aforementioned equations are solved for each increment i, using mid-increment velocity values for accuracy purposes [Gavin, 2018].

$$\{\ddot{u}\}_{(i)} = [M]^{-1}\left(\{F\}_{(i)} - [C]\{\dot{u}\}_{(i)} - [K]\{u\}_{(i)}\right) \tag{3.5}$$

$$\{\dot{u}\}_{(i+\frac{1}{2})} = \{\dot{u}\}_{(i-\frac{1}{2})} + \frac{\Delta t_{(i+1)} + \Delta t_{(i)}}{2}\{\ddot{u}\}_{(i)} \tag{3.6}$$

$$\{u\}_{(i+1)} = \{u\}_{(i)} + \Delta t_{(i+1)}\{\dot{u}\}_{(i+\frac{1}{2})} \tag{3.7}$$

There is no need to iterate to achieve a solution, so every increment is calculated in a residual amount of time. However, for a correct estimation of the nodal accelerations – and consequently of velocities and displacements – the time increment Δt has to be conditionally small or else the solution rapidly diverges. It is then legitimate to consider the explicit solver conditionally stable. This means that while the implicit solver can achieve convergence through immensely large increments, the explicit solver is time-restrained by the Courant–Friedrichs–Lewy (CFL) rule, which states the following:

> "The full numerical domain of dependence must contain the physical domain of dependence." [Laney, 1998]

The simplified equation for linearly elastic materials, allows for an estimation of the stable time increment [Simulia, 2019].

$$\Delta t = min\left(\frac{L_e}{c_d}\right), \quad c_d \approx \sqrt{\frac{E}{\rho}}, \tag{3.8}$$

where L_e, c_d, E and ρ represent the length of an element, the local maximum wave speed across the material, the Young's modulus and the material's density respectively.

The Courant-Friedrichs-Lewy rule determines that any partial differential equation system is only stable if the time increment Δt is inferior to the time taken by a oscillation wave to cross one single element throughout the model [Courant et al., 1928]. This means that the total roll forming simulation time is controlled by the smallest element in the sheet metal.

Since the stable time increment is usually very small, explicit simulations require a much larger amount of increments to complete a simulation when compared to the implicit solver. As such, it is necessary to apply certain features to the model in order to speed up the simulation. There are many variables that can be changed in order to accelerate the simulation; however, the ones that are usually manipulated when setting up an explicit roll forming simulation are the speed, the size of the elements and the mass of the system.

- The speed of the simulation can be increased by upscaling the rate to which the sheet metal passes through the rolls. This is common practise when simulating quasi-static processes; depending on the problem, the speed can be increased to values as high as 1/200 of the speed of a stress wave through the material c_d [Jung, 1998]. Since the increased speed is bound to introduce kinetic energy in the model, it is necessary to monitor the results lest the simulation results in non-static processes [Talebi-Ghadikolaee et al., 2020].

- The mass of the model has an influence in the Courant-Friedrichs-Lewy condition as well, and can be manipulated to accelerate the total simulation time. According to equation 3.8, if the mass is augmented by a scaling factor of f_{ms}, then the stable increment time is increased by $\sqrt{f_{ms}}$. This factor can be applied globally in the model or on an element-by-element basis. One way of applying mass scaling is by pre-determining a target stable increment time; in certain conditions, the mass scaling factor can reach values as high as 10^6 [Jiao et al., 2013]. Nevertheless, mass scaling depends largely on the problem at hand and is not easily predictable; therefore, constant kinetic energy monitoring is advisable.

- Finally, the element size can be controlled by mesh refinement. A finer mesh will inevitably lead to a decrease of the stable increment time. It is then vital to verify that the mesh is not unnecessarily refined in order to not hinder the simulation's computational cost.

By default, an explicit simulation is ran in single precision, i.e the solver uses 32-bit words. However, for a large number of increments (more than 300 000 [Simulia, 2019]), the double precision parameter – resorting to 64-bit length words – is required as the amount of round-off errors associated with the central difference method (equations 3.6 and 3.7) will accumulate leading to erroneous results.

3.1.3 Comparison and Conclusion

Both solvers can be used to effectively simulate a roll forming process. Table 3.1 summarises the advantages that would facilitate the simulation of a roll forming process and the disadvantages that one would have to overcome to properly model it.

Table 3.1: Advantages and disadvantages of using each solver in a roll forming process simulation.

	Advantages	Disadvantages
Implicit	The implicit solver is unconditionally stable. It is also ideal for quasi-static problems, as inertial forces are not considered.	Under-constrained problems can lead to simulation abortion and convergence can be hard to obtain in highly non-linear processes, ultimately increasing the total simulation time.
Explicit	The explicit solver handles highly non-linear problems in a more efficient way. No iteration is needed to calculate each increment and as such, no cutbacks will affect the simulation running time.	The large number of increments lead to round-off errors that have to be compensated by resorting to double precision analyses. Furthermore, to speed up the simulation one has to modify time and mass constraints that may influence the simulation results in an unpredictable manner. It is then necessary to monitor kinematic forces to not incur in erroneous analyses.

3.2 Part and Geometry Modelling

A roll forming process involves forming rolls, a sheet metal to be formed and additional components of the roll forming line such as guiding rolls. Therefore, the first step to take when modelling a roll forming process and the type of problem at hand dictates what sort of part is to be generated.

- Deformable part: an arbitrarily shaped part that can be meshed and deformed under load.
- Discrete rigid part: it shares some similarities to a deformable part, such as the possibility to assume any arbitrary shape and be meshed but it cannot be deformed under load.
- Analytical rigid part: similarly to the discrete rigid part, it cannot be deformed. Their difference relies on the fact that an analytical body is not meshed, allowing the simulation to generally take up less computational cost than if discrete rigid or solid bodies were used. Its geometry is defined by an analytical equation, rather than a mesh.

The modelling of a deformable part depends on the analysis subject of the roll forming simulation. Generally, the forming is the main aspect of a roll forming process so the deformable part is generally the sheet metal, while the rolls are modelled as rigid bodies. However, one could

consider the rolls as deformable in order to study their behaviour throughout the simulation; this solution implicates an extremely large increase in computational cost.

If the roll forming line is symmetrical, there is a possibility to only design half of the model. This consideration allows for a significant computational cost reduction in the simulation.

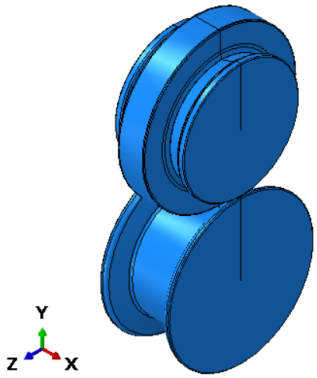

Figure 3.1: Modelling of a set of analytical rigid rolls in Abaqus.

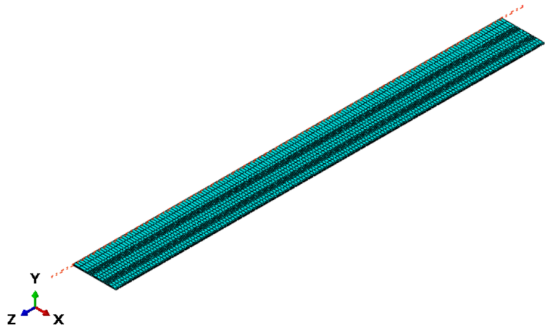

Figure 3.2: Modelling of half of a meshed deformable sheet metal strip in Abaqus, with the symmetry plane represented in red.

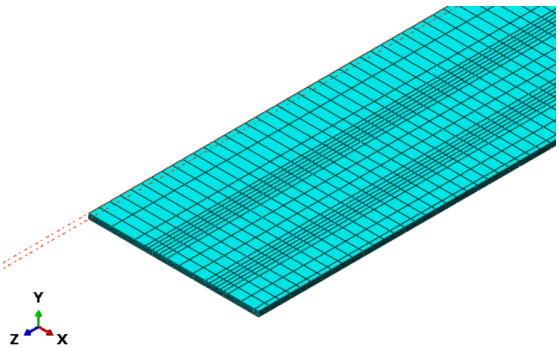

Figure 3.3: Detail of the modelled sheet metal, with the symmetry plane represented in red and with a mesh refinement in the bending zones and in the strip edge.

Even though the sheet metal can be modelled as a symmetrical body, the roll geometry is imported from COPRA®RF, meaning that throughout this work they are modelled as a whole.

3.3 Material Modelling

For a roll forming simulation the essential material properties to input into the programme are the material's density, Young's modulus, Poisson's coefficient, work hardening model and plastic yield surface. There is always the possibility to model other material behaviours such as fracture or creep for instance. However, for a wider scope, the aforementioned parameters can represent the process reliably. The sheet material is thus modelled as a linearly elastic material with isotropic hardening. The elastic behaviour is then modelled by Hooke's law given by equation 3.9. It relates the tensile stress and strain behaviour of a material through a constant of proportionality inherent to each material: the Young's modulus [Roylance, 1996].

$$\sigma(\varepsilon) = E\,\varepsilon, \tag{3.9}$$

where E is the Young's modulus, σ is the uniaxial stress and ε is the strain. On the other hand, the plastic behaviour is modelled by Swift's work hardening Law [Sener and Yurci, 2016] and the von Mises isotropic yield surface. It is relevant to point out that despite the fact that anisotropy [Bonab and Mazdak, 2014] is an inherent feature in sheet metal forming processes, the material was modelled with an isotropic approach. This was a simplification taken into consideration since the study of anisotropy is out of the scope of this thesis and facilitates a more expedite approach for the problem at hand.

Albeit that there is a vast number of isotropic and anisotropic work hardening models, the Swift's Law is one of the most widely used plasticity models for quasi-static processes. It relates the tensile stress to which a test piece is submitted to its true strain, and is given by equation 3.10 [Sener and Yurci, 2016].

$$\sigma(\varepsilon_p) = K(\varepsilon_p + \varepsilon_o)^n\,, \tag{3.10}$$

where ε_p is the effective plastic strain and ε_o, K and n are material parameters. The application of this equation results in a set of points from which the work hardening curve for the considered material can be drawn.

3.4 Contact Modelling

The contact modelling is crucial to the success of a roll forming simulation. Not only is the contact an extremely complex subject that needs to be accurately represented, it is also the agent responsible for the transverse bending that will cause the forming of the sheet metal. As such, the interaction of the different contact bodies has to be analysed in depth to ensure that the obtained results do not turn out to be erroneous.

In Abaqus, the contact is modelled between all the different parts that come in touch through the definition of contact pairs; one of the surfaces is defined as master and the other one as slave. These interactions are enforced through contact algorithms that avoid contact penetration which

which would otherwise occur to some extent between rolls and sheet metal. The available algorithms vary depending on the chosen solver:

- The explicit solver relies on two main contact pair algorithms: kinematic and penalty algorithms [Simulia, 2019].
- The implicit solver also relies on a penalty algorithm; furthermore, it counts on two other formulations that are variations of the aforementioned contact enforcement: Lagrange multiplier and augmented Lagrange algorithms.

The explicit kinematic contact enforcement is a predictor/corrector algorithm. For every increment i, the kinematic state of the slave nodes is calculated for increment i+1 and the positions of the interfering slave nodes is corrected [Neto, 2014]. This operation happens without artificial added stiffness to the elements; however this algorithm can cause the sheet metal to stick excessively to the roll, adopting a more plastic behaviour. Moreover, this algorithm also entails kinematic energy loss in the system [Simulia, 2019].

On the other hand, the penalty contact enforcement algorithm, usable by both implicit and explicit solvers, does not predict nodal interference. This algorithm allows nodal penetration up to a certain overclosure and stiffens the element in order to correct excessive penetration [Nour-Omid and Wriggers, 1987]. The drawback inherent to this contact formulation resides on the fact that the added element stiffness can reduce the stable time increment of an explicit simulation [Simulia, 2019].

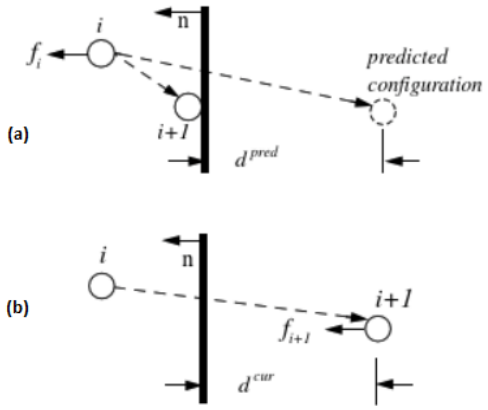

Figure 3.4: Physical representation of the (a) kinematic predictor algorithm and (b) penalty contact algorithm [Hibbitt, 1999].

In figure 3.4 the kinematic and penalty algorithms are compared. The kinematic algorithm predicts the configuration of the node in increment i+1 and corrects its displacement by the distance d^{pred}. The penalty algorithm allows the penetration of the node at increment i+1 and applies a force f^{pred} to correct the node by a distance of d^{cur} at increment i+2. This force involves an increase in the element's stiffness, as represented by equation 3.11.

$$f_{i+1} = (kd^{cur})_{i+1} \tag{3.11}$$

It can be inferred that the penalty method is the equivalent of applying a spring to the penetrating nodes. Figure 3.5 illustrates this behaviour applied to two surfaces in contact.

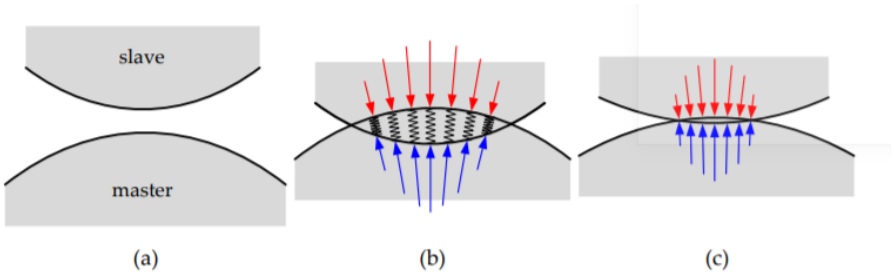

Figure 3.5: Physical interpretation of the penalty contact enforcement method: (a) initial configuration; (b) configuration after penetration; (c) equilibrium state [Neto, 2014].

Two other formulations are often resorted to in implicit simulations: the Lagrange multiplier method and the augmented Lagrange method [Neto et al., 2016]. The Lagrange multiplier method introduces additional degrees of freedom to enforce contact constraints; however this increases the computational cost of the simulation, as new variables are introduced in the problem. The augmented Lagrange method is a compromise between the two aforementioned approaches [Neto et al., 2016].

Friction can also be modelled, as it is an inherent parameter to sheet metal forming. However it is going to be disregarded throughout this study as it is a valid simplification: it allows to reduce the computational cost of the simulation ending up having little influence on the longitudinal strain on the sheet metal [Safdarian and Naeini, 2014] while still yielding reliable results [McClure and Li, 1995].

3.5 Boundary Conditions

The boundary conditions in an FEA model are the representation of the physical phenomenons that occur in a simulation. They are meant to represent the problem correctly while simplifying it so as not to over constrain the model which could result in a waste of computational time.

In a roll forming simulation the boundary conditions applied to the sheet metal and to the rolls should result represent the forming process, while avoiding rigid body motions.

To simplify the model, instead of conveying motion to the sheet metal and forcing it into the roll forming line, the motion can be applied to the rolls in order to facilitate the modelling, as illustrated by figures 3.10 and 3.11. The sheet metal is thus fixed, as illustrated by figures 3.6 to 3.9. Three boundary conditions are evident in these illustrations:

- A symmetry condition in the x-direction;
- a stabilisation condition in three nodes in the y-direction

- a continuous feeding to the roll forming line condition in the z-direction.

Rotational motion can also be applied to the rolls; however this requires a kinematic modelling of the problem. Moreover, if the rolls are driving the sheet metal, friction also has to be modelled [Lindgren, 2005].

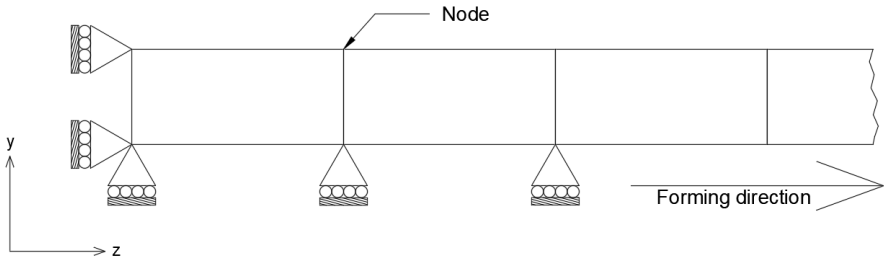

Figure 3.6: Boundary conditions applied to the back end of a modelled fixed sheet metal strip, YZ plane.

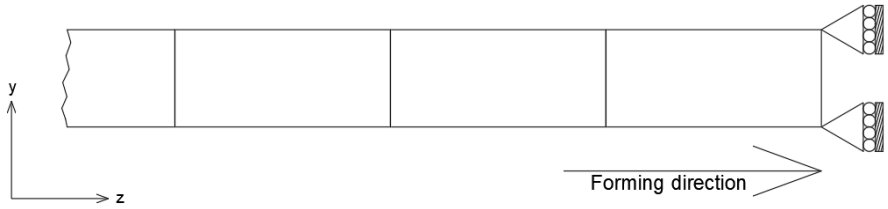

Figure 3.7: Boundary conditions applied to the front of a modelled fixed sheet metal strip, YZ plane.

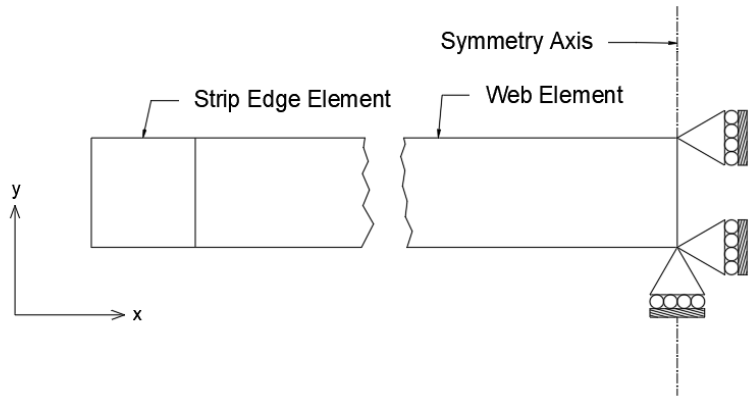

Figure 3.8: Boundary conditions applied to the back end of a modelled fixed sheet metal strip, XY plane.

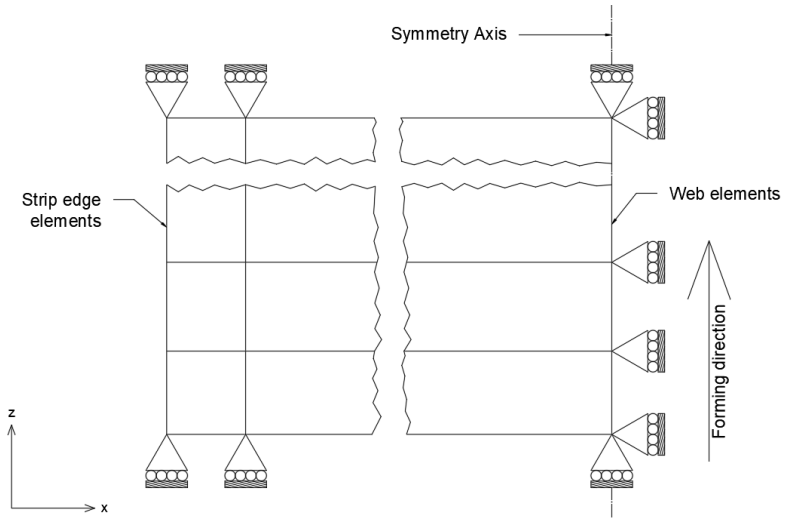

Figure 3.9: Boundary conditions applied to the totality of a modelled fixed sheet metal strip, XZ plane.

Three nodes in the y-direction are locked to stabilise the sheet metal in between stations (illustrated in figure 3.6), and the nodes in the Z-direction are locked to keep a constant length in order to simulate a continuous sheet metal feeding procedure (illustrated in figures 3.6, 3.7 and 3.9). In the x-direction, all the nodes belonging to the symmetry plane are locked to model the symmetry condition, as illustrated in figures 3.8 and 3.9.

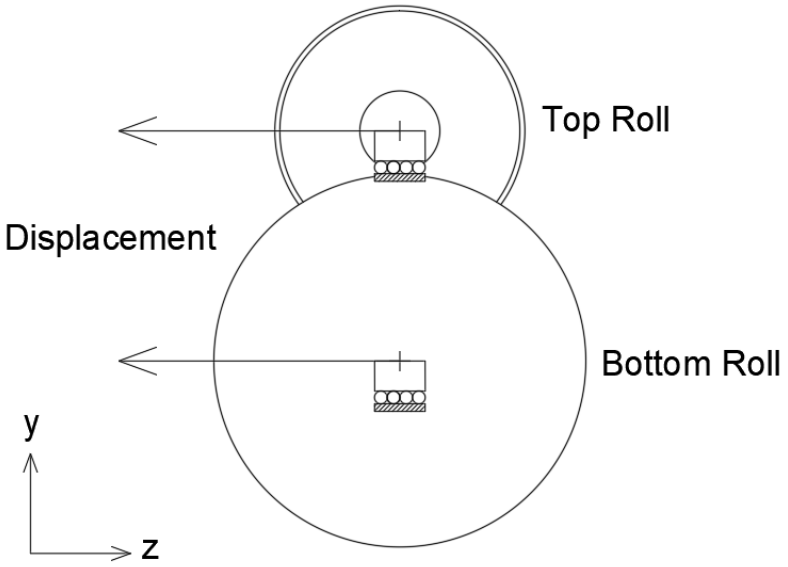

Figure 3.10: Projection of a set of rolls onto the YZ plane; the rolls' rotation is locked as well as the translation in y-direction, as the forming takes place in the z-direction.

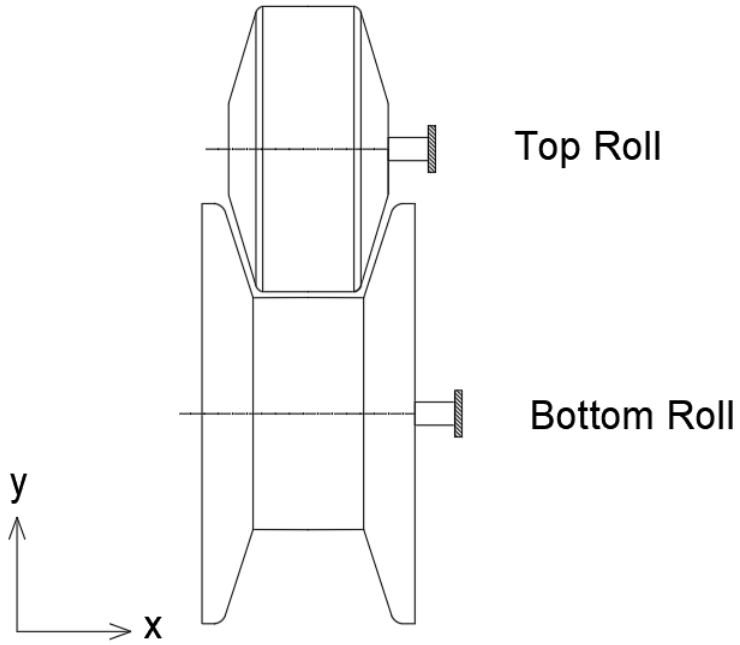

Figure 3.11: Projection of a set of rolls onto the XY plane; in this plane, the rolls produce no movement, as if they were submitted to an encastre.

Figures 3.10 and 3.10 illustrate the boundary conditions applied to the rolls. A translational motion is applied to the rolls in order to form the sheet metal into the desired cross-section, while all other degrees of freedom are blocked. This consists in a simplification of a process that otherwise would consider roll rotation and friction.

3.6 Element Types

The mesh refinement and element choice are essential parameters for any FEA simulation. COPRA® FEA RF uses a fully integrated solid and linear hexahedral element with an updated Lagrangian feature and enhanced assumed strain fields (Element type 7). As such solid fully integrated elements will also be considered for the roll forming modelling in Abaqus. Additionally, a linear shell element [Liang et al., 2019] and a solid continuum hexahedral element [Hellborg, 2007], both with reduced integration, will be studied as well since metal forming simulation with this sort of element is common practise. The next sections will be dedicated to expose pros and cons inherent to each type of element.

3.6.1 Solid 8-Node Fully Integrated Elements (C3D8 and C3D8I)

The considered fully integrated linear hexahedral elements have eight integration points and three degrees of freedom per node. Two fully integrated elements will thus be analysed in further chapters: the C3D8 and the C3D8I.

- The C3D8 element is a fully integrated element frequently used for small strain linear structural analysis as it usually gives very stiff response under the plastic domain [Simulia, 2019].
- The C3D8I is a fully integrated element equipped with an incompatible modes feature that grants the element thirteen additional internal degrees of freedom (added to the three degrees of freedom inherent to brick elements). It gives a much more pliant response to plasticity, particularly in bending, than the C3D8 element [Simulia, 2019].

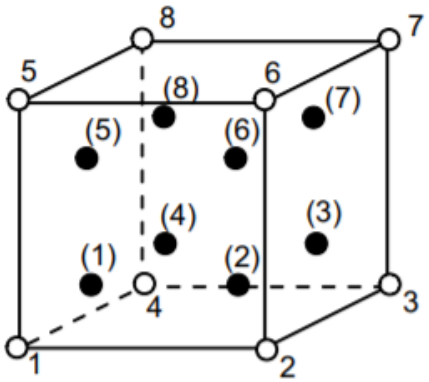

Figure 3.12: Solid 8-node fully integrated element; the integration points are denoted in white, while the nodes are denoted in white.

The main problem with the usage of fully integrated elements is shear locking. Shear locking happens because linear elements are unable to replicate pure material bending, the process illustrated by figure 3.13. Instead, fully integrated elements behave as illustrated in figure 3.14.

Figure 3.13: Ideal element behaviour under a pure bending load (the integration points are represented by the red dots) [Simulia, 2019].

Figure 3.14: Linear fully integrated element behaviour under a pure bending load (the integration points are represented by the red dots) [Simulia, 2019].

The upper integration points – the red dots that mark the intersection of the discontinuous segment – will assume stress in direction 1 (σ_{11}) as tensile while the lower integration points will

assume σ_{11} as compressive. The stress in direction 2, σ_{22}, is non-existent as the discontinuous lines have not suffered any length change for both cases. However, the angle between the segments created by the integration points in figure 3.14 has changed while it remains constant in figure 3.13. This implies that fully integrated elements subjected to pure bending consider the existence of an additional shear stress, τ_{21}, which is not supposed to exist in pure bending situations [Natal, 2017]. This will cause overly stiff responses to bending loads.

One solution to overcome this problem resides in the incompatible modes element though the addition of internal degrees of freedom to fully integrated elements; the more pliant response due to the enhanced displacement fields might yield adequate results for the simulation of roll forming processes [Bui and Ponthot, 2008].

The equivalent element in COPRA® FEA RF is element type 7.

3.6.2 Solid 8-Node Elements with Reduced Integration (C3D8R)

Another solution to overcome the shear locking problem resides in reduced integration elements, such as the C3D8R. These elements have one integration point and three degrees of freedom. As illustrated by figure 3.15, the fact that the reduced integration element only has one integration point solves the appearance of spurious shear stresses.

Figure 3.15: Linear element with reduced integration under a pure bending load (the integration points are represented by the red dots) [Simulia, 2019].

However, one has to be cautious when using reduced integration elements, as a new numerical problem is introduced: hourglassing. Hourglassing is a numerical instability associated to the lack of stiffness of an element due to the fact that it only possesses one integration point; this causes nodal deformation while no energy is being applied. An artificial hourglass control has to be added to the system to avoid these zero-energy deformations, introducing system induced energies. These energies have to be kept in check and cannot weight too much on the total internal energy of the model [Boulbes, 2010]. Another solution consists in refining the mesh; in roll forming simulations, reduced integrated elements must constitute a mesh with several elements over the thickness.

The equivalent element in COPRA® FEA RF is element type 117.

3.6.3 Planar 4-Node Shell Elements with Reduced Integration (S4R)

Shell elements (S4R) are used to model parts with a negligible thickness when compared to its width and length [Simulia, 2019]. This sort of element has a user-defined amount of integration points over the thickness. However, being a planar element, an analysis to shear strain/stress through the thickness of the sheet metal is rendered impossible.

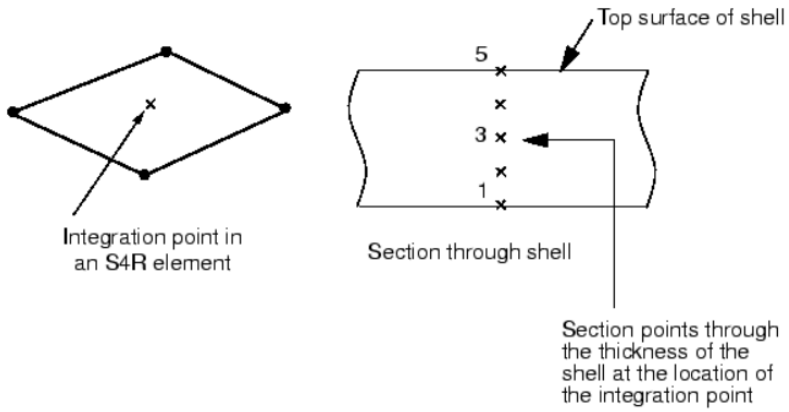

Figure 3.16: S4R element with five Simpson integration points through the rendered thickness.

There are advantages to the usage of this sort of elements:

- Computationally inexpensive in Abaqus [Simulia, 2019];
- Correct representation of springback phenomenons [Hellborg, 2007].

Nevertheless, there are also several disadvantages associated with the usage of shell elements with reduced integration[Willmann, 2020]:

- The small bending radii inherent to roll forming processes is incompatible with the usage of shell elements as bending is not well represented, unless the mesh is highly refined [Willmann and Bischoff, 2019].
- For thicker sheet metals, the usage of shell elements is inadequate, as the ratio between the thickness of the sheet metal and its width/length becomes larger.
- The strains and stresses in the thickness direction cannot be represented by conventional shell elements.
- The element can be prone to excessive artificial stiffening for large strains.

3.6.4 Hourglass Control in Abaqus

There are three main hourglass controls that are the subject of study in this dissertation: the enhanced hourglass control (EHC), the total stiffness hourglass control (TSHC) and the relaxed stiffness hourglass control (RSHC). These features can significantly influence the final outcome of a roll forming simulation as the enforcement of hourglass control is made by adding artificial stiffness to elements prone to zero-energy deformation.

- Enhanced hourglass control: it is a method that is more suitable for displacement solutions for models presenting coarse meshes with linear elastic materials. It also provides increased resistance to hourglassing for nonlinear materials; nevertheless, it is prone to generating an

overly stiff responses in problems displaying plastic yielding under bending. It is recommended to use in hyperelastic materials [Simulia, 2019].

- Total stiffness hourglass control: it is the most recommended hourglass control algorithm for quasi-static and transient simulations. This hourglass control is the default setting for Abaqus/Standard [Simulia, 2019].

- Relaxed stiffness hourglass control: it is the most computationally expensive hourglass mode control of the three. It is used in dynamic simulations where there is a chance of sudden dynamic loading. This hourglass control is the default setting for Abaqus/Explicit [Simulia, 2019].

3.6.5 Comparison and Conclusion

It was seen that the response that the elements provide varies significantly under load, depending on their formulation.

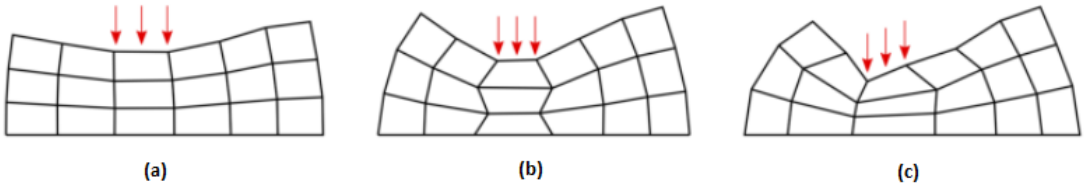

Figure 3.17: Unstable element responses to the same load: (a) stiff behaviour, (b) numerical instability (hourglassing) and (c) physical instability (element collapse) [Bieber, 2020].

In figure 3.17, three element related instabilities are represented. A stiff behaviour is expected to occur in element C3D8, while the hourglassing effect can be observed in elements such as the C3D8R and S4R, due to the reduced integration. If the physical collapse of the element takes place, the roll forming process is most likely underconstrained or poorly modelled.

In chapter 4 the different elements will be studied more exhaustively to understand how they behave in different loading situations. Nevertheless, the theoretical information mentioned throughout this chapter is reported in table 3.2; at the end of chapter 4 these premises will be corroborated/disproved in order to correctly model a roll forming simulation.

Table 3.2: Theoretical advantages and disadvantages of using each element in a roll forming simulation.

Element	Advantages	Disadvantages
C3D8	Will allow a direct comparison with COPRA® FEA RF's solid element.	Inadequate for sheet metal forming simulations of any kind.
C3D8I	Correct representation of bending. Allows the interpretation of stresses along the thickness of the sheet metal.	The element's dimensional ratio has to be quasi cubic. Can still be prone to shear/volumetric locking phenomenons.
C3D8R	Computationally inexpensive. Also allows a stress/strain analysis over the thickness of the sheet metal.	Prone to hourglassing. Requires a fine mesh to yield accurate results.
S4R	Computationally inexpensive. Does not require elements over the thickness given that it consists in a planar element.	Difficult to correctly model the contact in explicit simulations. The model is not adequate for thicker sheet metals.

3.7 Mesh Refinement

Mesh refinement is also an extremely important topic and it is closely related to the selected element. Since it is computationally inefficient to analyse the sheet metal with a constant mesh refinement, localised refinement has to be carried out to obtain reliable results. To accurately represent the roll forming process, especially in the bending areas and the strip edge, the following considerations can be established:

- Minimum of three elements over the width of the sheet metal' bending zone(s) for an accurate representation of the bending process.
- Transition elements, slightly larger than the bending zone elements, next to the bending zone(s) are recommended, especially next to the sheet metal's web, where the elements are larger. A smooth change in element size is considered a good practice in FEA, as errors in larger elements can be transferred into finer elements [Fagan, 1992].
- A locally refined area on the strip edge is required, in order to correctly represent the longitudinal strain in this area.

Figure 3.18 illustrates the aforementioned conditions being applied to a sheet metal mesh. In this example, the sheet metal has four elements to represent the two bending zones and one row of transition elements on each side of the bending zones. Additionally, a row of larger transition elements between the web and one of the bending zones was added as well. Since only half of the sheet metal was modelled for symmetry purposes, the symmetry axis is also denoted.

The refinement of a sheet metal in the thickness direction will have to do with the choice of elements, and some conclusion can be drawn from chapter 4 in that regard.

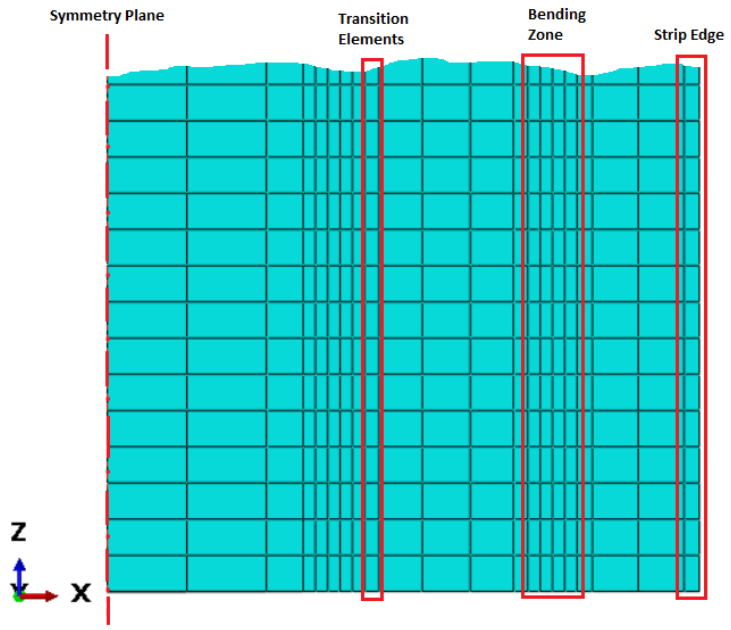

Figure 3.18: Example of a meshed symmetrical sheet metal with four bending zones combined with transition elements.

Finally, the refinement of the mesh along the length of the sheet metal has to be done in order to keep the elements as cubic as possible, to ensure an adequate nodal distribution throughout the model.

Chapter 4

Element Technology Study

In order to understand how to implement a roll forming model in Abaqus, one must assess beforehand the behaviour of elements C3D8, C3D8R, C3D8I and S4R (as described in chapter 3) in terms of stiffness and distortion when faced with basic loads, such as tensile or bending. Resorting to quasi-static processes, it is intended to evaluate the application of the aforementioned elements in roll forming simulations.

In a first instance, single elements will be submitted to tensile and bending test simulations. The goal of the tensile test is to compare the evolution of stress in each element as a function of its total strain using the generated stress-strain curves. That will provide some insight regarding the response of these elements to the same applied uniaxial displacement. On the other hand, the single element bending test is meant to replicate the distortion of an element submitted to bending loads. The objective of the bending test simulation is to compare the behaviour of the modelled elements in terms of stiffness when subjected to moments. Since roll forming is a process that heavily relies in the sheet metal's transversal bending, this test enables a prediction of each element's deformation in the subsequent roll forming analysis.

The third test consists in a beam bending analysis that can be compared to Timoshenko's equations for beams subjected to bending. Although roll forming depends on the material's plastic deformation, this test has to be kept in the elastic domain so that the simulation results can be compared to an analytical model. The goal of this test is to analyse the behaviour of a discretised structure when subjected to bending moments, varying the type of element that constitutes its mesh. All the tests are carried out in Abaqus/Standard, using the implicit solver.

4.1 Single Element Analysis

This test consists in subjecting a single element to a load, or a set of loads, and boundary conditions in order to predict its behaviour to the different scenarios to which it is submitted. The idea behind these tests consists in analysing how a single element fares when subjected to simple loads such as bending and tensile loads. They will then be evaluated in terms of stiffness and likeliness to distort under the applied loads.

4.1.1 Single Element Tensile Test

The tensile test purpose is simple; it consists in locking one end of a 1 mm sided cube and applying a 5 mm displacement to the other end, as illustrated by figure 4.2a and 4.2b. Each node of the considered elements have only three degrees of freedom; as such, the rotation of every fixed element does not need to be blocked.

In this chapter, as well as throughout the subsequent chapters, the modelled material will be the HSS DP800. The elastic properties of the DP800 are reported in table 4.1 and its density is 7800 kg/m^3.

Table 4.1: Elastic properties of the HSS DP800.

E [MPa]	210×10^3
ν [-]	0.3

The plasticity of the DP800 steel is modelled according to Swift's plasticity law (equation 3.10), using the parameters reported in table 4.2 [Figueiredo, 2016]. Furthermore, the material is modelled to yield isotropically, following the von Mises yield surface.

Table 4.2: Swift law's parameters for DP800 steel.

ε_0 [-]	0.00151
K [MPa]	1361.29
n [-]	0.157

The work-hardening curve of the DP800 steel is represented by figure 4.1.

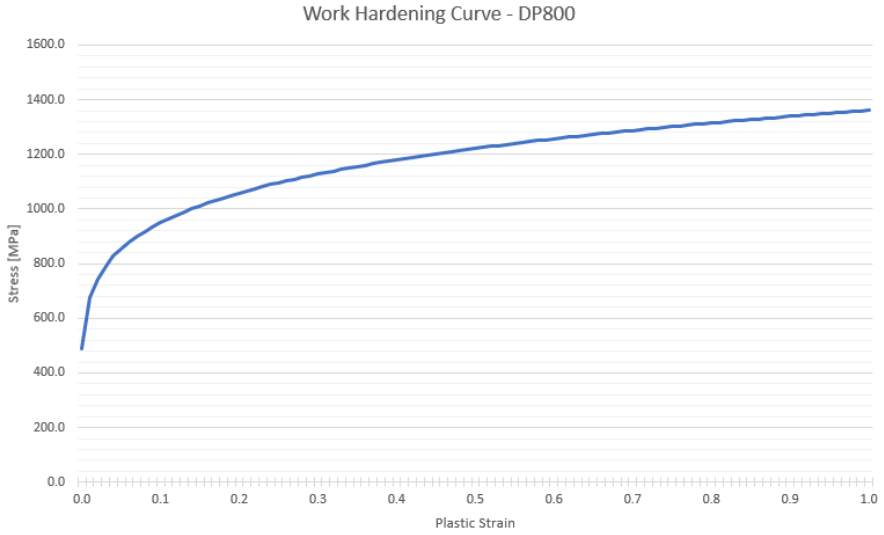

Figure 4.1: Work hardening curve of the DP800 steel.

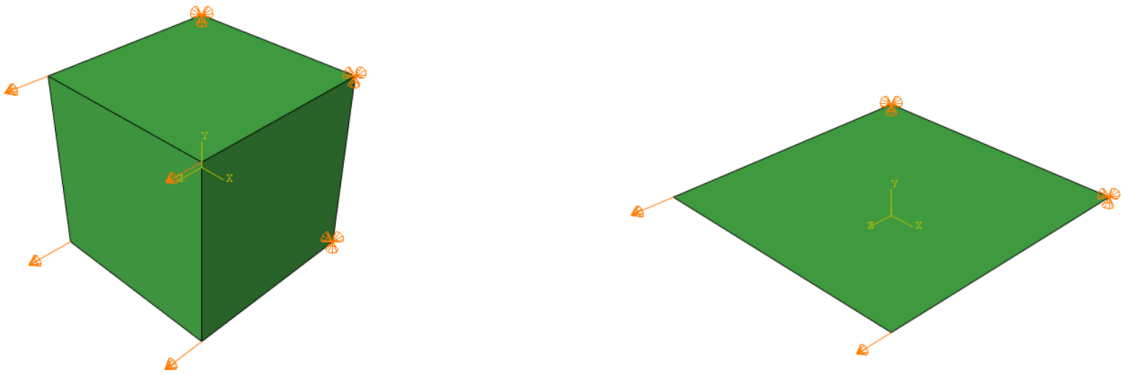

(a) Solid Elements. (b) Shell Elements.

Figure 4.2: Boundary conditions set for the single-element tensile test.

Four elements are tested under these conditions: C3D8, C3D8R, C3D8I and S4R. In order to compare their behaviour throughout each tensile test simulation, a graphical analysis has to be carried out. Two curves will be generated: the stress-strain curve and the internal energy curve for each element. The internal energy is represented in Abaqus by the parameter ALLIE and can be calculated through the equation 4.1, where the more relevant variables are ALLSE – recoverable strain energy – ALLPD – energy associated with the plastic deformation – and ALLAE – the energy associated with hourglass control. The definition of the remaining variables can be found in the abbreviation list, even though their weight is negligible for the problem at hand.

$$ALLIE = ALLAE + ALLPD + ALLSE + (ALLCD + ALLDMD + ALLDC + ALLFC) \quad (4.1)$$

These plots will allow an assessment of the stiffness of each element throughout the simulation. After simulating every element in the aforementioned conditions, the graphics in figure 4.3 and 4.4 were generated.

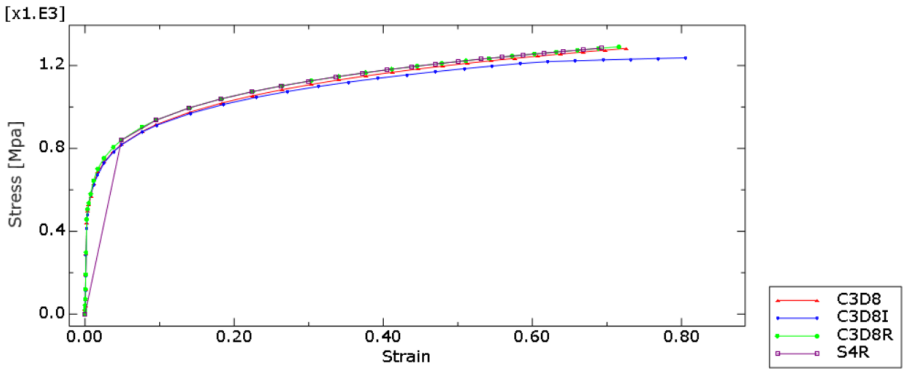

Figure 4.3: True stress as a function of true strain curves for the four elements submitted to a tensile test.

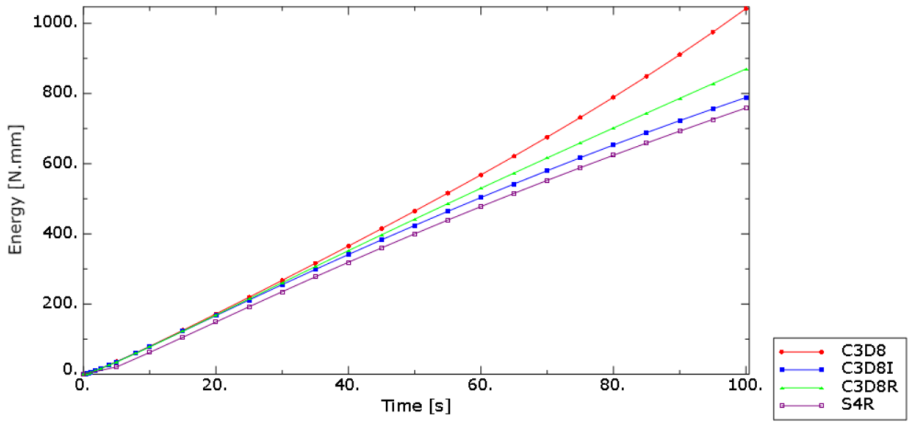

Figure 4.4: Internal energy curves for the four elements submitted to a tensile test, over the time of simulation.

From figure 4.3, one can infer that – as expected – the elastic domain behaviours of the solid continuum elements are similar to one another. However, the shell element exhibits an erratic stress/strain behaviour, even though the element was modelled with the same material properties. This observation can indicate a poor capacity of the reduced integration shell element to replicate the elastic behaviour of the sheet metal, which can lead to an underestimation of the springback phenomenon. In the plastic domain, the differences in the stress evolution throughout the simulation become more apparent; the reduced integration elements' curves eventually overlap and exhibit a slighter stiffer behaviour than the other elements while the C3D8I is clearly more pliant under tensile loads than the remainder.

From figure 4.4, it is deducible that the required energy to deform each element is different for every case. The fully integrated element C3D8 is the stiffest element as its deformation demands more energy involved in the tensile test, while the S4R is the least stiff.

In order to better understand the variables that regulate the behaviour of the different elements, a decomposition of the internal energy can be carried out. Among the variables described in equation 4.1, only the energies associated with elastic strain (ALLSE), plastic strain (ALLPD) and hourglass control (ALLAE) – in the case of reduced integrated elements – are relevant for this particular simulation. The internal energy is also plotted to ascertain the relative weight of each variable.

Both elements with full integration have the same behaviour under tensile loads: according to figures 4.5 and 4.6 the elements are under full plasticity, given that the internal energy and plastic dissipation energy curves are completely overlapped. The artificial energy in both fully integrated elements is naturally non-existent as hourglassing does not occur.

Concerning the reduced integration element C3D8R, one can already observe a weight of around 5% of the artificial energy in the total internal energy. Even though it does not represent a very significant fraction of the internal energy, it does have a small effect in the final results. This sort of influence has to be avoided (according to the User's Manual [Simulia, 2019], system-induced energies should be kept below 5%) in order to obtain reliable results.

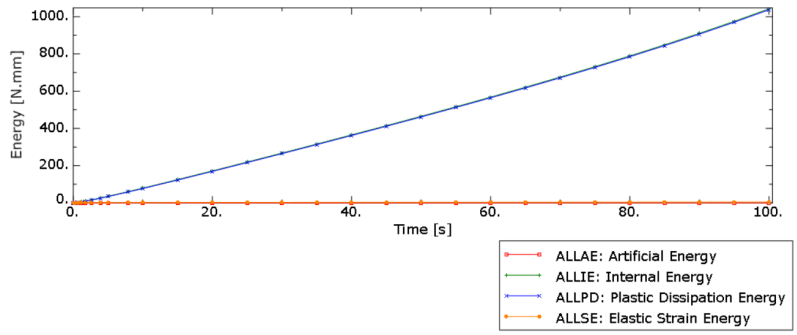

Figure 4.5: Energy balance of a C3D8 element subjected to a tensile test.

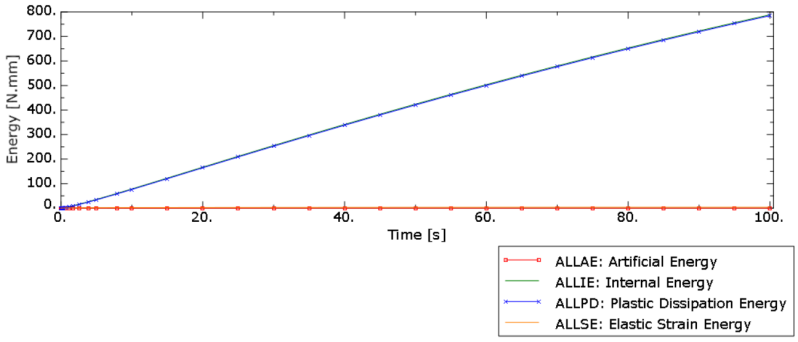

Figure 4.6: Energy balance of a C3D8I element subjected to a tensile test.

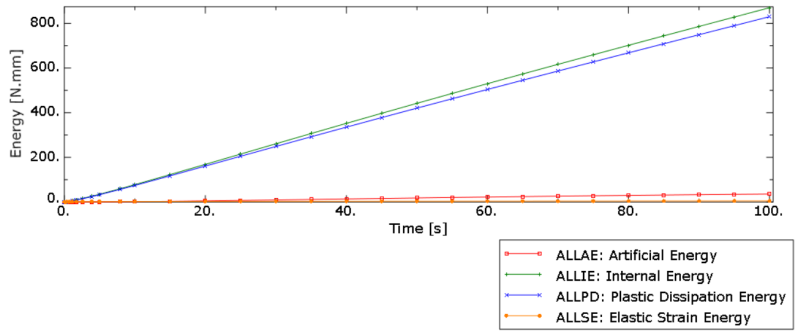

Figure 4.7: Energy balance of a C3D8R element subjected to a tensile test.

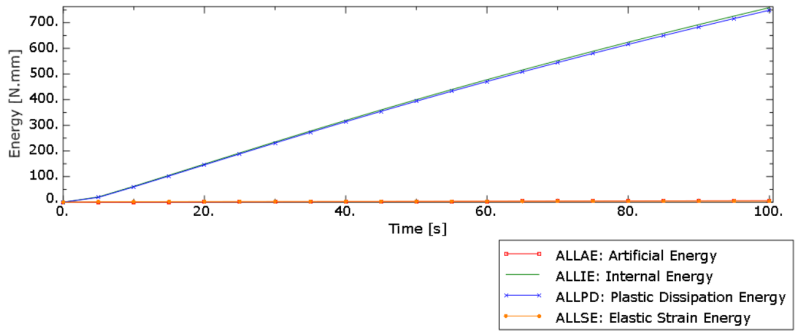

Figure 4.8: Energy balance of a S4R element subjected to a tensile test.

Finally, the S4R element is marginally affected by the hourglass control associated energy in a fraction that is safely below the allowable maximum fraction of the internal energy value.

4.1.2 Single Element Bending Test

Even though the tensile test revealed a first glimpse on the behaviour of the different considered elements, it is not enough to characterise bending loads. Since transversal bending is the most important deformation in roll forming processes, understanding the elements' behaviour when subjected to bending loads is of the utmost importance. As such, different models were devised so as to analyse the behaviour of different elements in terms of stiffness and deformed geometry. This test consists in applying tension displacements to the top nodes of a face of a single solid element and compression displacements to the bottom ones, while pinning the other end of the cube (as seen in figure 4.9a). For the shell element, the setup has to be distinct; since the S4R is a plane element, one edge will be encastred while the other one will be subjected to a rotational displacement along the Z-axis, as represented in figure 4.9b.

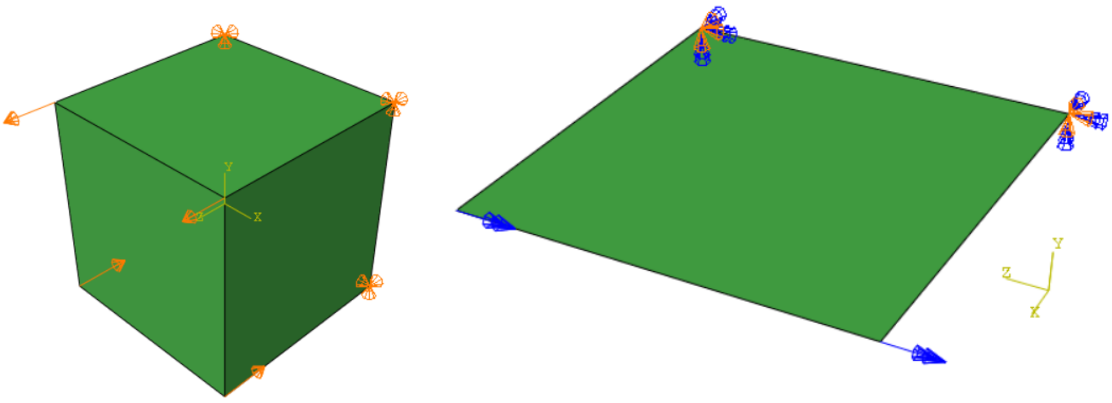

(a) Solid Elements. (b) Shell Elements.

Figure 4.9: Boundary conditions set for the single-element bending test.

In figures 4.10 to 4.13, a side view of each element distortion after a bending load is depicted. Furthermore, the von Mises stress (given by equation 4.2) was plotted, so as to observe the stress state of each element at the end of the simulations. It is fairly noticeable that the fully integrated elements are stiffer under bending loads than the reduced integration elements.

$$\sigma_{VM} = \sqrt{\frac{1}{2}\left[(\sigma_{xx}-\sigma_{yy})^2+(\sigma_{yy}-\sigma_{zz})^2+(\sigma_{zz}-\sigma_{xx})^2\right]+3\left(\tau_{xy}^2+\tau_{yz}^2+\tau_{zx}^2\right)}, \tag{4.2}$$

where σ_{xx}, σ_{yy} and σ_{zz} are the normal stresses in the respective directions while τ_{xy}, τ_{yz} and τ_{zx} are the shear stresses.

Naturally that due to the planar nature of the shell element, the von Mises equation could be rewritten as follows:

$$\sigma_{VM} = \sqrt{\sigma_{xx}^2 + \sigma_{yy}^2 + \sigma_{xx}\sigma_{yy} + 3\,\tau_{xy}^2} \tag{4.3}$$

Equation 4.3 outlines one of the inherent problems of the shell element: the lack of stresses in the thickness direction. For thicker sheet metal strips, choosing a shell element can lead to misguided analyses as the bending behaviour might be poorly represented.

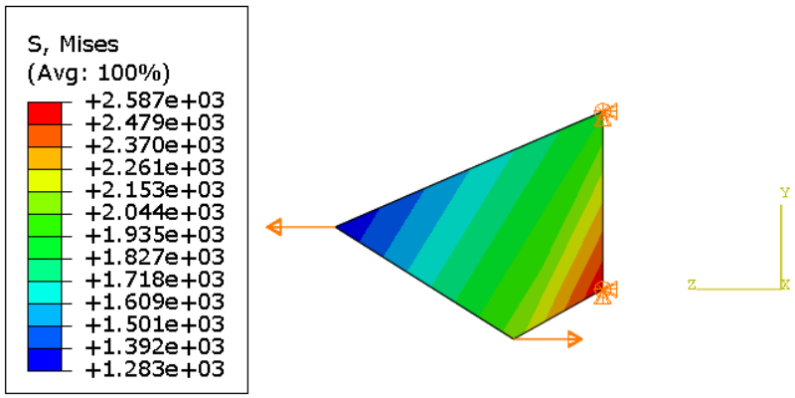

Figure 4.10: Deformation of the C3D8 element under a bending load (side view).

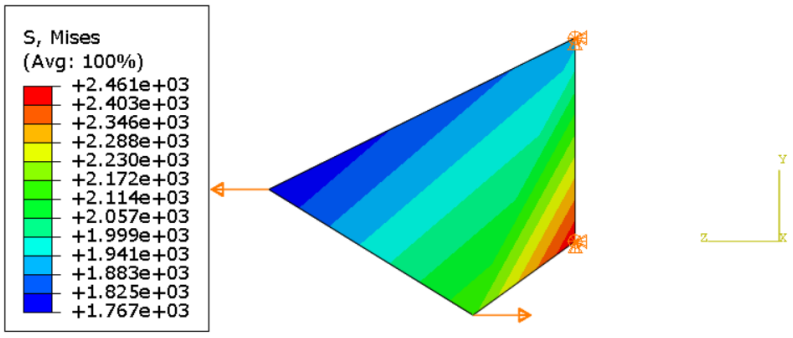

Figure 4.11: Deformation of the C3D8I element under a bending load (side view).

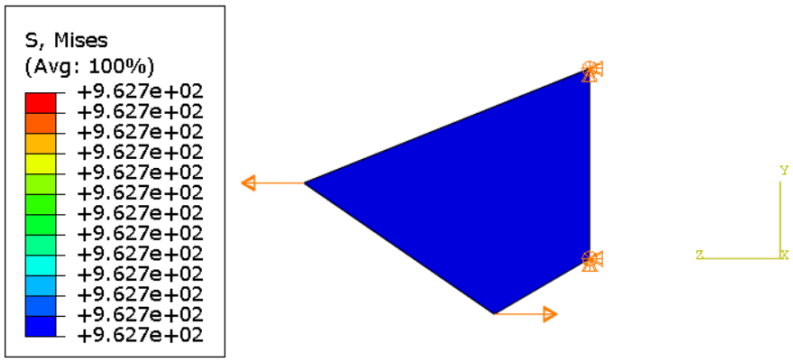

Figure 4.12: Deformation of the C3D8R element under a bending load (side view).

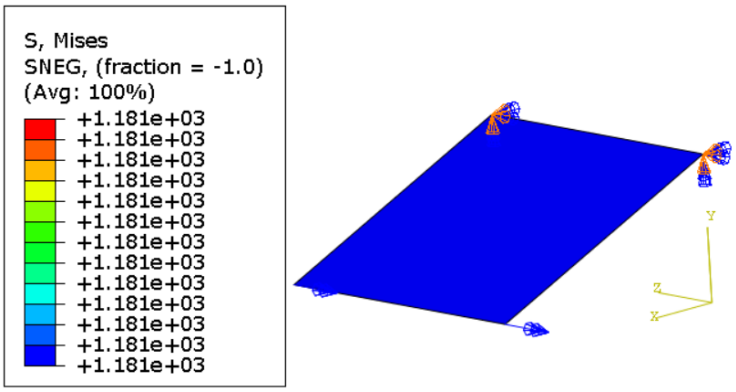

Figure 4.13: Deformation of the S4R element under a bending load (side view).

For this test, it is important to analyse the final geometry of the element, the stress-strain curve and the internal energy evolution over time in order to get a sense of the stiffness of the elements.

As stated in Abaqus' User Manual, the C3D8I element is used to accurately represent bending; internal degrees of freedom are added to suppress the shear locking hindrance. However, these elements are fairly sensitive to spurious deformations due to the additional internal degrees of freedom, requiring a finer mesh in areas prone to distortion. Figure 4.15 illustrates the aforementioned behaviour, since the element distorted irregularly as one of its faces caved in; nevertheless, this distortion is merely associated with an internal degree of freedom, since the nodes themselves are displaced co-linearly as illustrated by the same figure.

The contour plots in figures 4.14, 4.15 and 4.16 represent the nodal displacements along the x-axis. This plot provides an insight to the element's deformation when subjected to a simulated bending load. The displacement of the nodes comprising the C3D8 element in the x-direction was predominant in the contracted nodes in the z-direction – as illustrated by figures 4.14 and 4.10 – whereas the opposite is verified for the other two solid nodes: the nodes that are pulled in the z-direction are more prone to displacements in the x-direction. Moreover, the value for nodal displacements along the x-axis of the C3D8I element are twice as high to those observed in the C3D8 element, which hints towards a stiffer behaviour of the latter. Finally, the fact that there is only one integration point in the C3D8R element makes any conclusion regarding the correlation between stiffness and nodal displacement purely speculative, as bending can only be correctly simulated with several layers of reduced integration elements.

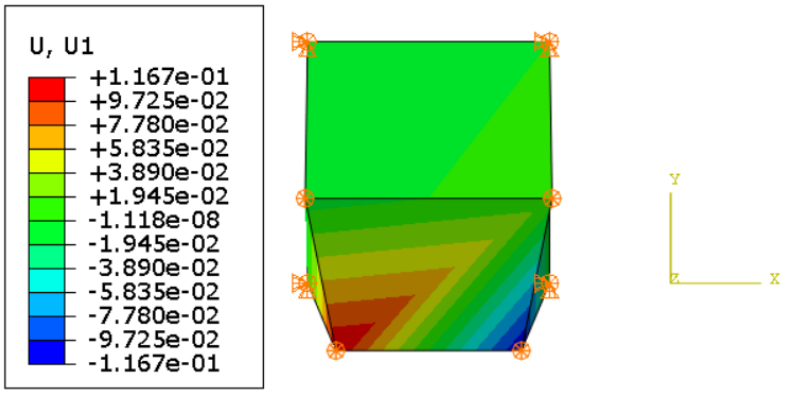

Figure 4.14: The C3D8 element exhibits a small transversal deformation, as it can be observed from the nodal displacements in the x-direction.

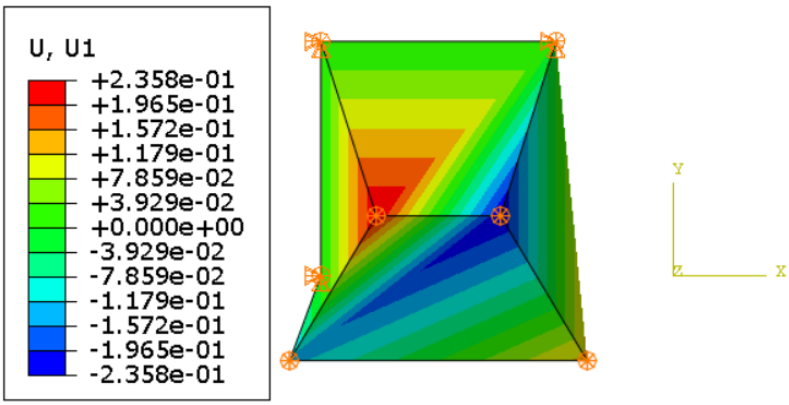

Figure 4.15: The C3D8I element distorted heavily, presenting a high transversal deformation and spurious deformations along the side faces of the cube. This is due to the additional degrees of freedom associated with the incompatible modes.

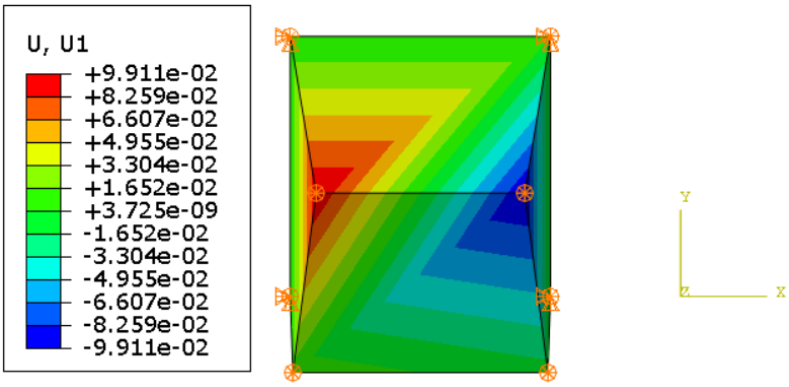

Figure 4.16: The C3D8R exhibits the smallest transversal deformation of the considered solid elements, as it can be observed from the nodal displacements in the x-direction.

The stress-strain curves for the bending simulations are represented in figure 4.17 while the internal energy curves are represented in figure 4.18. It is also relevant to mention that the boundary conditions in the S4R model are different due to the planar nature of the shell element, which

can influence the obtained results to some extent. As such, the main focus will be the analysis and comparison of the solid continuum elements.

From figure 4.17 it can be observed that the plastic behaviour of the C3D8R element has a lower value of strain than the rest of the elements. This is due to a spurious zero-energy mode – or hourglass mode – which consists in a deformation that is not associated with strain energy. That is naturally an artificial displacement, impossible outside a computational simulation context as deformation without strain does not exist; inherently to the single integration point of the C3D8R, these zero-energy modes are prone to be recurrent if one does not take care of properly refining the mesh or adding an hourglass control feature when resorting to these elements.

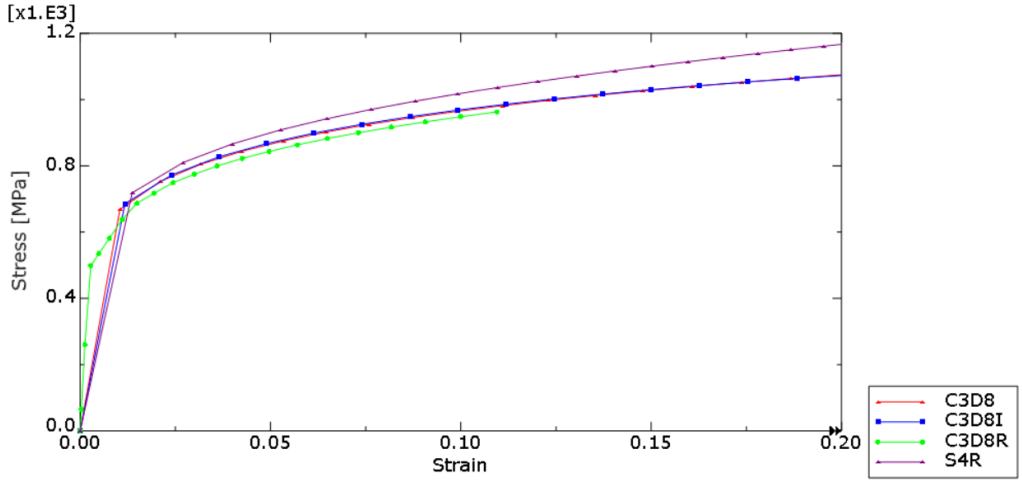

Figure 4.17: Stress-Strain curves for the four elements submitted to a bending test.

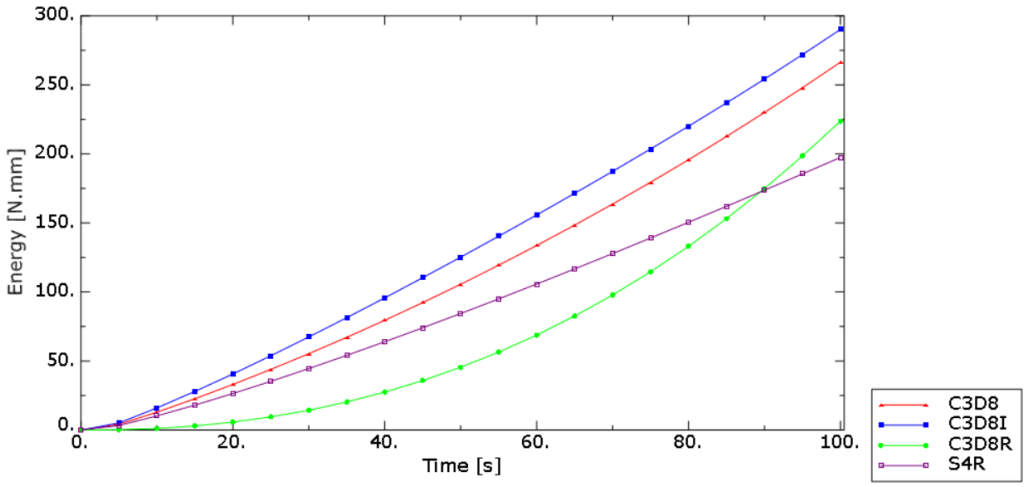

Figure 4.18: Internal energy curves for the four elements submitted to a bending test.

On the other hand, figure 4.18 provides an insight into the internal energy associated to each element throughout the simulation. According to this plot, the C3D8I element is the stiffest element, as more energy is needed to deform it. However, this behaviour can be justifiable by the

distortion of the element's face, which can lead to erroneous predictions of the strain values, leading to a higher energy estimation. The least stiff element is the C3D8R; nevertheless the evolution of its internal energy throughout the simulation progresses at a faster rate than the remainder.

Similarly to the previous test, in order to better understand the internal behaviour of a reduced integration element compared to a fully integrated one, the energy balance of the C3D8R and C3D8I elements were plotted in figures 4.19 and 4.20. The same variables – ALLIE, ALLSE, ALLAE and ALLPD – were plotted.

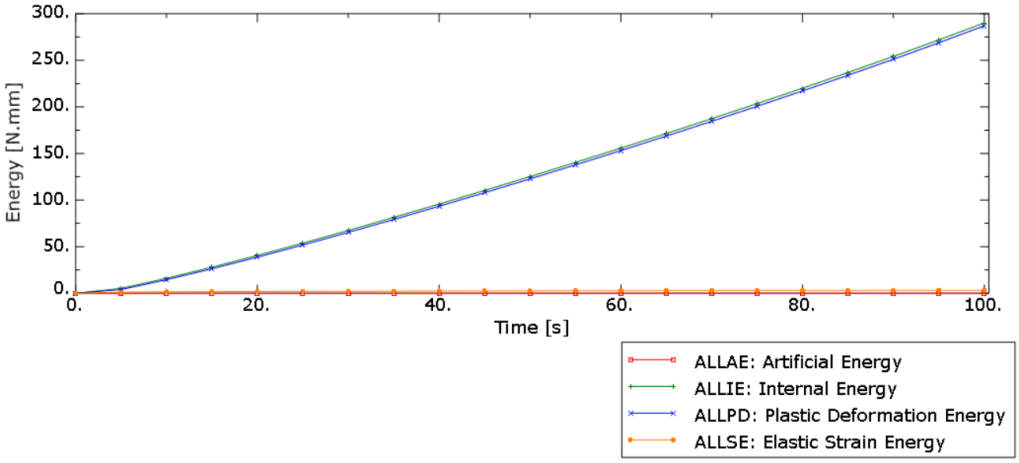

Figure 4.19: Plot of the internal energy balance of the C3D8I element.

By analysing figure 4.19 one can observe that the greater weight parcel in the internal energy of the C3D8I element is represented by the plastic dissipation energy, while the elastic strain energy is negligible and the artificial energy is non-existent. As seen in section 4.1.1, this is the expected behaviour for a fully integrated element in the plastic domain subjected to bending loads. However, in the face of any abnormality concerning the energy balance in this element, one can infer that the the C3D8I cannot be the basis of a very coarse mesh, lest excessive distortions such as the one observed in figure 4.19 occur, leading to overestimated values of stress.

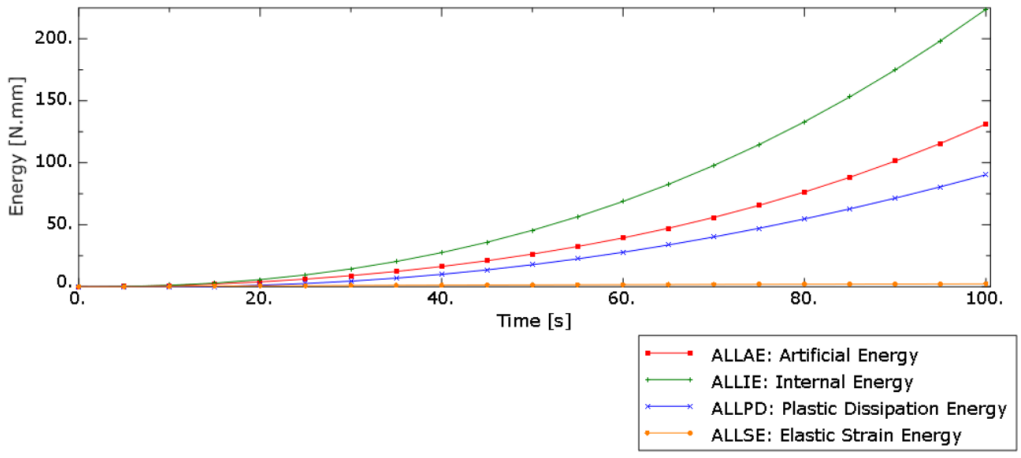

Figure 4.20: Plot of the internal energy balance of the C3D8R element.

Finally, it can be concluded by observing figure 4.20 that the C3D8R's artificial energy represents more than half of the internal energy at the end of the simulation. This value indicates that the internal energy values are misleading, as the artificial energy is caused by a fictitious increase in the element stiffness that should have a weight of no more than 5% of the ALLIE variable. Furthermore, the value for the plastic dissipation energy is around three times lower than the one reported in figure 4.19, corroborating the premise that the nodal displacements in the C3D8R element were mostly due to zero–energy modes. This inference confirms that this element can never be used in a single element layer sheet metal, or in a multilayered coarse mesh, as the element will most likely present hourglass modes when subjected to bending loads.

4.2 Beam Bending Analysis

Throughout subsection 4.1, single-element simulations are carried out to verify how they fared under tensile and bending loads and to compare them with each other. However there is a necessity to compare their behaviour with theoretical conjectures in order to ascertain about their viability for roll forming modelling.

Therefore, a simple bending model based in Timoshenko's beam theory is created, in order to analyse the bending behaviour of each element in the elastic domain. The reason why this test is carried out in a purely elastic domain resides on the fact that the analytical equations proposed by Timoshenko and Goodier [Timoshenko and Goodier, 1934] are only valid for those conditions. The amount of elements through the thickness is also an important variable to consider, as seen in subsection 4.1.2.

The adopted beam bending model is based on a study carried out by Augarde and Deeks [Augarde and Deeks, 2008] and follows the configuration given by figure 4.21.

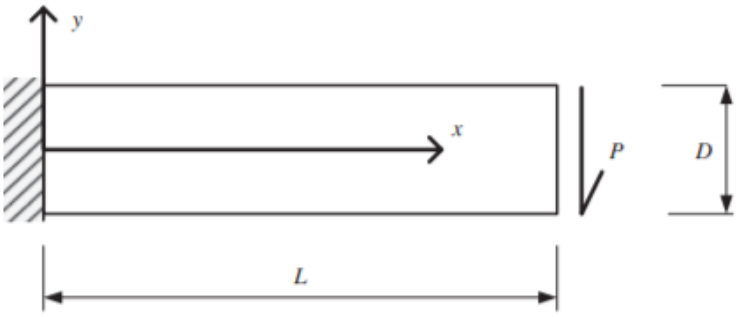

Figure 4.21: Proposed cantilever beam for the Timoshenko analysis [Augarde and Deeks, 2008].

The study is based on Timoshenko and Goodier's theory of elasticity which proposes the following equations for the stress field on the beam [Timoshenko and Goodier, 1934]:

$$\sigma_{xx} = \frac{P(l-x)y}{I}; \tag{4.4}$$

$$\sigma_{yy} = 0; \tag{4.5}$$

where I is the second moment of inertia and P is the force applied along the free edge of the beam. Timoshenko also proposes the following correlation between the beam's displacement field and the force:

$$u_{yy} = -\frac{P}{6EI}\left[(3\nu y^2(L-x) + (4+5\nu)\frac{D^2 x}{4} + (3L-x)x^2\right] \tag{4.6}$$

where E is the Young's modulus and ν is the Poisson's coefficient. The parameters given by table 4.3 are defined to build the bending model.

Table 4.3: Designated parameters to build the bending model.

D	1 [mm]
L	80 [mm]
W	20 [mm]
E	210000 [MPa]
ν	0.3
u_{yy}	5 [mm]
I_{zz}	1.6667 [mm^4]

The model is built by creating an encastre in one of the beam's ends onto an analytical rigid surface – in order to easily obtain the vertical reaction forces – and by applying a 5mm displacement in the free edge, as represented in figure 4.22.

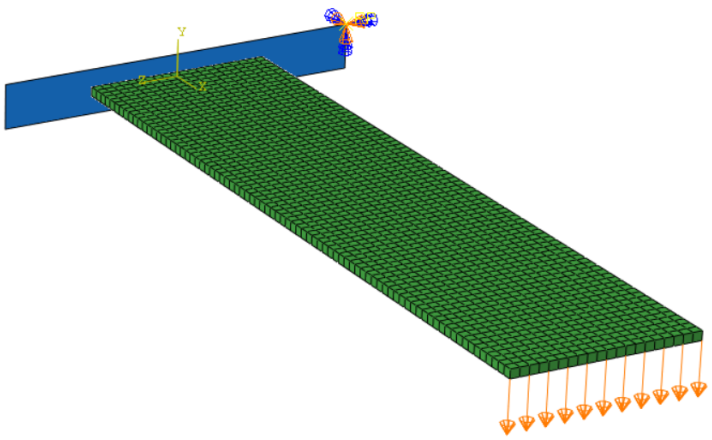

Figure 4.22: Assembly and boundary conditions for the modelled beam.

From that displacement, a theoretical prediction of the vertical reaction force can be obtained; the comparison between the analytical and simulated results enables the user to infer about the stiffness and bending behaviour of the tested elements.

From the equation 4.6 the expected exerted force can be obtained. From then on, the stress field can be analysed to a set of different coordinates on the beam and subsequently compared to the stresses obtained from each Abaqus simulation.

The chosen point to be analysed was the point with the coordinates x=40mm, y=0.5mm, z=0mm and the analytical results are reported in table 4.4.

Table 4.4: Theoretical values obtained from the Timoshenko's equations.

σ_{xx}	123.03 [MPa]
σ_{yy}	0.00 [MPa]
P	10.253 [N]

Some preliminary deductions can be inferred from the previous section before even simulating the model at hand; according to what is explained in section 3.6 one could predict that the behaviour of a C3D8 one-element thick sheet metal will be too stiff on account of the materialisation of parasitic shear stresses. On the other hand, a C3D8R one-element thick sheet metal will most likely exhibit a relaxed behaviour, underestimating the values of the reaction force and the stresses along the beam.

The table 4.5 shows the reported values after simulating the bend and analysing the nodal variables of the longitudinal and transversal stresses at coordinates (40mm, 0.5mm, 0mm), and the reaction force in the analytical rigid body at the end of the simulation. The charts in figures 4.23 and 4.24 allow for a more expedite visual analysis of the aforementioned results for the longitudinal stress and the vertical reaction force. The red line indicates the values reported in table 4.4 for each correspondent variable.

Table 4.5: Obtained results for the longitudinal and transversal stresses and vertical reaction forces, depending on the element and the number of layers across the thickness.

Element (number of layers)	$\sigma_{xx}\,[MPa]$	$\sigma_{yy}\,[MPa]$	Reaction Force [N]
C3D8 (1 Element)	56.62	-40.81	8.67
C3D8 (3 Elements)	116.33	-3.58	14.50
C3D8R (1 Element)	0.01	0.00	0.11
C3D8R (3 Elements)	100.45	0.51	9.99
C3D8I (1 Element)	124.06	0.65	10.54
C3D8I (3 Elements)	122.70	0.62	10.42
S4R (11 integration points)	124.55	0.00	10.54

According to the results reported in table 4.5, three of the simulated models originated stress and force values that differed to the theoretical ones by less than 5%. Two of the models were the ones simulated with the C3D8I element (one and three elements over the thickness of the sheet metal), while the other one was simulated with the S4R element. It is important to mention that the transversal stress value is, according to Timoshenko's model, null. As such, one can immediately dismiss the one-layer thick C3D8 model as a viable bending model given that the longitudinal and transversal stress values were crassly misjudged. The refinement of the mesh using the C3D8

element clearly improves the quality of the results obtained, as more elements across the thickness of the sheet metal result in more approximated values to the theoretical ones. Similarly, one could also immediately discard the one-layer thick C3D8R model as one element through the thickness barely yields any results. The refinement of the mesh, once again, improves the quality of the results as these approach those reported in table 4.4. The values in table 4.5 were transferred to the charts 4.23 and 4.24 in order to provide a more expedite visual analysis.

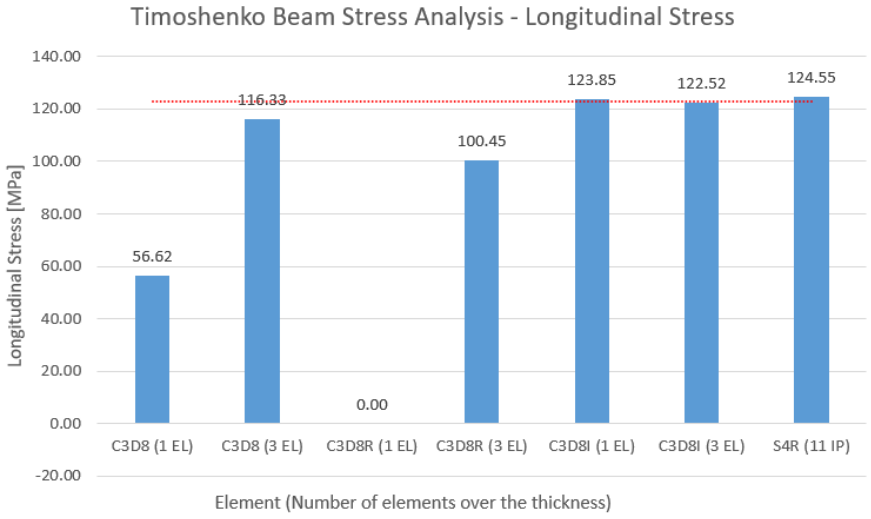

Figure 4.23: Longitudinal stress in node (40, 0.5, 0) [mm] at the end of the bending simulation and theoretical longitudinal stress represented in red.

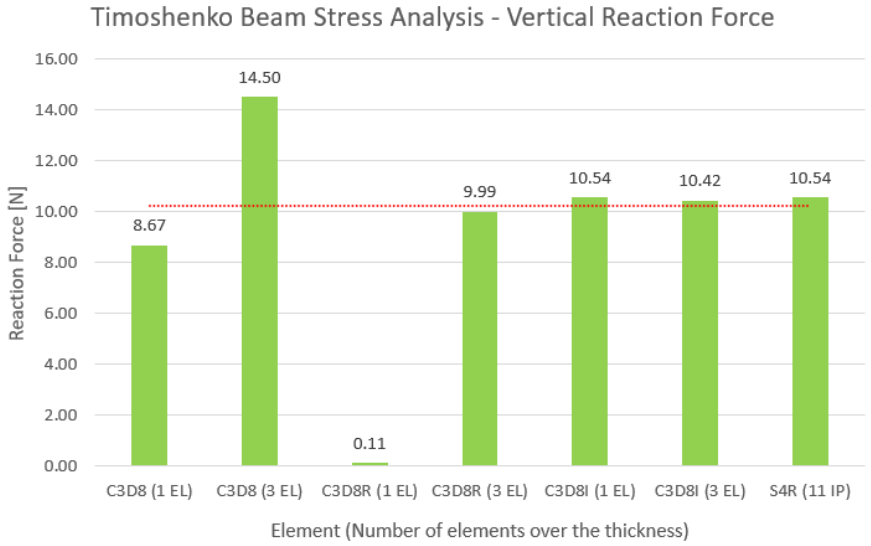

Figure 4.24: Vertical reaction forces in the analytical rigid body at the end of the bending simulation and theoretical vertical reaction force represented in red.

From chart 4.23, one can confirm that the incompatible modes and shell elements are the models that predict more accurately the value of longitudinal stress in bending behaviour. The model

meshed with one layer of C3D8R elements over the thickness clearly under predicted the value of longitudinal stresses, hence corroborating the conjecture mentioned at the beginning of this section. The model meshed with one layer of C3D8 also under predicted this value, reinforcing the idea that this element is not formulated to predict bending behaviour with a small amount of elements over the thickness; further refining the mesh would result in an unnecessarily computationally expensive simulation. Moreover, the three element thick reduced integration model also underestimated the value of the longitudinal stress, revealing a relaxed behaviour under elastic bending. On the other hand, the values obtained when modelling with S4R and C3D8I are very similar to the ones obtained analytically.

Finally, from chart 4.24, it is inferable that the three element thick C3D8R model, along with the C3D8I and S4R models, predicted accurately the vertical reaction force at the encastre. On the other hand, the C3D8 and one layered C3D8R models did not yield favourable results. The C3D8 model with one element layer over the thickness underestimated the magnitude of the reaction force while the opposite happened as the mesh is refined.

Based on the analysis carried out to figures 4.23 and 4.24 as well as to the table 4.5, one can extract the following conclusions:

1. C3D8R element is not a viable solution when considering one layer of elements over the thickness in stress-strain related problems. An accurate representation of the results requires a fine mesh associated with several elements over the thickness.

2. The overestimation of the vertical reaction force in the three layered C3D8 mesh suggests that the element is too stiff and that even in small-strain bending in the elastic domain the parasitic shear stresses lead to erroneous results.

3. The C3D8I element yields very accurate results when compared to the analytical results depicted in table 4.4, even when considering the one element thick mesh.

4. The S4R also yields accurate results, even though an analysis through the sheet metal's thickness is impossible.

4.3 Comparison and Conclusions

The previous sections were meant to test the elements under basic loading conditions such as tensile forces and bending, to analyse their behaviour. This chapter represents an important part of the dissertation because it allows the comprehension of element behaviour in a more simple context than roll forming. Since simulating roll forming involves complex features such as contact and highly non-linear material deformation, this preliminary study is important to set the foundations to the element choice and mesh refinement. Therefore, the conclusions drawn in this chapter allow for a prediction of the applicability of the studied elements in roll forming modelling and the advantages and shortcomings associated with each one.

These pros and con are represented in table 4.6.

Table 4.6: Conclusions regarding the advantages and disadvantages of using each element in a roll forming process simulation.

Element	Advantages	Disadvantages
C3D8	Serves as a control experiment, meant to compare the final results of a roll forming simulation obtained with a fully integrated element with and without incompatible modes.	Cannot represent plasticity, especially bending, in an accurate and reliable way.
C3D8I	Represents elastic bending in conformity with the analytical Timoshenko equations.	The proneness to mesh distortion (as seen in figure 4.11) indicates a need to refine the mesh in order to produce reliable results.
C3D8R	Regarded by the scientific community as the go-to element to represent sheet metal forming processes. The fact that it only contains one integration point, solves the shear locking problem (section 3.6.2).	Prone to hourglassing (section 3.6.2) and artificial stiffness.
S4R	In Abaqus, this sort of element is inexpensive and suitable for general applications in sheet metal forming problems. The preliminary tests using this element were satisfactory, as the element represented the stresses in accordance to the theoretical model in section 4.2.	The usage of this element renders an analysis through the thickness of the sheet metal impossible. Furthermore, the element is known to misrepresent sharp bending radii, needing a very fine mesh refinement to accurately represent them.

Chapter 5

Roll Forming Model Description and Evaluation Parameters

In order to assess the viability of Abaqus (focusing in its Explicit solver) as an effective FEA package for roll forming simulations, one must establish evaluation parameters applied in order to compare the obtained results with the ones carried out in COPRA® FEA RF.

Naturally, the profile's final geometry will be an essential factor which can be analysed based on a cross section geometry outline, angles of the profile's bends and sheet thickness. Furthermore, the longitudinal strain will allow for a quantitative comparison of the simulations carried out in Abaqus with the ones carried out in COPRA® FEA RF. Finally, the computational time expended to complete a full simulation, all the while producing reliable results, must also be an object of study. Each one of these topics will be scrutinised throughout the following sections.

It is also important to define an analysis plane along the length of the profile in order to generate a cross-section in which these parameters can be evaluated. Naturally, this plane has to be defined in an analogue way to both FEA packages, to ensure that the results are comparable. The front end of the sheet metal – where contact is first established – is not a viable solution as this section is discarded at the end of a real process. Moreover, the mesh can become distorted and generate erroneous estimations of plastic strain; as such, the plane that cuts the modelled sheet metal's length in half will be studied.

5.1 Model Description

First and foremost, the model has to be described in order to understand what is relevant to analyse after the simulation is done. Most of the simulations in Abaqus are carried out in Abaqus/Explicit, except for one, for solver comparison purposes.

The intended cross-section consists in a symmetrical C-channel, illustrated in figure 5.3. This cross-section represents the intended final geometrical configuration of the profile. The dimensions of the sheet metal are reported in table 5.1 and in figures 5.1, 5.2 and 5.3.

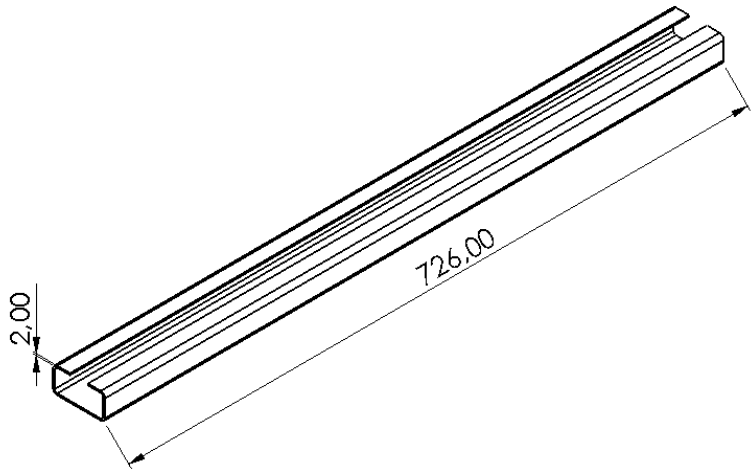

Figure 5.1: Isometric view of the theoretical geometry of formed sheet metal (dimensions in mm).

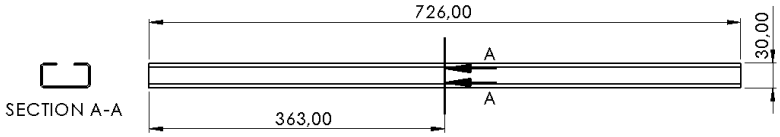

Figure 5.2: Side view of the sheet metal strip and location of the analysed cross section, section A-A (dimensions in mm).

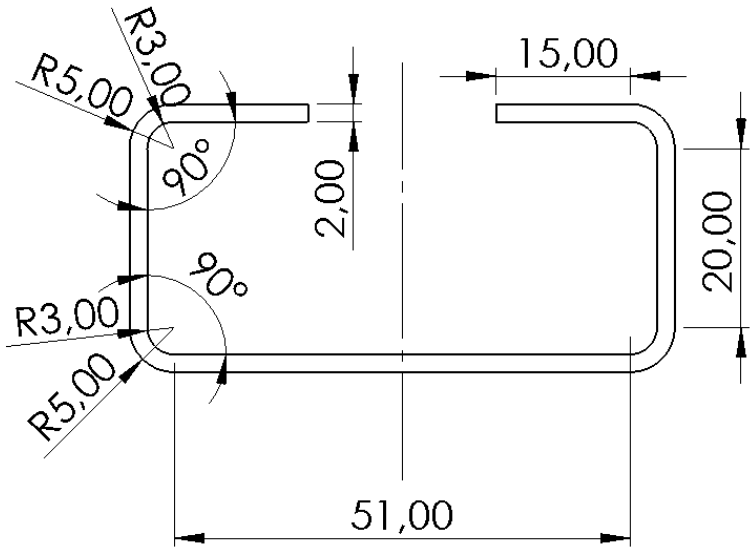

Figure 5.3: Detailed view of section A-A, illustrating the theoretical final cross-section of the C-channel profile including a symmetry axis and the dimensions in mm.

Table 5.1: Dimensions of the modelled sheet metal.

Dimension	Magnitude [mm]	Direction in the Model
Length	726 [mm]	Z-Axis
Width	72.56 [mm]	X-Axis
Thickness	2 [mm]	Y-Axis

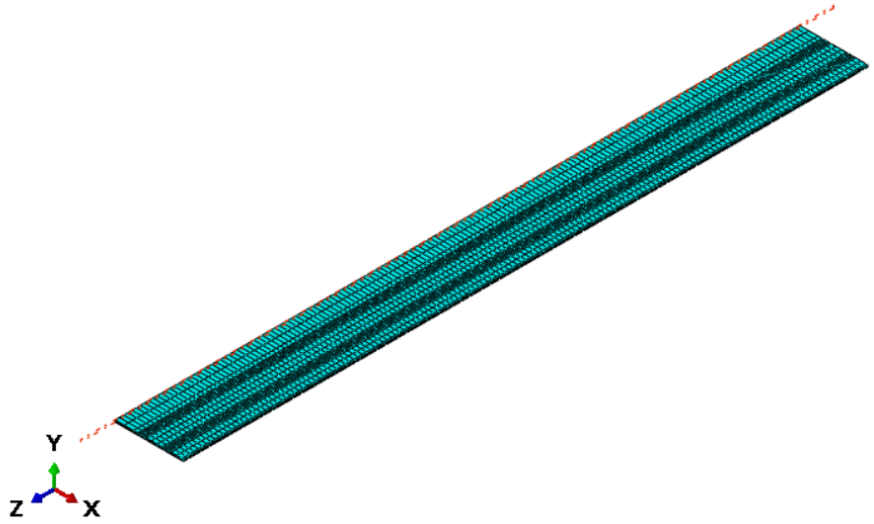

Figure 5.4: Isometric view of the modelled sheet metal strip, already meshed, with the symmetry plane depicted in red.

The sheet metal was modelled as a deformable solid body and the rolls as analytical rigid bodies. Since the profile is symmetrical, only half of the sheet metal was modelled. The chosen material for the sheet metal is the same as mentioned in chapter 4, the high strength steel DP800.

The roll forming project was made through COPRA®RF and subsequently imported into Abaqus. The model consists in fourteen stations: thirteen forming stations and one guiding station in which no forming occurs. The distance between stations is 220mm and the total displacement of the rolls amounts to 3380mm.

For each station, a step is created. For explicit simulations, as it is described in section 3.1, the time span of these steps depends on the speed necessary to accelerate the simulation in a way where the quasi-static condition of the problem is respected, while reducing the total simulation time. The chosen speed was based in the speed of sound in steel; according to Simulia's manuals regarding advanced topics in explicit simulations applied to quasi-static models, the speed of the forming tools should be limited to a maximum of 1% of the speed of sound in the sheet metal [Simulia, 2005a]. The speed of sound in steel is, in average, 5000m/s [Granta Design Limited, 2019] – and as such, the theoretical maximum allowable speed of the rolls would be 50m/s. Applying a 0.3 safety coefficient to this value, to ensure a minimal influence of kinetic forces during the simulation, yields a translation speed of 15m/s which is then implemented on the modelled rolls.

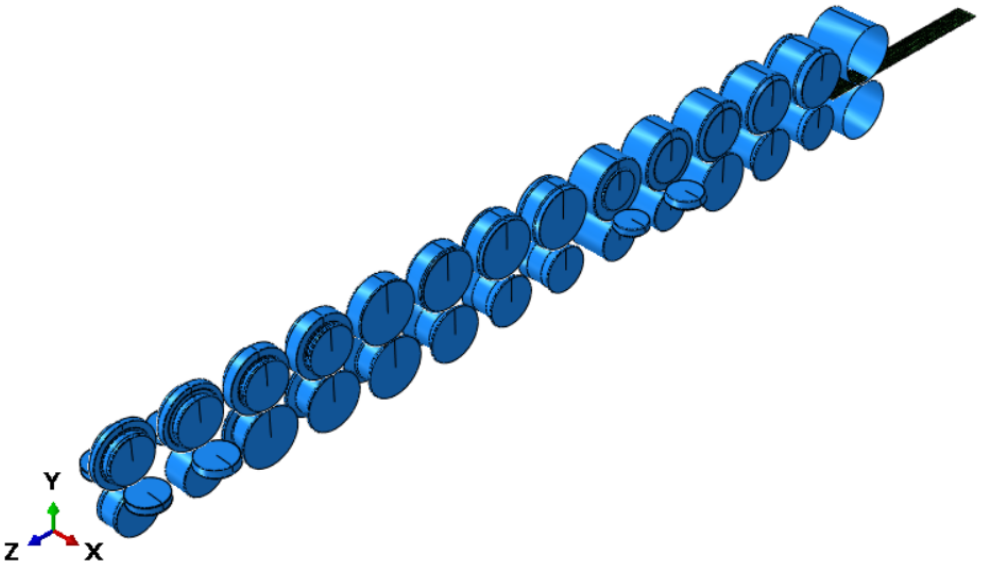

Figure 5.5: The assembled model for the C-channel roll forming simulation. The consecutive roll stations are distanced by 220mm and move simultaneously along the z-axis in order to form the fixed sheet metal into a profile.

The contact was modelled as a series of contact pairs consisting in the outer surface of the rolls – the master surfaces – and the outer surface of the sheet metal – the slave surface. As previously stated, friction will not be contemplated in this model, as it simplifies the simulation and reduces computational time; as such the interactions are modelled as frictionless and with a hard normal contact behaviour (as opposed to softened contact in which the tolerance to penetration is higher). The penalty algorithm was the chosen contact enforcement formulation, as described in section 3.4.

The boundary conditions were modelled in accordance to what was described in chapter 3:

- The front and back nodes of the sheet metal are locked in the forming direction to simulate a continuous feeding of the coil.
- The nodes of the sheet metal belonging to the symmetry axis are locked in the X-direction.
- Three back nodes of the sheet metal belonging to the symmetry axis are locked in the Y-direction to avoid rigid body motions.
- the rollers have all their degrees of freedom locked at their reference points, except for the displacement in the forming direction.

The roll displacement, as previously stated, is of 3380mm at a speed of 15000mm/s. Consequently, the total simulation time is set at 0,2253 seconds.

Figure 5.6 illustrate the aforementioned imposed boundary conditions for the sheet metal and for the roll stations.

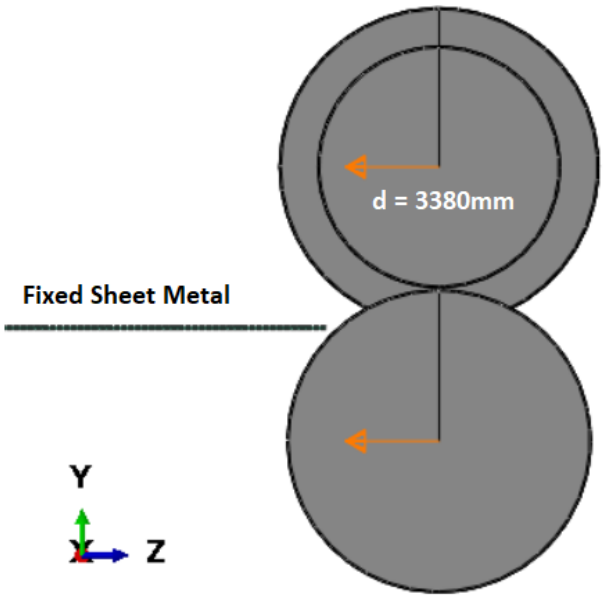

Figure 5.6: Fixed sheet metal and the displacement applied to the rolls and represented in orange.

The mesh was created with the COPRA® to FEA pre-processing tool, that allows for a fast mesh refinement in the areas that are going to be analysed, such as the bending areas and the strip edge (as seen in figure 3.18, section 3.7). Table 5.2 describes the different meshes and associated elements that, in light of the conclusions taken from chapter 4, will be used throughout the different simulations. A simulation with the C3D8 element, theoretically unfit to replicate sheet metal forming simulations, will be carried out to compare the obtained results with the remainder fully integrated elements.

Table 5.2: Different elements and mesh discretisation over the thickness used to carry out roll forming simulations.

Element Type	Elements/Thickness	Number of Nodes	Number of Elements
C3D8	One	7216	3423
C3D8I	One	7216	3423
C3D8I	Two	10824	6846
C3D8I	Four	18040	13692
C3D8R	Four	18040	13692
C3D8R	Six	25256	20538

After the simulations are finished, the results can be analysed and subsequently compared with the theoretical cross section. All the results will be extracted from a cross section located in midway along the length of the sheet metal (as illustrated in figure 5.2), for consistency purposes.

5.2 Angle Measurement and Sheet Thickness

The quality of the profile's geometry at the end of the simulation can be assessed through the comparison between the theoretical cross section (drawn using the pre-processing tool COPRA®RF) and the simulation results obtained in both Abaqus and COPRA® FEA RF. The geometry is one of the parameters that can be comparable without the use of an external post-processing tool; by extracting the geometrical outline of the mid-length cross-section and overlapping them in any commercial CAD software (AutoCAD for instance), one can compare the cross sections in terms of bending angles. This allows for a qualitative – detection of any twisting/warping effects on the web – and for a quantitative analysis – value of the bending angles.

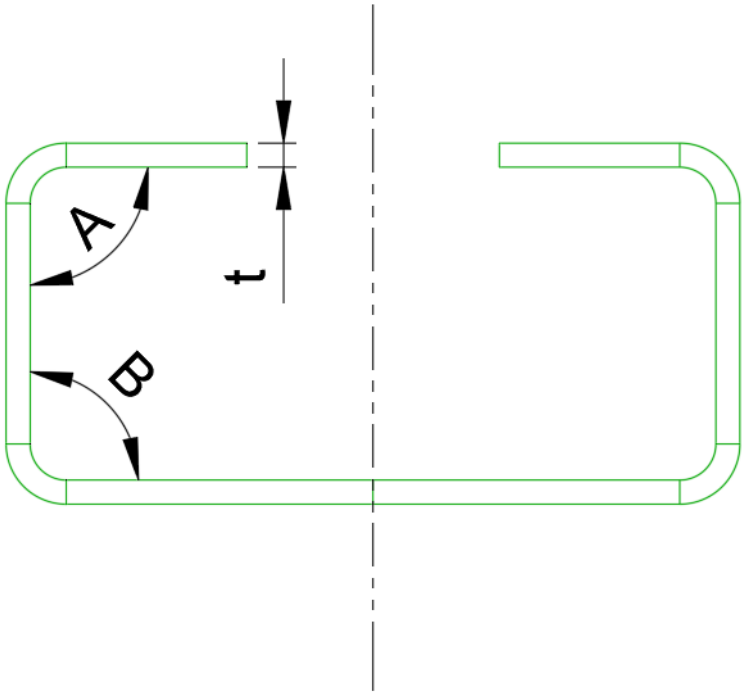

Figure 5.7: Evaluation parameters of the obtained cross-section's geometry; two bending angles (A and B) and the sheet thickness.

The angle values for bends A and B, seen in figure 5.7 will be reported in a table in two different moments: while the midsection of the sheet metal is being formed in the last station and at the end of the simulation (after springback). On the other hand, the sheet thickness will be evaluated through a cross sectional contour plot.

The sheet thickness is an interesting parameter to analyse because it indicates which areas of the sheet metal were subjected to thinning. Excessive thinning can lead to defects such as necking, tearing and wrinkling [Jung, 2017]. This analysis will also contribute to a better understanding of the element's pliancy under transversal bending and other roll forming associated deformations.

Using the previous method, the sheet thickness can also be obtained. However, using AutoCAD to extract the sheet metal thickness in the bending zones consists in an error prone process.

As such, the post-processing tool COPRA®PostDraw is used; not only does it allow to extract nodal values for Abaqus and COPRA® FEA RF under a consistent extrapolation scheme, it also calculates the sheet thickness in a given cross section.

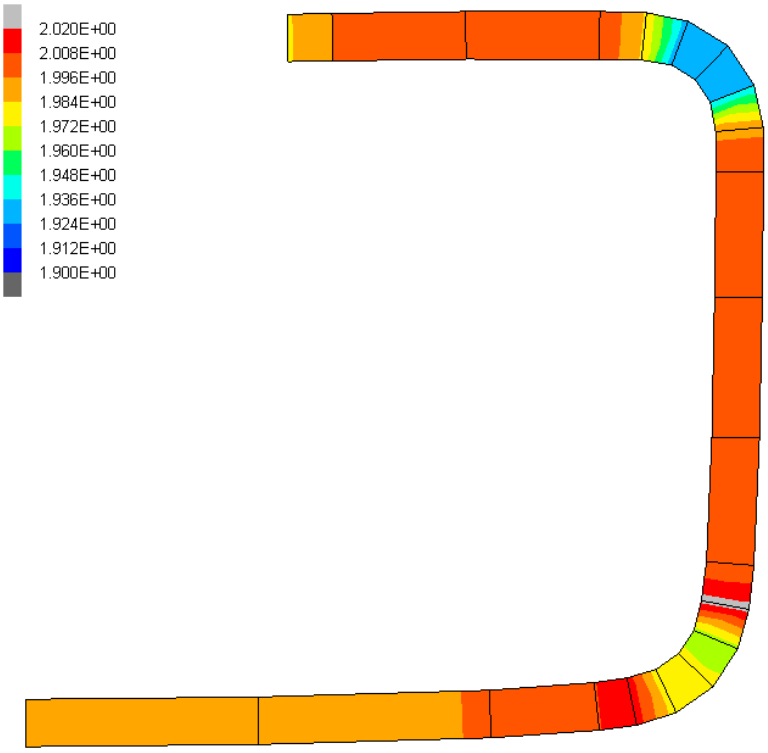

Figure 5.8: Example of a PostDraw sheet thickness result for a COPRA® FEA RF roll forming simulation.

5.3 Longitudinal Strain

Longitudinal strain is one of the most important analysis parameters in roll forming. The peak longitudinal strain is a good indicator to the possibility of the existence of defects [Panton et al., 1996] such as twists, longitudinal bowing and end flare – among others, as seen in section 2.1.5 – and it is one of the key aspects to analyse when performing an FEA analysis of a roll forming process. There are two main longitudinal strain analyses that are carried out for each simulation:

- An analysis to a section of the profile (150mm, midsection of the sheet metal) inside the last pair of rolls (at 3000 seconds), such as the one represented in figure 5.9.

- A single node's longitudinal strain history analysis throughout the simulation (as a chart depicting longitudinal strain as a function of time).

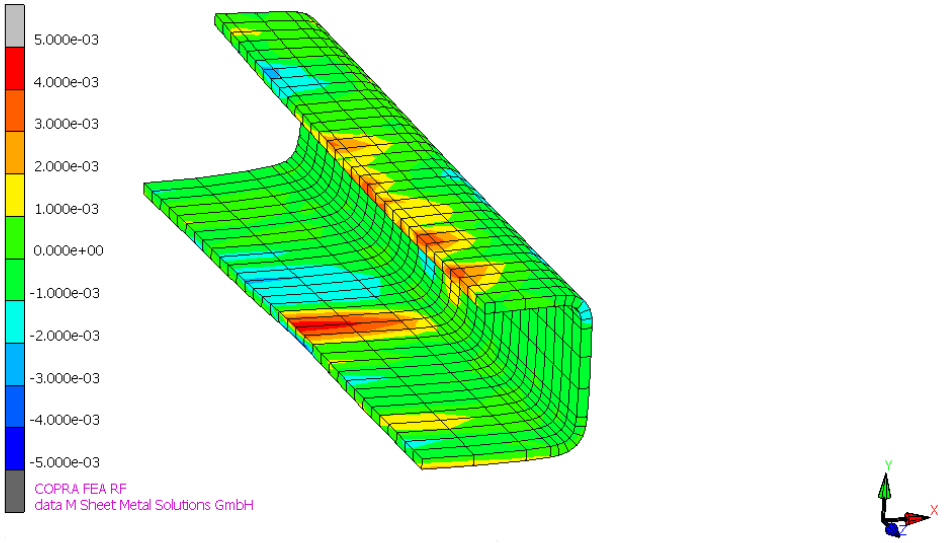

Figure 5.9: Example of a section of the sheet metal while passing through the last forming station. The variable in display is the longitudinal strain and the current view will be used throughout the entire analysis.

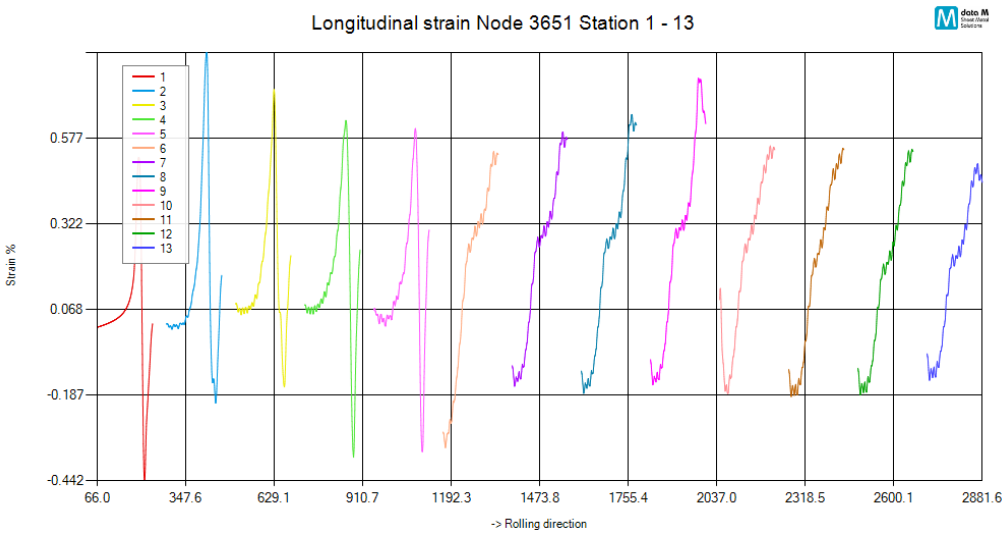

Figure 5.10: Example of a plot of the longitudinal strain in a single midsection node throughout a roll forming simulation carried out in COPRA® FEA RF. Each station represents a colour and the displacement is given in mm.

5.4 Computation Time

The computation time represents the efficiency of a simulation. In both industrial and academic contexts it is paramount to be as fast as possible while producing reliable results. As such, the CPU time spent simulating a roll forming process consists in an important comparison parameter of both FEA packages.

As seen in section 3.1, there are multiple modelling factors that condition both solvers when it

comes to simulation time; nevertheless, it is still interesting to analyse how Abaqus/Explicit fairs when put head-to-head with COPRA® FEA RF.

All the simulations were run under the same conditions and with the same Abaqus and COPRA® versions.

5.5 Extrapolation of the Integration Point Values and Comparison

Comparing the results obtained in Abaqus with the ones simulated in COPRA/MSC Marc, especially when it comes to contour plots, is not a straightforward task.

The tensor values are calculated at the integration points (Gauss points) inside the elements (as explained in section 3.6) and are then extrapolated to the nodes. The way that each FEA package does this extrapolation differs. As such, the visual representation of simulated results depends heavily on the method of extrapolation and averaging of results. Figure 5.11 illustrates this very phenomenon in which four different result interpretation schemes for the same simulation in Abaqus yielded very different results for the Von Mises stress, which can lead to analysis mistakes.

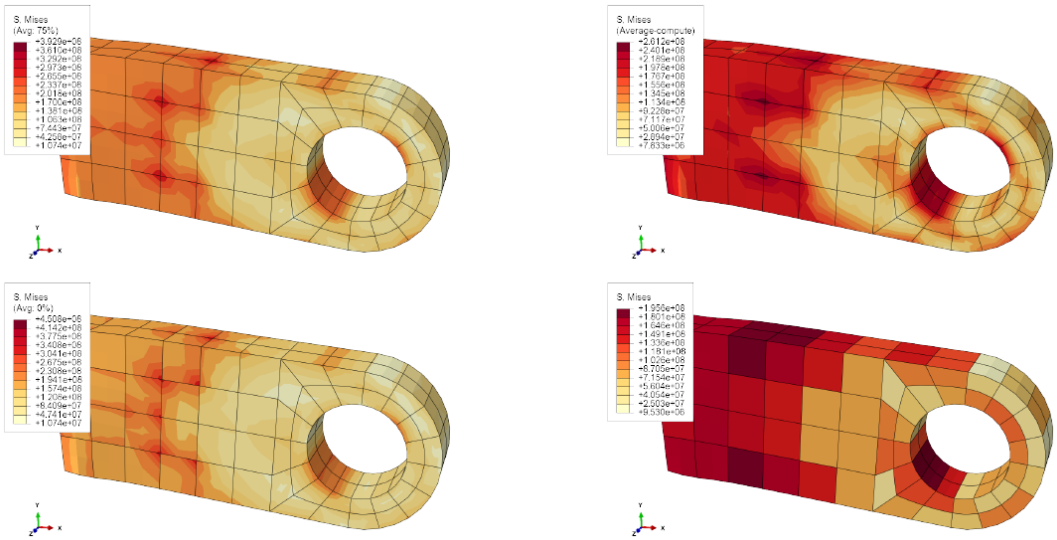

Figure 5.11: Von Mises stress in a simple lug, modelled as ideally plastic, encastred on the left and pulled downwards through the hole on the right. All four figures show the same simulation result. Due to the extrapolation and averaging method applied to the values from the integration points, the maximum and minimum nodal value vary from one visualisation method to another [Baeker, 2018].

In MSC Mentat, MSC Marc's post-processor, the user is given the choice of three extrapolation modes: linear, translation and average [MSC Software, 2019]. On the other hand, Abaqus enables the user with the choice of extrapolating the scalar values before or after averaging them; the extrapolation mode depends on several factors:

"For contour plots of element-based field output variables, Abaqus/CAE applies computations to the output database results to form the contour values. The computations vary according to the following criteria:

- the chosen quantity to plot (field output or discontinuities),
- the selected averaging options,
- the selected result regions,
- the requested type of contour plot (line, banded, or quilt)." [Simulia, 2019]

Since the comparison of extrapolated tensor values in the nodes is difficult to carry out in an accurate way, one has to resort to the source of these values: the integration points. As such, it is important to come up with solutions to effectively extract tensor values from the Gauss points.

The most efficient solution, and the solution adopted for the result analysis throughout the next chapter, is recurring to an external post-processor. There are several viable options, such as Matlab [G. Papazafeiropoulos, 2017]; however, the in-house post processing tool COPRA® PostDraw will be used. PostDraw not only consists in an effective post processing tool but it is also specialised in roll forming simulations.

Chapter 6

Results and Discussion

Throughout this chapter, the results of the simulations will be analysed and discussed in order to obtain conclusions about the efficiency of Abaqus when used to model roll forming processes. As stated in the previous chapter, one forming simulation was carried out using Abaqus/Standard, three in COPRA® FEA RF – using element 7 and element 117 –, while the remainder were carried out using Abaqus/Explicit – resorting to elements C3D8I, C3D8R and C3D8. All the springback simulations were carried out in Abaqus/Standard. The simulation carried out using Abaqus/Standard did not reach the end as convergence issues were encountered, even after several attempts in optimising the model. The multiple simulations using the C3D8I element are mostly meant to analyse the effect of mesh refinement and the likeness of the obtained results when compared to COPRA® FEA RF. The multiple simulations carried out using the C3D8R element are designed to assess the effect of the hourglass control parameters. There are three main hourglass mode controls: the total stiffness (TSHC), relaxed stiffness (RSHC) and enhanced (EHC) hourglass control. Finally, the usage of element C3D8 (unfit for representing bending in a correct way, as seen in section 4) serves as a basis for comparison with the remainder fully integrated elements. Shell elements were also considered for analysis; nevertheless, preliminary studies using this element suggested that the final forming of this particular profile was incompatible with the usage of element S4R.

As stated in the previous chapter, data M's experimental code to convert Abaqus result files into MSC Marc result files – in combination with the MSC Marc post processor and the in-house post-processor COPRA® PostDraw – allowed for the comparison of the results in a consistent way (i.e. with the same extrapolation method and visualisation settings). The values of the von Mises stress, longitudinal strain and total equivalent plastic strain are analysed, as well as the geometrical outcome of the cross-section (angles and sheet thickness) and the computational time.

This chapter is organised by dedicating a section to each relevant evaluation parameter and comparing the results obtained in Abaqus to the ones simulated using COPRA® FEA RF.

6.1 Strain Analysis

Two strain variables are to be compared throughout this section: the total equivalent plastic strain and the longitudinal strain, as described in chapter 5. The longitudinal strain is a variable of utmost importance in roll forming as it usually serves as a reference to predict the outcome of the process since a high value of longitudinal strain can indicate the presence of defects on the final product. On the other hand, the total equivalent plastic strain, given by an absolute scalar value, allows for a quick visualisation of the areas most affected by plastic strain in every direction (including shear strain behaviour).

6.1.1 Total Equivalent Plastic Strain

The total equivalent plastic strain, as stated in chapter 5, is an absolute scalar value that represents the magnitude of the strain to which the sheet metal was submitted. It is a good indicator of the material's plastic yielding; as such, this parameter is deemed useful to compare the magnitude of strain for each simulation.

The first figures in this chapter represent a cross section view of the results of a simulation carried out in COPRA® FEA RF (figure 6.1b) and of the results of another one carried out in Abaqus/Explicit, obtained using one layer of C3D8I elements (figure 6.1a).

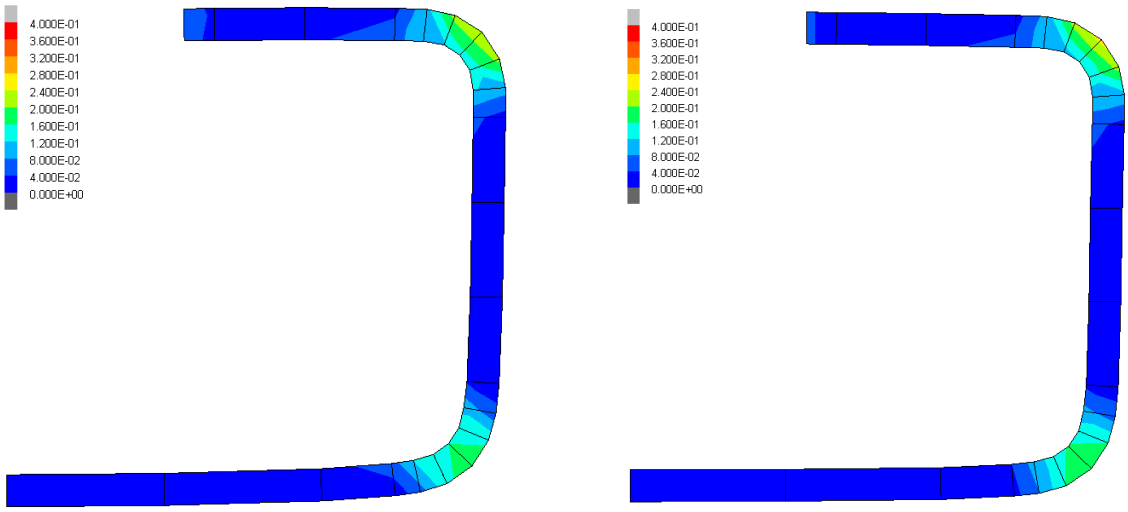

(a) Simulation carried out in Abaqus/Explicit.

(b) Simulation carried out in COPRA® FEA RF.

Figure 6.1: Cross section of a roll formed C-Channel profile (a) modelled in a mesh composed of C3D8I elements, with one layer of elements over its thickness and simulated in Abaqus/Explicit; (b) modelled in a mesh composed of type 7 elements, with one layer of elements over its thickness and simulated in COPRA® FEA RF. The contour plot illustrates the total equivalent plastic strain distribution at the end of the simulation.

The strain distribution, as well as the strain values, are similar throughout the cross section. Nevertheless, the transition from the bending zone to the flange/web is smoother in figure 6.1b, even if only slightly. The total strain values also cover a larger width of the strip edge in figure 6.1a than in figure 6.1b. The drawbacks of only using one layer of elements through the thickness of the sheet metal are apparent: the neutral axis does not exist, as it cannot be represented with two Gauss points over the thickness.

A simulation was also carried out using the C3D8 element (fully integrated linear element, prone to volume and shear locking) to corroborate the hypothesis that it is too stiff for an accurate bending representation. Figure 6.2 illustrates that premise, as the element isn't as pliant and does not present the same values for total equivalent plastic strain.

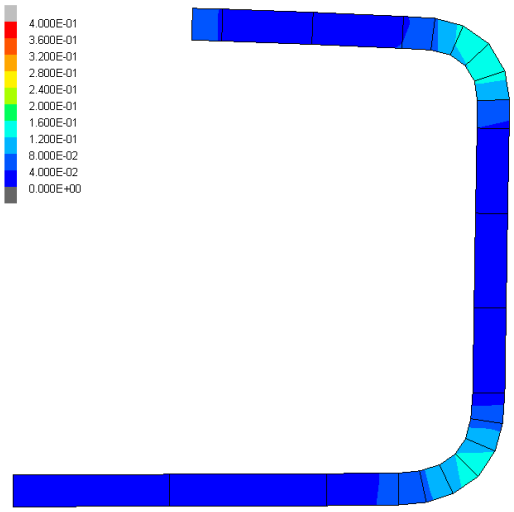

Figure 6.2: Cross section of a roll formed C-Channel profile modelled in a mesh composed of C3D8 elements, with one layer of elements over its thickness and simulated in Abaqus/Explicit. The contour plot illustrates the total equivalent plastic strain distribution at the end of the simulation.

A mesh refinement through the thickness of the sheet metal allows for the representation of a neutral axis. The addition of another layer of elements through the thickness of the sheet metal does not only allow for a reduction of the element size but also doubles the number of integration points, enabling a more reliable representation of the results. Naturally, with the inclusion of additional Gauss points near the surface of the sheet metal, the extrapolation of results changes the plastic strain nodal values, increasing them, as illustrated by figure 6.3.

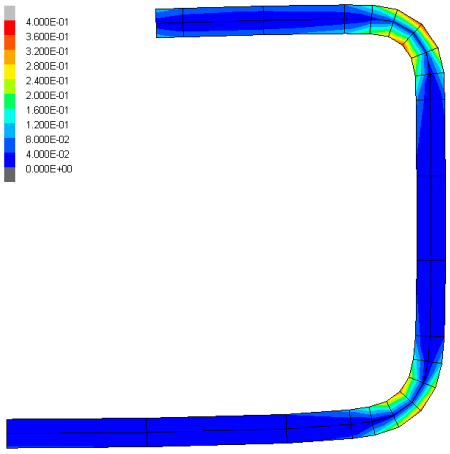

Figure 6.3: Cross section of a roll formed C-Channel profile modelled in a mesh composed of C3D8I elements, with two layers of elements over its thickness and simulated in Abaqus/Explicit. The contour plot illustrates the total equivalent plastic strain distribution at the end of the simulation.

A further mesh refinement is done to verify the results obtained in figure 6.3; in both FEA packages simulations were carried out using additional layers of elements. In the case of the simulation carried out with Abaqus/Explicit, four layers of elements with incompatible modes (C3D8I) were used, as illustrated by figure 6.4a. For a more accurate comparison with COPRA® FEA RF, a simulation with four layers of fully integrated EAS (enhanced assumed strain) elements was carried out as well.

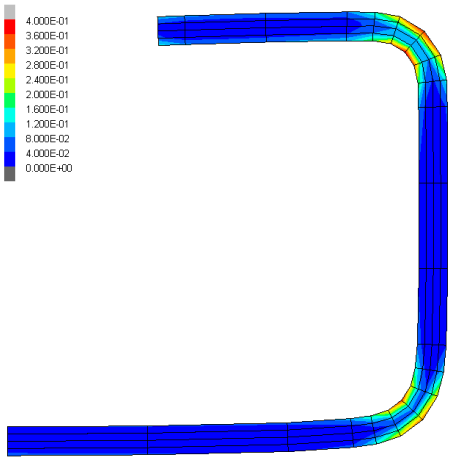

(a) Simulation carried out in Abaqus/Explicit.

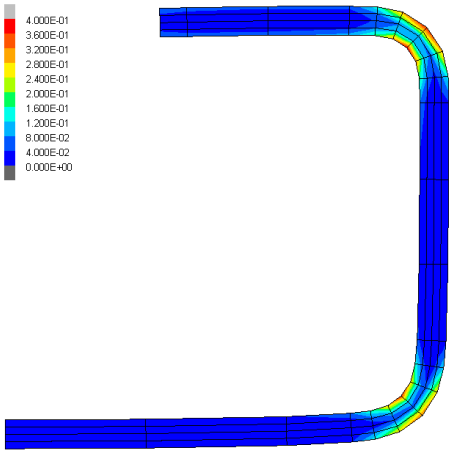

(b) Simulation carried out in COPRA® FEA RF.

Figure 6.4: Cross section of a roll formed C-Channel profile (a) modelled in a mesh composed of C3D8I elements, with four layers of elements over its thickness and simulated in Abaqus/Explicit; (b) modelled in a mesh composed of type 7 elements, with four layers of elements over its thickness and simulated in COPRA® FEA RF. The contour plot illustrates the total equivalent plastic strain distribution at the end of the simulation.

From observing figures 6.4a and 6.4b, one can conclude that the strain distribution in both contour plots is very similar. Furthermore, it follows the distribution verified for the results yielded by the model with two layers of C3D8I elements through the thickness of the sheet metal. It is also interesting to point out a slight displacement of the neutral axis towards the interior of the bending zone, behaviour that is theoretically expected (as explained in chapter 2) and that is verified in both contour plots.

Four other simulations were carried out, this time using elements with reduced integration (C3D8R). Three simulations were carried out with four layers of elements across the sheet metal using different hourglass mode controls. These hourglass mode controls will be the mechanism applied by the solver to surpass the numerical issues related to zero-energy deformations, as explained throughout section 3. Hourglass mode controls can prevent numerical issues in the simulation but can also hinder the final outcome of a simulation; the ones considered for analysis are:

- Total stiffness hourglass control (TSHC)
- Relaxed stiffness hourglass control (RSHC)
- Enhanced hourglass control (EHC)

To ease the visualisation of the plots and tables throughout this section, the superscribed abbreviations will be used throughout the the following chapter to indicate the type of hourglass mode control used in each simulation.

The final simulation resorting to reduced integration elements is meant to assess the effect on mesh refinement (four layers of elements to six) in a C3D8R sheet metal using the total stiffness hourglass control (TSHC).

Furthermore, one simulation was also carried out using the reduced integration element from MSC Marc's library, which is never used by data M to simulate roll forming processes. What can be observed from the outcome of these simulations is that this particular model of roll forming is poorly represented by two hourglass control modes, as the final geometrical shape of the profile is drastically different from what would be expected. The relaxed stiffness hourglass control mode represents the geometry quite well, despite yielding an underestimated strain value distribution when compared to figure 6.4b.

To understand if the misrepresentation of the strain values is innate to the elements with reduced integration, a simulation using MSC Marc's element 117 (also with reduced integration) [MSC Software, 2019] was carried out.

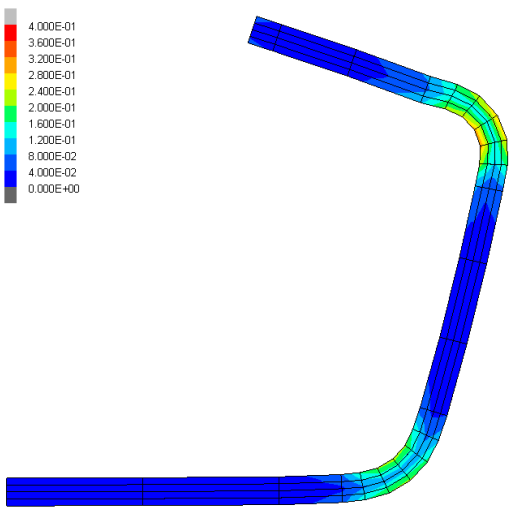

(a) Stiffness based hourglass mode control.

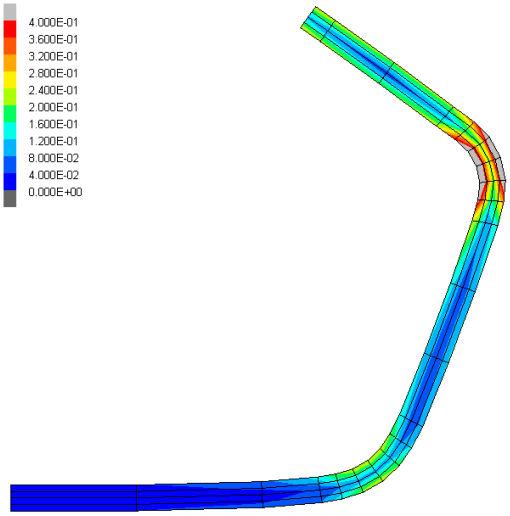

(b) Enhanced hourglass mode control.

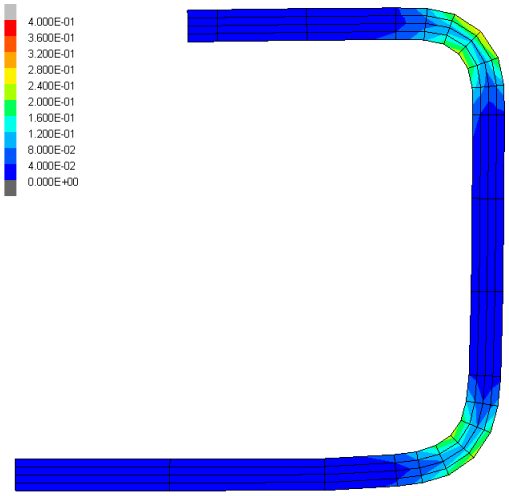

(c) Relax Stiffness hourglass mode control.

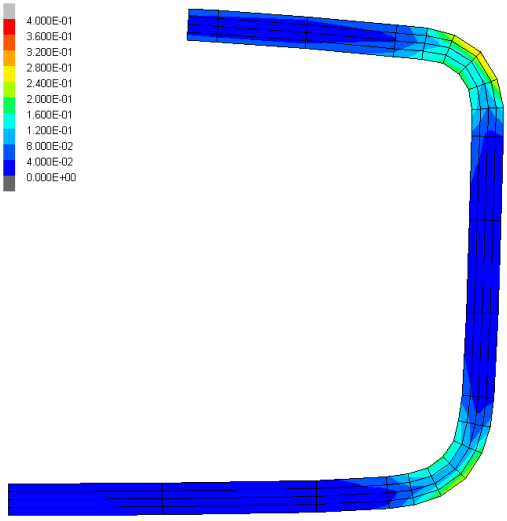

(d) MSC Marc's element 117.

Figure 6.5: Cross section of a roll formed C-Channel profile modelled in a mesh composed of C3D8R elements, with four layers of elements over its thickness and simulated in Abaqus/Explicit with (a) stiffness based hourglass control, (b) enhanced hourglass control, (c) relax stiffness hourglass control. A simulation was carried out in COPRA® FEA RF using element 117, represented in (d). The contour plot illustrates the total equivalent plastic strain distribution at the end of the simulation.

The simulation carried out using element 117, which yielded the results illustrated by figure 6.5d, are also not in accordance to what is shown in figure 6.4b.

By comparing figures 6.5a and 6.5b with 6.5d with figure 6.4b, one can infer that the reduced integration elements in Abaqus show an overly stiff behaviour to accurately represent roll forming processes under the conditions delineated in chapter 5. The enhanced strain hourglass mode proved to be inadequate for this sort of application and should be discarded for simulations with plastic deformation, even though it exhibits higher values of equivalent plastic strain. The stiffness

based hourglass mode also yields an unacceptable result, as the geometric outcome of the profile is not depicted in accordance to the results obtained with COPRA ® FEA RF. The relax stiffness hourglass control, depicted by figure 6.5c, represents the expected final geometry correctly but underestimates the maximum strain values.

To observe if the mesh refinement has a positive effect on the prediction of the maximum plastic strain values after the forming of a C-Channel profile using C3D8R elements with Abaqus/Explicit, another simulation was carried out resorting to a six-layered mesh of reduced integration elements, using the total stiffness based hourglass control.

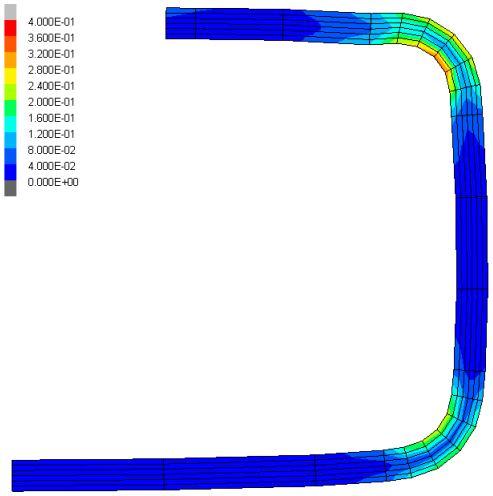

Figure 6.6: Cross section of a roll formed C-Channel profile modelled in a mesh composed of C3D8R elements, with six layers of elements over its thickness and simulated in Abaqus/Explicit with stiffness based hourglass control. The contour plot illustrates the total equivalent plastic strain distribution at the end of the simulation.

By observing figure 6.6, one can conclude that the mesh refinement improved the forming geometry as well as the strain distribution throughout the cross section. However, some geometrical anomalies are still noticeable, such as hourglassing near the upper bending zone, as well as a more faded representation of the neutral axis in the same area. Finally, one can notice a underestimation of the maximum plastic strain values.

6.1.2 Longitudinal Strain

The longitudinal strain in the forming direction, especially at the strip edge, is also a fundamental subject of study, given that it consists in one of the most important variables in roll forming. As seen in chapter 2, the longitudinal strain has a major influence in the probability of obtaining defects in the final product. As such, an isometric view of a small section of the sheet metal will be analysed, as well as the elements that form the strip edge at the aforementioned section. Its orientation will be remain constant, as explained in figure 5.10, while the axis system will be omitted for legibility. Furthermore a plot is drawn, depicting the history of the longitudinal strain values of a node in the midsection of the sheet metal, throughout the simulation.

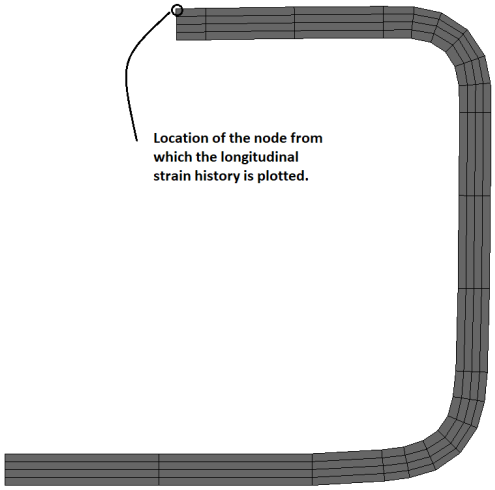

Figure 6.7: Cross sectional view of a roll formed C-Channel profile; the cross section is a projection of the profile on the transversal midplane (XY). The marked node in the figure, will be used to plot a history of the longitudinal strain throughout the simulation.

Similarly to the study carried out in section 6.1.1, the first analysis concerns the C3D8I element, with one element over the thickness, compared to COPRA ® FEA RF's element 7.

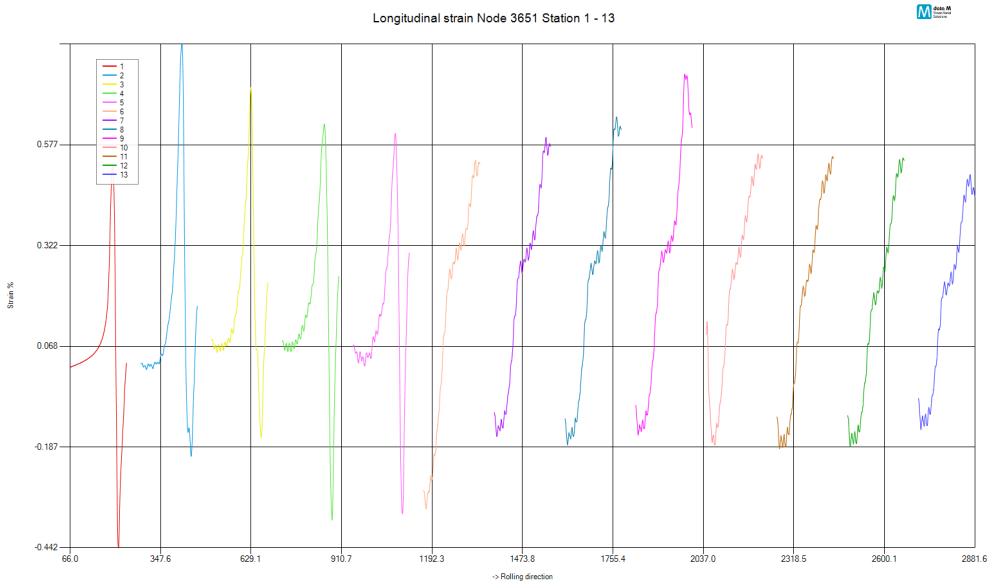

Figure 6.8: Nodal longitudinal strain of a simulation carried out in COPRA ® FEA RF using a mesh composed of one layer of type 7 elements; each colour in the plot represents a station. The rolling distance is in [mm].

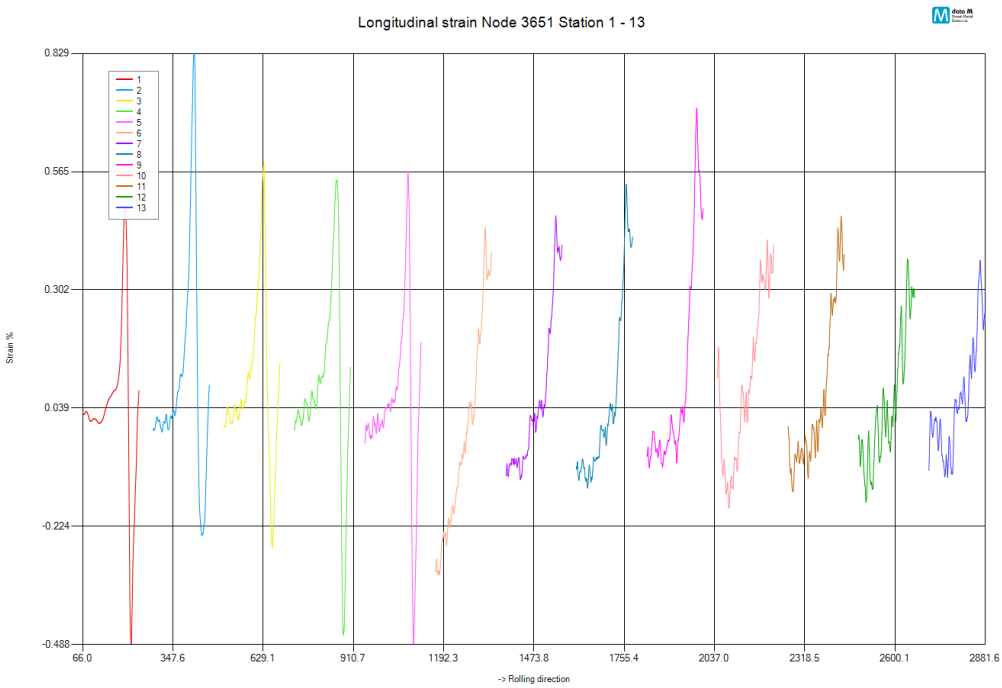

Figure 6.9: Nodal longitudinal strain of a simulation carried out in Abaqus/Explicit using a mesh composed of one layer of C3D8I elements; each colour in the plot represents a station. The rolling distance is in [mm].

Chart 6.9 allows for the observation of the longitudinal strain in one node throughout the simulation. The chosen node is located along the strip edge, as indicated by figure 6.7. As seen in chapter 2, every time that the sheet metal strip undergoes a pass through a roll station, there is a phase of material tension followed by a contraction of the steel. This becomes evident when analysing the plot, as every station plot indicates this behaviour. The results can be analysed as follows:

- The first five stations form the first bend of the flange, closer to the strip edge, leading to higher values of longitudinal strain in the studied node.
- The following stations are responsible for the forming of the second bend of the flange, further away from the strip edge, leading to lower values of longitudinal strain.
- As stated in chapter 2, the first station is usually demanding in terms of design, as the beginning of the forming takes place, leading to a higher longitudinal strain.
- Station four and five include auxiliary lateral rolls for the consolidation of the forming process. As such, there is a heavy material contraction throughout both passes.
- The final stations have little effect on the node's longitudinal strain, in both contraction and tension, as it can be observed in the chart.

As for the longitudinal strain verified in the last station, a comparison of the sheet metal behaviour in each simulation can be established using a section of the sheet metal undergoing a

forming process inside the last pair of rolls. Figures 6.10b and 6.10a illustrate the longitudinal strain in the last station for both Abaqus/Explicit and COPRA ® FEA RF simulations.

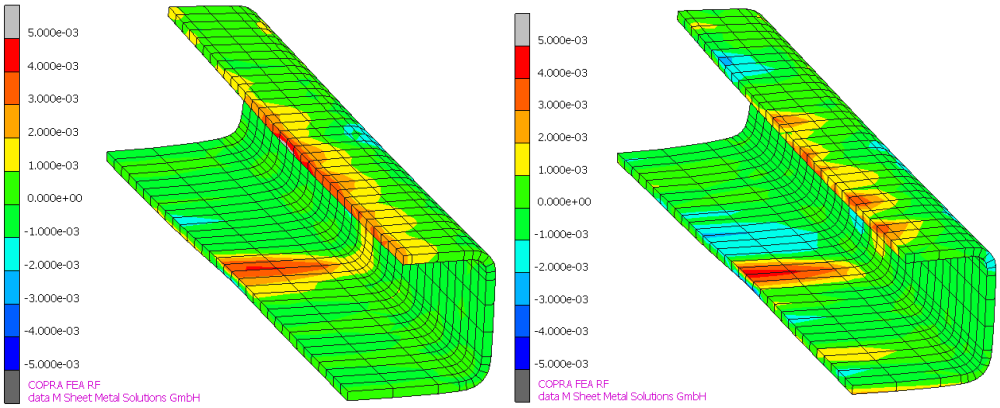

(a) Simulation carried out in COPRA® FEA RF. (b) Simulation carried out in Abaqus/Explicit.

Figure 6.10: Section of a roll formed C-Channel profile (a) modelled in a mesh composed of element type 7, with one layer of elements over its thickness and simulated in COPRA® FEA RF and (b) modelled in a mesh composed of C3D8I elements, with one layer of elements over its thickness and simulated in Abaqus/Explicit. The contour plot illustrates the longitudinal strain distribution at the last station of rolls.

The minimum and maximum values of longitudinal strain are quite similar when comparing both plots. Furthermore, the longitudinal strain evolution throughout the simulations follow the same tendency.

The main difference between the two simulations resides on the smoothness of the strain distribution:

- The longitudinal strain results obtained by the simulation carried out in COPRA® FEA RF (figure 6.10a) yielded an even contour plot distribution from the strip edge (where the material is stretched) to the bending area. The plot (figure 6.8) made from the midsection node presents some oscillation in strain in each section but follows a mostly linear tendency.

- On the other hand, the longitudinal strain results obtained by the simulation carried out in Abaqus/Explicit (figure 6.10b) yielded an irregular contour plot. This suggests that the kinematic effects inherent to an explicit simulation affected the evolution of the longitudinal strain. The plot in figure 6.9 corroborates this assumption as the evolution of the longitudinal strain reveals the presence of vibrations throughout the simulation.

Further mesh refinement is applied through the thickness of the sheet metal to verify if the oscillatory effect can be mitigated by the extra layers of elements.

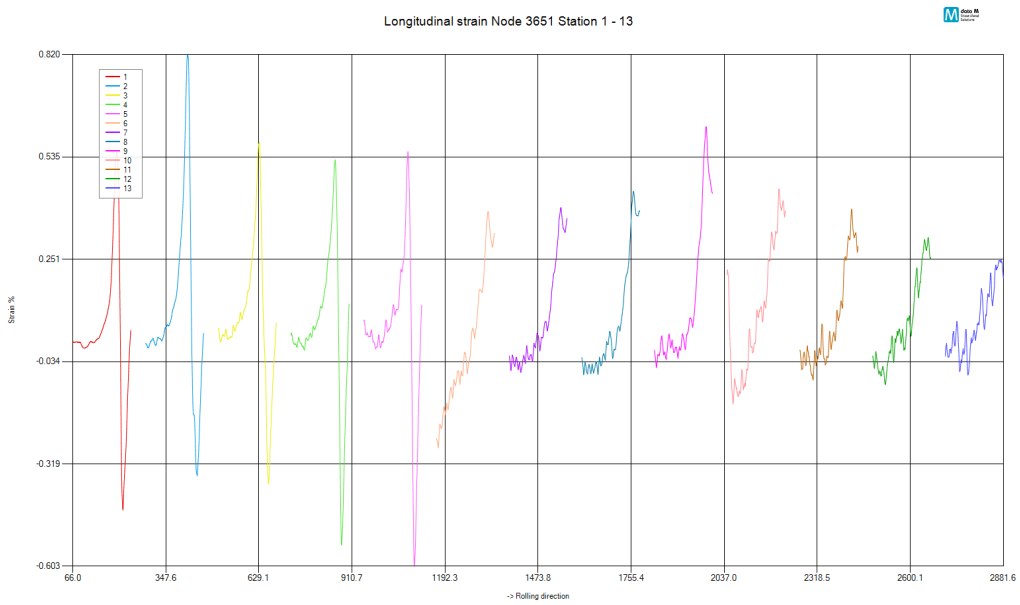

Figure 6.11: Nodal longitudinal strain of a simulation carried out in Abaqus/Explicit using a mesh composed of two layers of C3D8I elements; each colour in the plot represents a station. The rolling distance is in [mm].

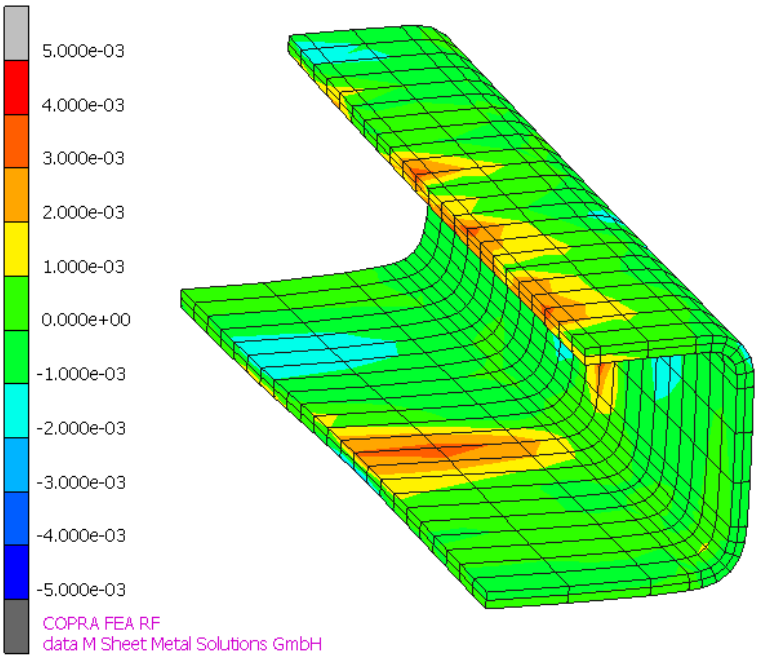

Figure 6.12: Section of a roll formed C-Channel profile modelled in a mesh composed of C3D8I elements, with two layers of elements over its thickness and simulated in Abaqus/Explicit. The contour plot illustrates the longitudinal strain distribution at the last station of rolls.

By analysing figure 6.11 one can conclude that the problem was partially mitigated for the first stations. However, the final stations still present a significant oscillatory behaviour. The contour plot in figure 6.12 representing the longitudinal strain in the final station is slightly smoother than

the one in figure 6.10b even though it is not as well distributed as the contour plot observed in figure 6.10a.

To understand the effect of the incompatible modes in the longitudinal strain values, the same exercise can be applied to the element C3D8 (with full integration, without EAS or additional displacement fields).

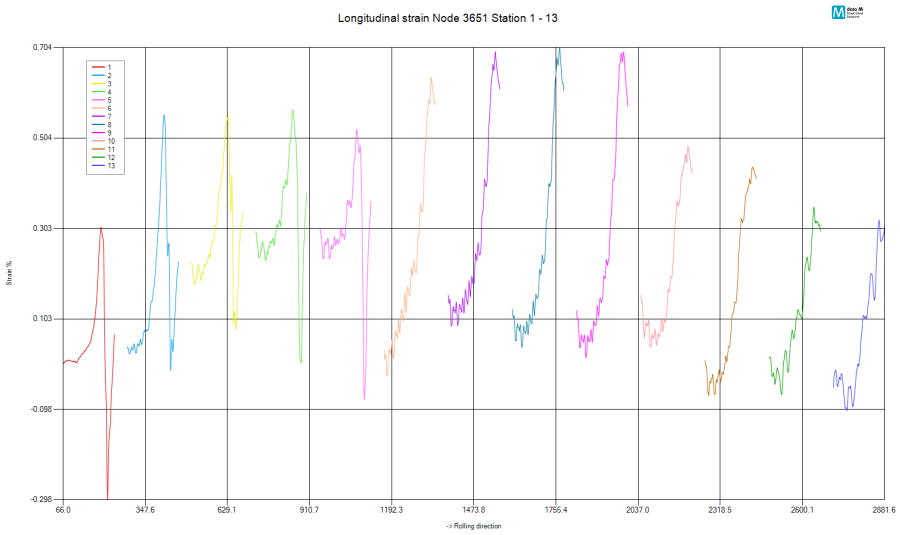

Figure 6.13: Nodal longitudinal strain of a simulation carried out in Abaqus/Explicit using a mesh composed of one layer of C3D8 elements; each colour in the plot represents a station. The rolling distance is in [mm].

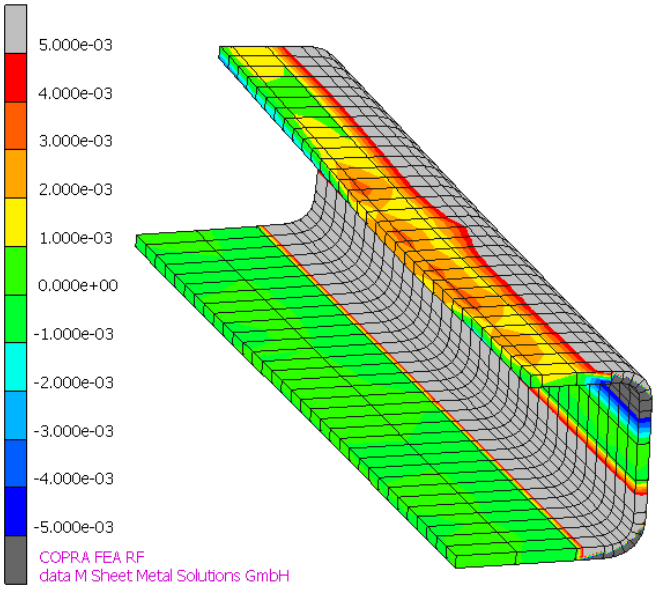

Figure 6.14: Section of a roll formed C-Channel profile modelled in a mesh composed of C3D8 elements, with one layer of elements over its thickness and simulated in Abaqus/Explicit. The contour plot illustrates the longitudinal strain distribution at the last station of rolls.

The C3D8 element is once again proven to be unfit for roll forming simulations; the maximum value of longitudinal strain occurs mostly in the bending areas, which should not happen. This phenomenon can be explained by the artificial stresses that are associated with shear locking in the bending areas, causing more material deformation around that region. Furthermore, the maximum and minimum values of longitudinal strain in the strip edge are inferior in magnitude to the ones obtained in the remainder simulations. Finally, it can be observed that there is a significantly inferior material compression in the first stations, when using this element.

Having analysed the longitudinal strain in sheet metal with less elements over the thickness, the simulations suing four layers of elements will now be analysed. Figures 6.15 and 6.16 illustrate the strain evolution and distribution after the simulation carried out in COPRA® FEA RF using MSC Marc's element type 7.

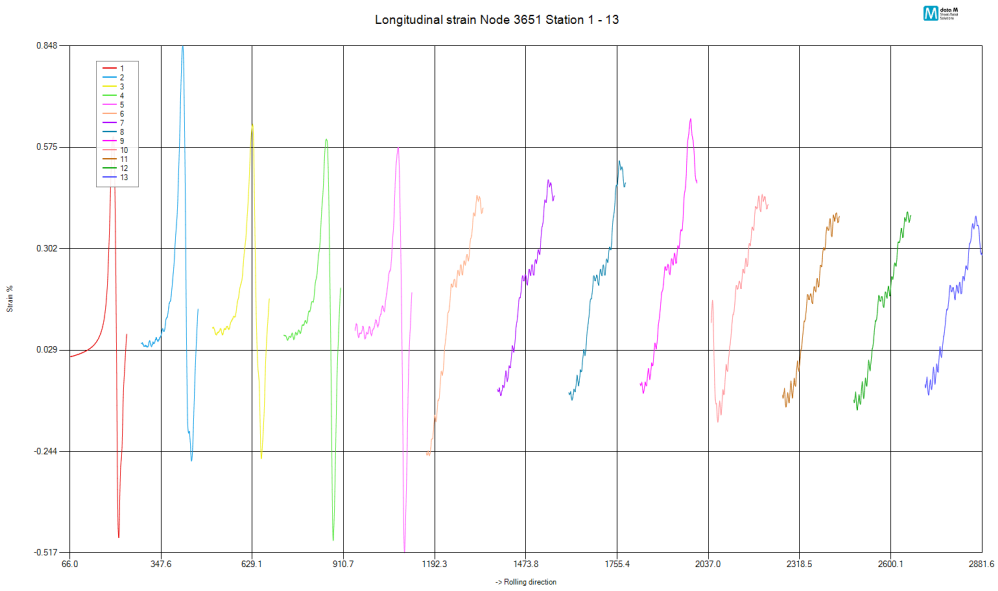

Figure 6.15: Nodal longitudinal strain of a simulation carried out in COPRA ® FEA RF using a mesh composed of four layers of type 7 elements; each colour in the plot represents a station. The rolling distance is in [mm].

The plot in figure 6.15 is consistent to the one in figure 6.8, that is, despite the refinement of the mesh through the thickness of the sheet metal, the strain evolution in the studied node follows the same behaviour. Moreover, the maximum and minimum values are approximately the same, which was to be expected, as the behaviour of the sheet metal should not change drastically.

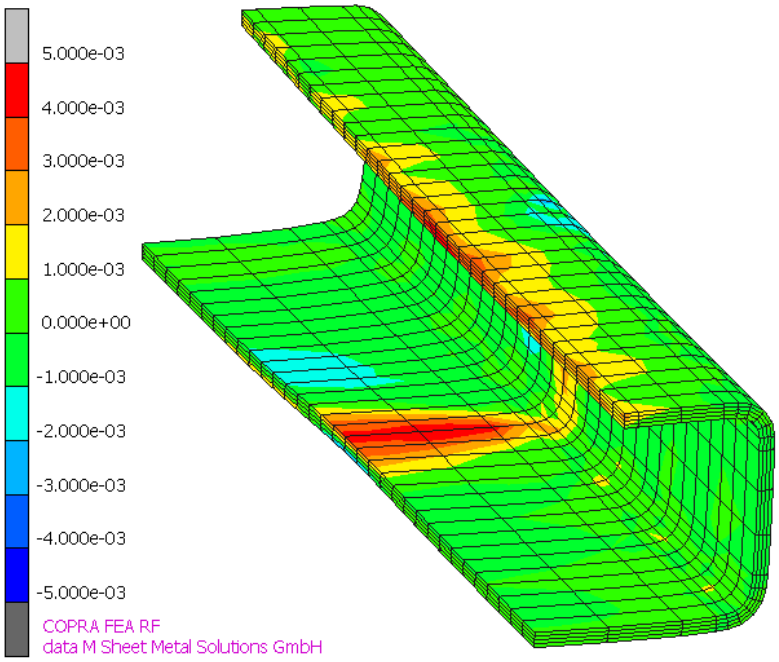

Figure 6.16: Section of a roll formed C-Channel profile modelled in a mesh composed of type 7 elements, with four layers of elements over its thickness and simulated in COPRA® FEA RF. The contour plot illustrates the longitudinal strain distribution at the last station of rolls.

The strain distribution along the strip edge of the sheet metal, illustrated by figure 6.16, is consistent to what is represented by figure 6.10a. The refinement of the mesh did not alter drastically the strain distribution. Since dataM Sheet Metal Solutions frequently uses one layer of element type 7 to accurately represent roll forming processes, this outcome is not unexpected.

By further refining the sheet metal with four layers of C3D8I elements, one can compare the outcome of the simulation with the results from the type 7 element models. Subsequently, an analysis to the reduced integration element C3D8R, with the different hourglass controls is also carried out.

Similarly to the outcome of the COPRA® FEA RF simulations, the mesh refinement along the thickness of the sheet metal did not alter the evolution of the longitudinal strain (depicted by figure 6.17), despite a small mitigation of the oscillatory behaviour in the first five stations. The maximum and minimum values represented in figure 6.17 are similar to the ones that can be observed in figure 6.16, revealing a very close resemblance to the results obtained with less refined meshes. The contour plot, illustrated in figure 6.18, is nevertheless very irregular and lacks the smooth distribution verified in both figures 6.10a and 6.16, due to the kinematic effects inherent to explicit simulations.

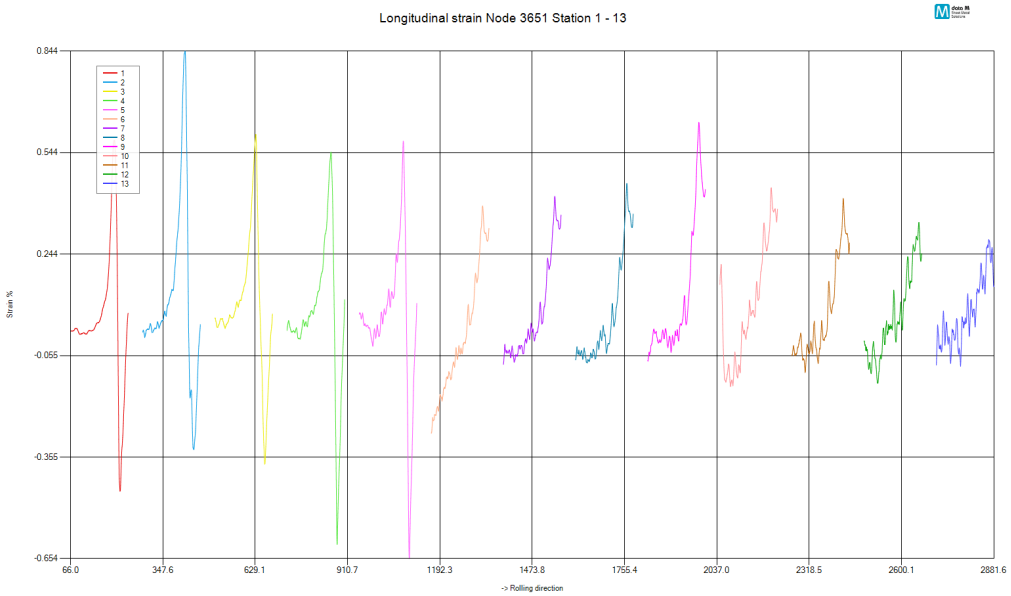

Figure 6.17: Nodal longitudinal strain of a simulation carried out in Abaqus/Explicit using a mesh composed of four layers of C3D8I elements; each colour in the plot represents a station. The rolling distance is in [mm].

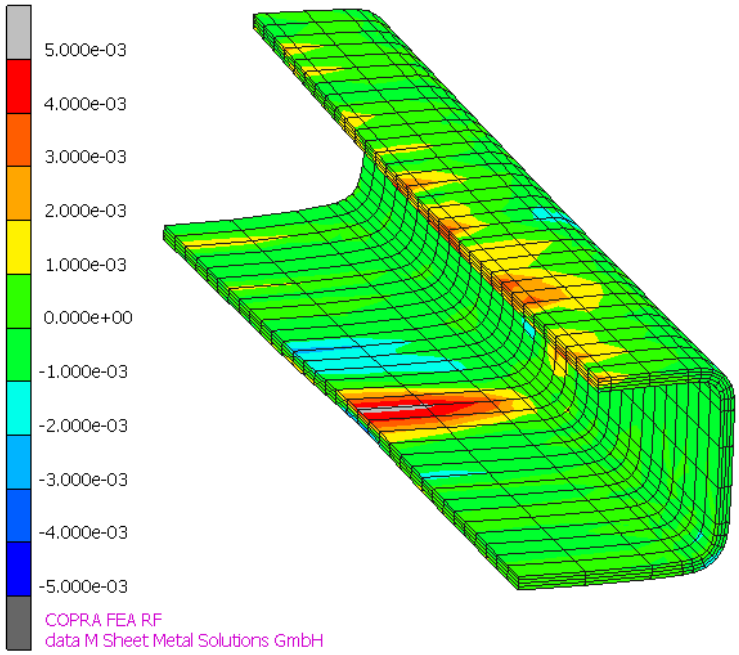

Figure 6.18: Section of a roll formed C-Channel profile modelled in a mesh composed of C3D8I elements, with four layers of elements over its thickness and simulated in Abaqus/Explicit. The contour plot illustrates the longitudinal strain distribution at the last station of rolls.

Finally, the reduced integration elements are analysed. It was already established that two of the hourglass mode controls are unfit to apply to the simulation of roll forming processes. However, the differences in longitudinal strain representation can still be analysed and compared.

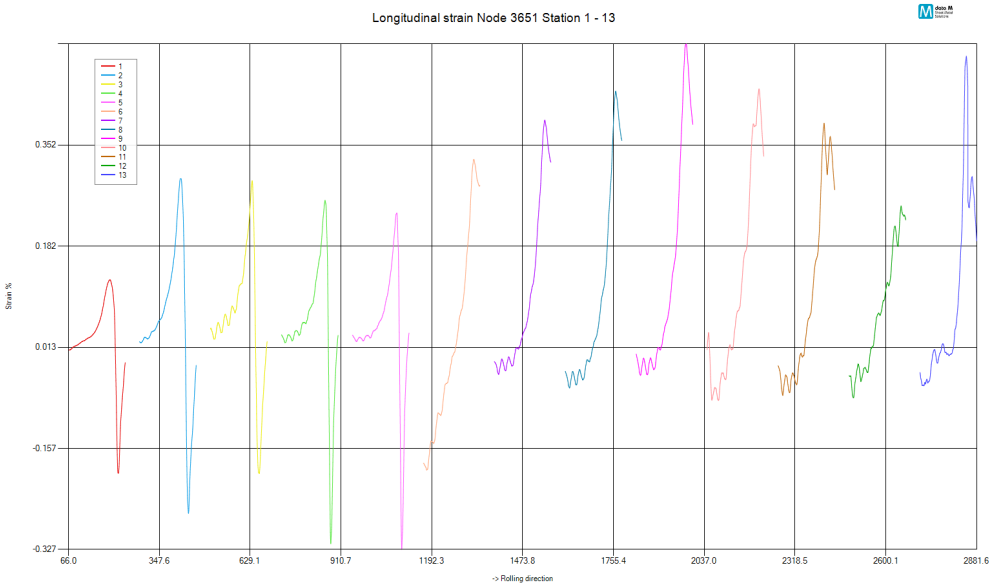

Figure 6.19: Nodal longitudinal strain of a simulation carried out in Abaqus/Explicit using a mesh composed of four layers of C3D8R elements with relaxed stiffness hourglass mode control; each colour in the plot represents a station. The rolling distance is in [mm].

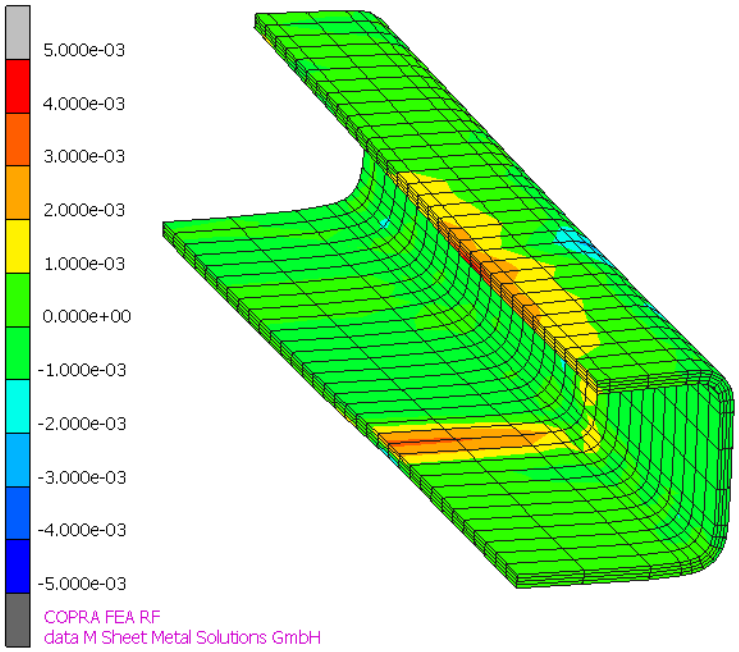

Figure 6.20: Section of a roll formed C-Channel profile modelled in a mesh composed of C3D8R elements using relaxed stiffness hourglass mode control, with four layers of elements over its thickness and simulated in Abaqus/Explicit. The contour plot illustrates the longitudinal strain distribution at the last station of rolls.

From figures 6.19 and 6.20, one can draw the following conclusions from the C3D8R element using relaxed stiffness hourglass control:

- The maximum values of longitudinal strain in chart 6.19, to the contrary of what is verified in the previous results, are registered in the last stations of the forming line.
- The maximum and minimum values of longitudinal strain in the chart are underestimated comparing to the previous analyses.
- The contour plot in figure 6.20 is much smoother than the ones verified in the C3D8I simulations.

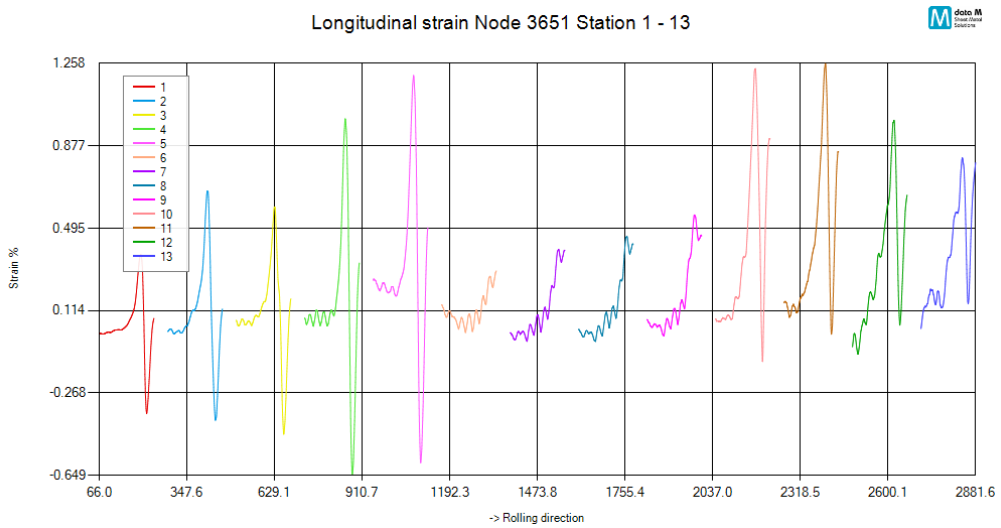

(a) C3D8R element with enhanced hourglass mode control.

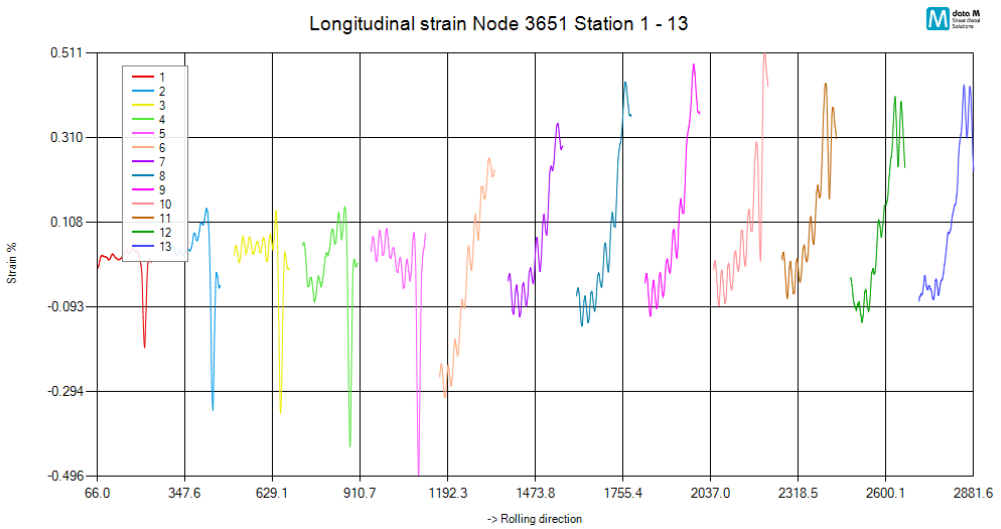

(b) C3D8R element with total stiffness hourglass control mode.

Figure 6.21: Nodal longitudinal strain of simulations carried out in Abaqus/Explicit using a mesh composed of four layers of C3D8R elements with (a) enhanced hourglass mode control and (b) total stiffness hourglass control mode; each colour in the plot represents a station. The rolling distance is in [mm].

The charts in figures 6.21a and 6.21b depict the longitudinal strain evolution of models using C3D8R elements with enhanced and total stiffness hourglass controls respectively. These hourglass control modes were already deemed unfit to represent roll forming in an accurate way; however, it is still interesting to point out the main differences between these results and the ones already discussed. The evolution of the longitudinal strain in plot 6.21a is the most similar in behaviour to the results obtained in COPRA® FEA RF, despite the gross overestimation of the maximum and minimum results. On the other hand, plot 6.21b depicts longitudinal strain evolution quite similar to the one in figure 6.19, while underestimating of the minimum and maximum values.

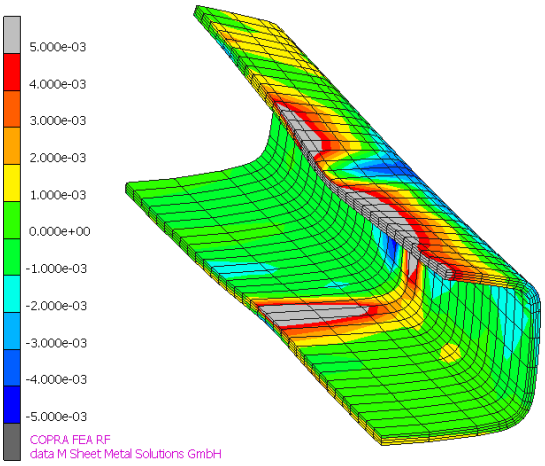

(a) C3D8R element with enhanced hourglass mode control.

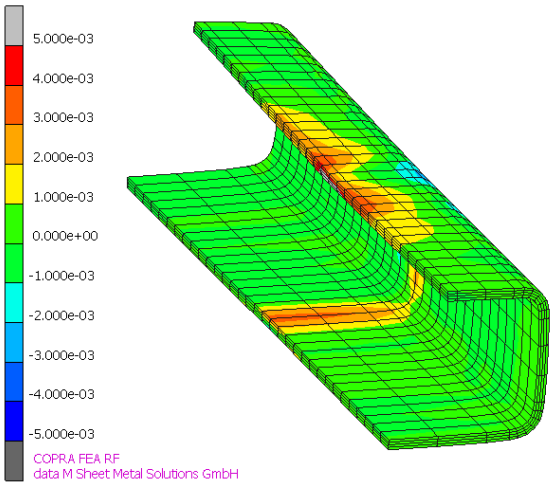

(b) C3D8R element with total stiffness hourglass control mode.

Figure 6.22: Section of a roll formed C-Channel profile modelled in a mesh composed of C3D8R elements using (a) enhanced hourglass mode control and (b) total stiffness hourglass mode control, with four layers of elements over its thickness and simulated in Abaqus/Explicit. The contour plot illustrates the longitudinal strain distribution at the last station of rolls.

While the enhanced hourglass control mode yields a very unsatisfactory result, the total stiffness approach yields a strain distribution similar to the one obtained in COPRA® FEA RF, as it is illustrated by figure 6.22b.

The summary of the maximum and minimum values of the longitudinal strain in a node in the strip edge of the sheet metal throughout each simulation can be consulted in table 6.1 and in figure 6.23 for an illustrative approach.

Table 6.1: Comparison of the maximum and minimum value of the longitudinal strain in the node of the sheet metal from which the strain history charts were plotted. The values were all taken using dataM Sheet Metal Solutions' in-house post-processing tool: FEA PostDraw.

Element	Layers/Thickness	Maximum Value (Station)	Minimum Value (Station)
C3D8	1	0.704% (Station 8)	-0.298% (Station 1)
C3D8I	1	0.829% (Station 2)	-0.488% (Station 1 and 5)
C3D8I	2	0.820% (Station 2)	-0.603% (Station 5)
C3D8I	4	0.857% (Station 2)	-0.634 (Station 5)
C3D8R (EHC)	4	1.258% (Station 11)	-0.649 (Station 4)
C3D8R (TSHC)	4	0.511% (Station 10)	-0.496 (Station 5)
C3D8R (RSHC)	4	0.522% (Station 9)	-0.327% (Station 5)
C3D8R (TSHC)	6	0.688% (Station 4)	-0.711 (Station 5)
Element 7	1	0.832% (Station 2)	-0.442% (Station 1)
Element 7	4	0.848% (Station 2)	-0.517% (Station 5)

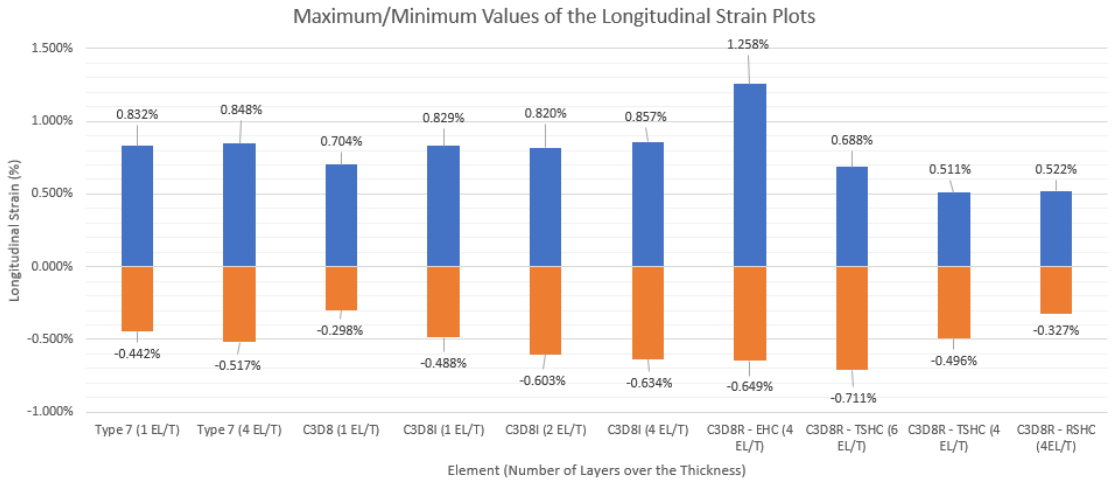

Figure 6.23: Chart with a plot of the minimum (represented in orange) and maximum (represented in blue) values of the longitudinal strain plots.

6.2 Stress Analysis

The von Mises stress (as explained in chapter 5), as a scalar value, gives out a good indication of the magnitude of the stresses to which the sheet metal is subjected and which areas of the sheet

metal are more affected after springback. In this chapter, similarly to the previous one, a small section of the sheet metal will be considered, in this case after springback, to analyse the von Mises stress at the very end of the roll forming process. The orientation of the sheet metal will also be the same as in the previous section. The maximum and minimum values of the residual stresses will then be reported for comparison.

Contrary to the previous section, the distribution of the von Mises stress in the contour plot varies significantly by refining the mesh through the thickness. This fact reinforces the idea that the analysis of stress in contour plots is highly dependent of the number of integration points across the thickness of the sheet metal.

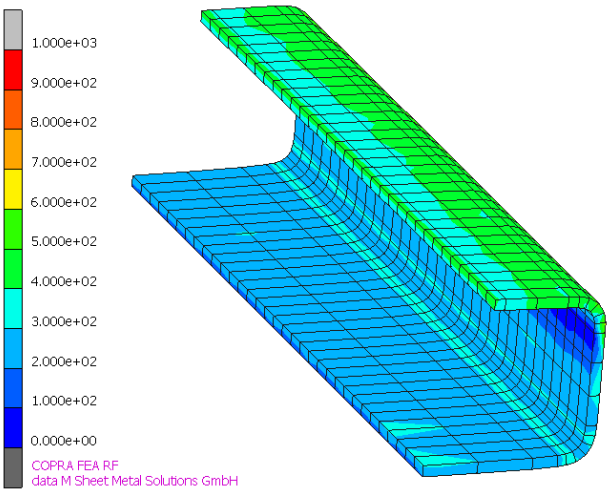

(a) One layer.

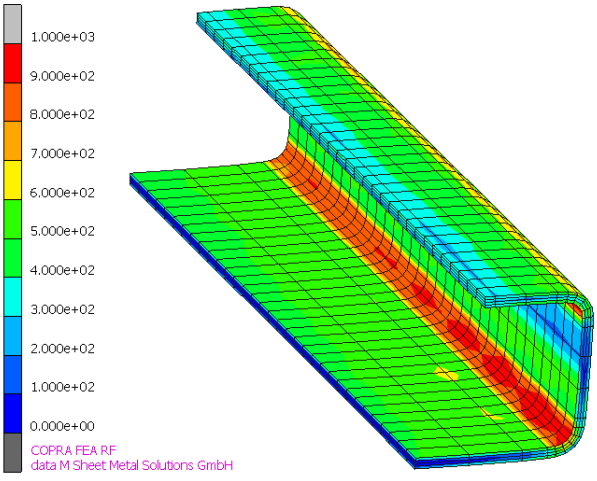

(b) Four layers.

Figure 6.24: Section of a roll formed C-Channel profile modelled in a mesh composed of type 7 elements with (a) one layer of elements over its thickness and (b) four layers of elements over its thickness and simulated in COPRA® FEA RF. The contour plot illustrates the von Mises stress distribution at the end of the simulation.

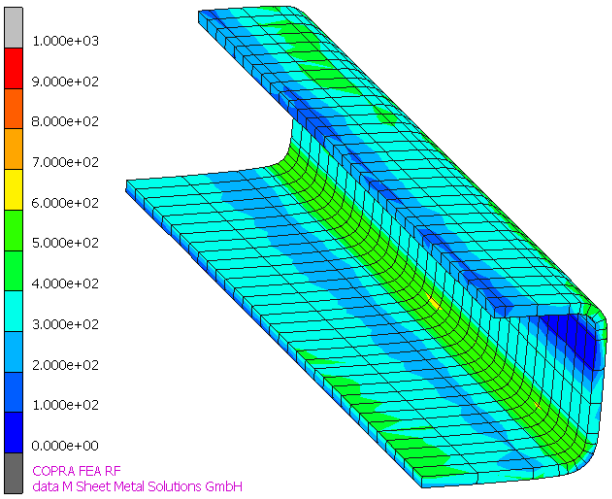

(a) One layer.

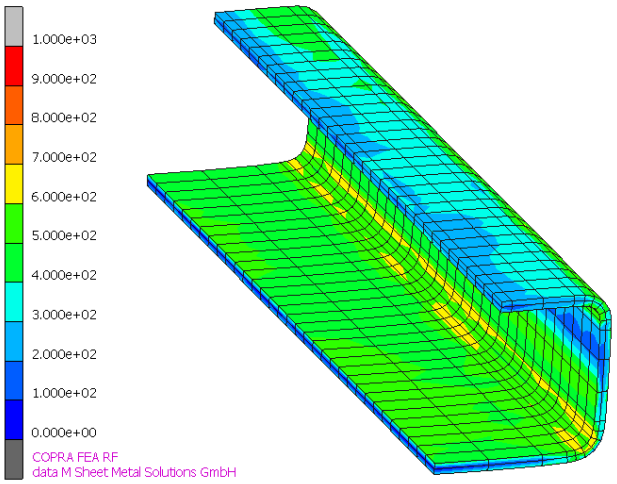

(b) Two layers.

Figure 6.25: Section of a roll formed C-Channel profile modelled in a mesh composed of C3D8I elements with (a) one layer of elements over its thickness and (b) two layers of elements over its thickness and simulated in Abaqus/Explicit. The contour plot illustrates the von Mises stress distribution at the end of the simulation.

By analysing figures 6.25a and comparing it to figure 6.24a, one can conclude that the stress distribution is much smoother in the simulation carried out using COPRA® FEA RF.

By further refining the mesh, as illustrated in figure 6.25b, one can notice the appearance of the neutral axis in the web as well as on the strip edge. Moreover, the stress distribution gets slightly closer to the one depicted in figure 6.24a than to the one in figure 6.25a, indicating that the mesh refinement tends to a stable distribution that can only be achieved with the increase of the number of integration points across the sheet metal's thickness.

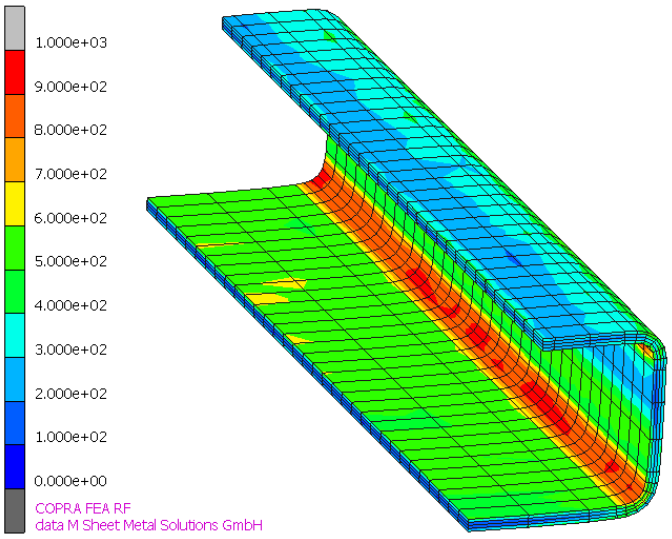

Figure 6.26: Section of a roll formed C-Channel profile modelled in a mesh composed of C3D8I elements with four layers of elements and simulated in Abaqus/Explicit. The contour plot illustrates the von Mises stress distribution at the end of the simulation.

By analysing figure 6.26 and comparing it to 6.24b, one can observe that the stress distribution is similar for both contour plots. This corroborated the assumption that a stress analysis requires several elements over the thickness to accurately represent the stress values.

Despite the likeness in stress distribution among the models with more layers over the thickness, the reduced integration elements yielded results that are not in accordance with figures 6.24b and 6.26.

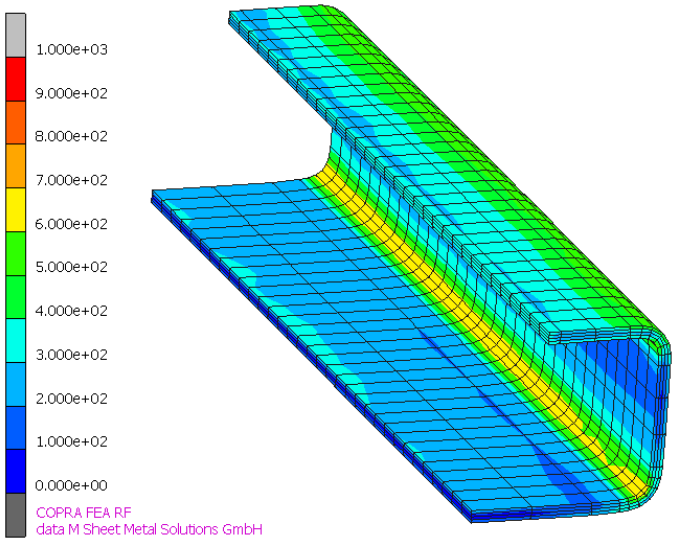

Figure 6.27: Section of a roll formed C-Channel profile modelled in a mesh composed of four layers of C3D8R elements with relaxed stiffness hourglass control and simulated in Abaqus/Explicit. The contour plot illustrates the von Mises stress distribution at the end of the simulation.

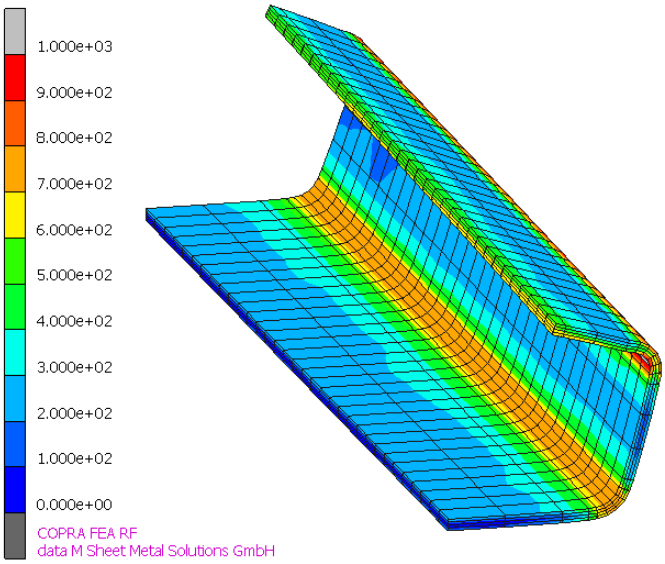

Figure 6.28: Section of a roll formed C-Channel profile modelled in a mesh composed of four layers of C3D8R elements with total stiffness hourglass control and simulated in Abaqus/Explicit. The contour plot illustrates the von Mises stress distribution at the end of the simulation.

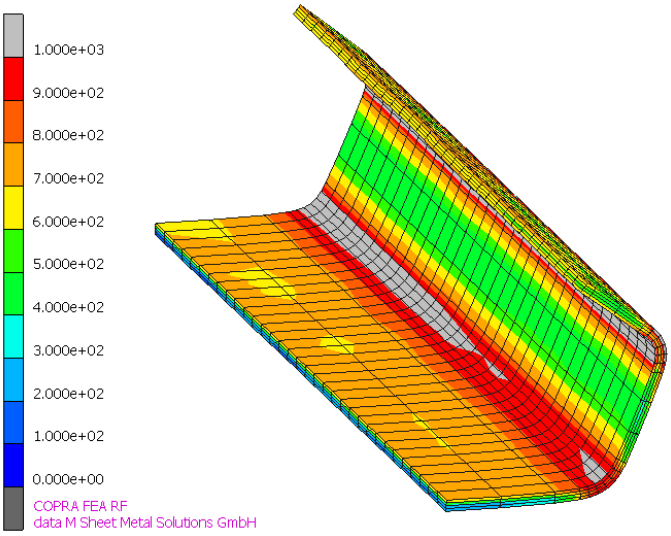

Figure 6.29: Section of a roll formed C-Channel profile modelled in a mesh composed of four layers of C3D8R elements with enhanced hourglass control and simulated in Abaqus/Explicit. The contour plot illustrates the von Mises stress distribution at the end of the simulation.

By analysing the results obtained using the reduced integration element with different hourglass mode controls (figures 6.27 to 6.29), the following conclusions can be drawn:

- The simulation carried out with the relaxed stiffness hourglass mode control yielded a distinct stress contour plot to the one in figure 6.24b; even though the stress distribution is somewhat similar, the values of stress throughout the sheet metal are underestimated.

- The simulation carried out with the total stiffness approach yields high values of stress in the strip edge, which does not occur in any other previous simulation.

- Finally, the simulation carried out with the enhanced hourglass control yielded grossly overestimated values of stress throughout the sheet metal.

Finally, the C3D8 element will be analysed. The von Mises stress distribution yielded at the end of the simulation is illustrated by figure 6.30.

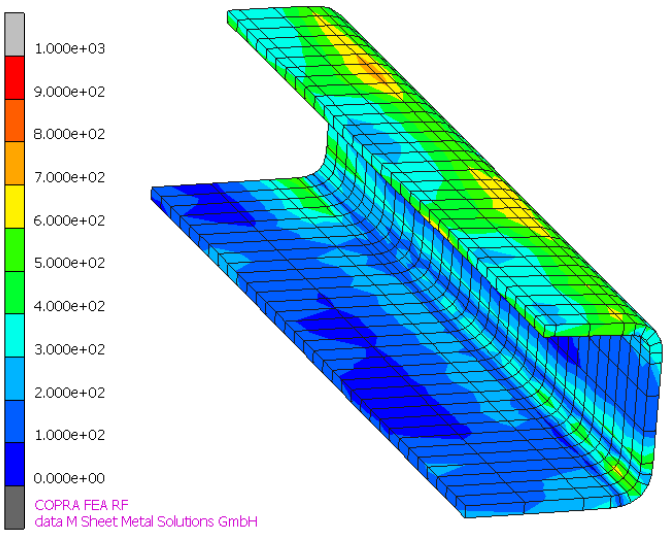

Figure 6.30: Section of a roll formed C-Channel profile modelled in a mesh composed of one layer of C3D8 elements and simulated in Abaqus/Explicit. The contour plot illustrates the von Mises stress distribution at the end of the simulation.

Similarly to the previous sections, the simulation of roll forming using C3D8 element yielded results that differ wildly from the reference ones. The higher values of stress are located in the upper flange, as opposed to the bending areas, where the stress values are higher for every other simulation.

Finally, following the same process as in section 6.1.2, a table is created with the minimum and maximum values of the von Mises stress for each analysed section. Albeit that the values are highly dependent of the number of elements throughout the thickness of the sheet metal, these numbers provide an insight to the residual stresses after the simulation takes place. Furthermore, since the values are post processed in identical ways (using a tool developed by data M to convert the Abaqus result files into MSC Marc files) there is no risk of having different extrapolation methods for different simulations.

The values input into the table are subsequently plotted into a chart for a more expedite comparison.

Table 6.2: Comparison of the maximum and minimum value of the von Mises stress in the mid-section of the sheet metal for each simulation. The values were all taken after the springback takes place and subsequently post-processed with the same tool in order to maintain the same extrapolation mode. The stress values are all in [Mpa].

Element	Layers/Thickness	Maximum Value [MPa]	Minimum Value [MPa]
C3D8	1	776.9	4.1
C3D8I	1	614.0	24.9
C3D8I	2	735.5	-35.6
C3D8I	4	994.6	54.6
C3D8R (EHC)	4	1235.0	145.9
C3D8R (TSHC)	4	1060.0	28.1
C3D8R (RSHC)	4	695.1	33.2
Element 7	1	711.1	-62.1
Element 7	4	982.8	19.6

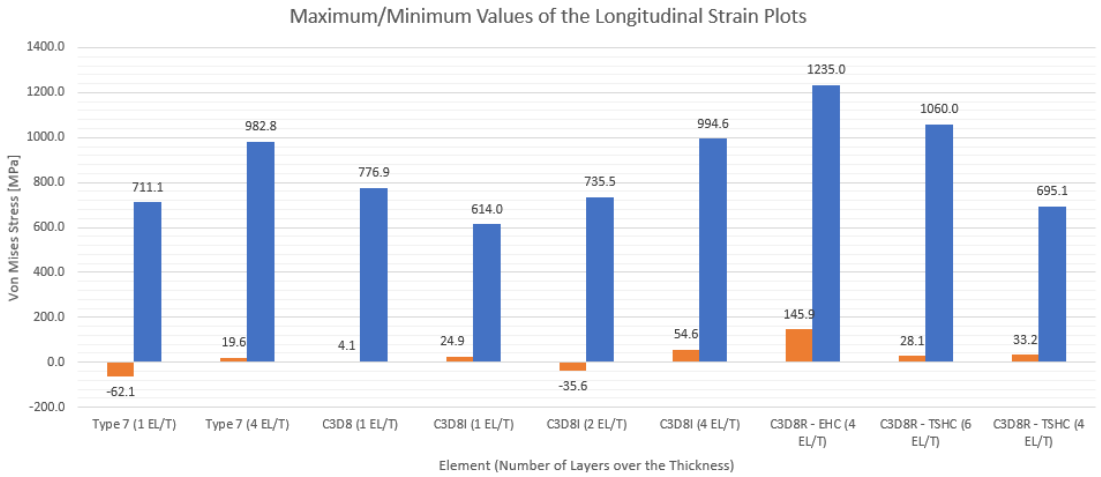

Figure 6.31: Chart with a plot of the minimum (represented in orange) and maximum (represented in blue) values of the von Mises stress for each section.

6.3 Geometrical Analysis

As stated in chapter 5, the geometrical analysis of the profile will be focused on the sheet metal thickness and the bending angles. The bending angles can be measured by taking the outline of the cross section illustrated in figure 5.2 into any CAD software. Figure 6.32 illustrates the cross section in question as well as the measured parameters.

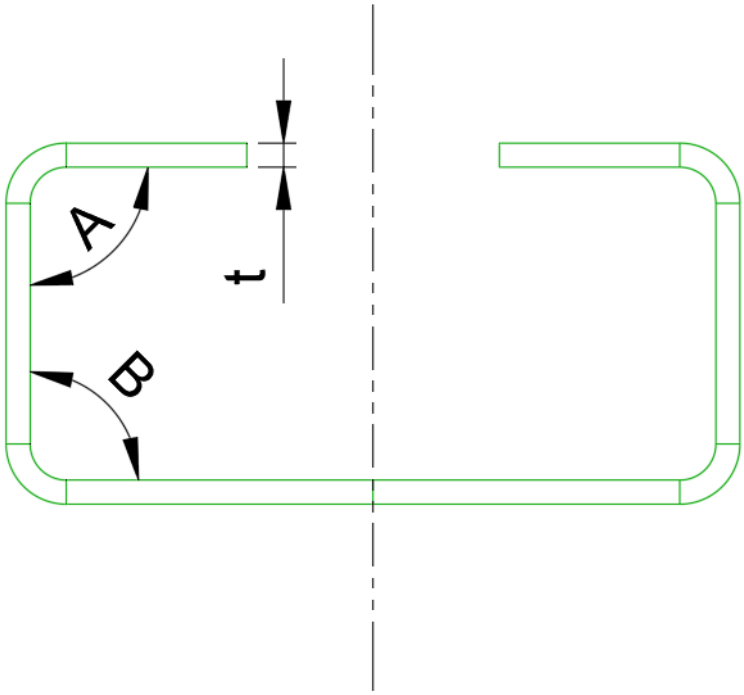

Figure 6.32: Symmetrical C-Channel cross-section and the parameters to be studied; "A" represents the first bending zone, "B" the second one and "t" represents the sheet metal thickness.

The first step in geometry analysis will be the measurement of the angle values. Using a tool developed by data M to convert the Abaqus files into MSC Marc files and subsequently exporting the contour of the profile midsection into a CAD software, the angles are measured and reported into table 6.3.

Table 6.3: Bending angle measurements for every profile obtained. The angles are in degrees and were measured in rollplane at the last station (station 13) and after forming.

Element	Layers/Thickness	In Rollplane		After Forming	
		Bend A	Bend B	Bend A	Bend B
C3D8	1	89.24	89.86	90.54	90.21
C3D8I	1	87.98º	90.10º	89.69º	92.65º
C3D8I	2	87.91º	90.21º	89.61º	91.88º
C3D8I	4	87.55º	90.05º	89.98º	91.61º
C3D8R (EHC)	4	90.16º	89.94º	106.39º	111.54º
C3D8R (TSHC)	4	90.26º	92.30º	97.62º	98.21º
C3D8R (RSHC)	4	90.21º	90.16º	91.03º	91.96º
C3D8R (TSHC)	6	90.33º	90.11º	91.84º	93.87º
Element 7	1	88.88º	89.96º	89.05º	91.02º
Element 7	4	88.13º	89.92º	90.00º	91.92º
Element 117	4	90.16º	89.87º	93.60º	92.69º

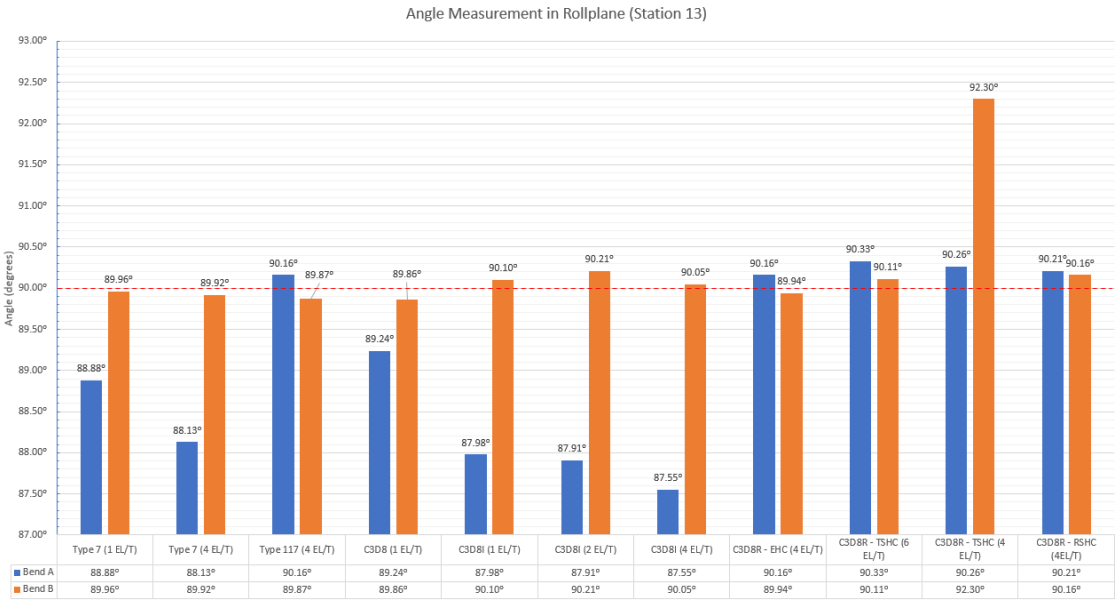

Figure 6.33: Plot of the angle measurements taken for each simulation in the station 13's roll plane. The red line indicates the theoretical angle that the profile should have at this stage (90º).

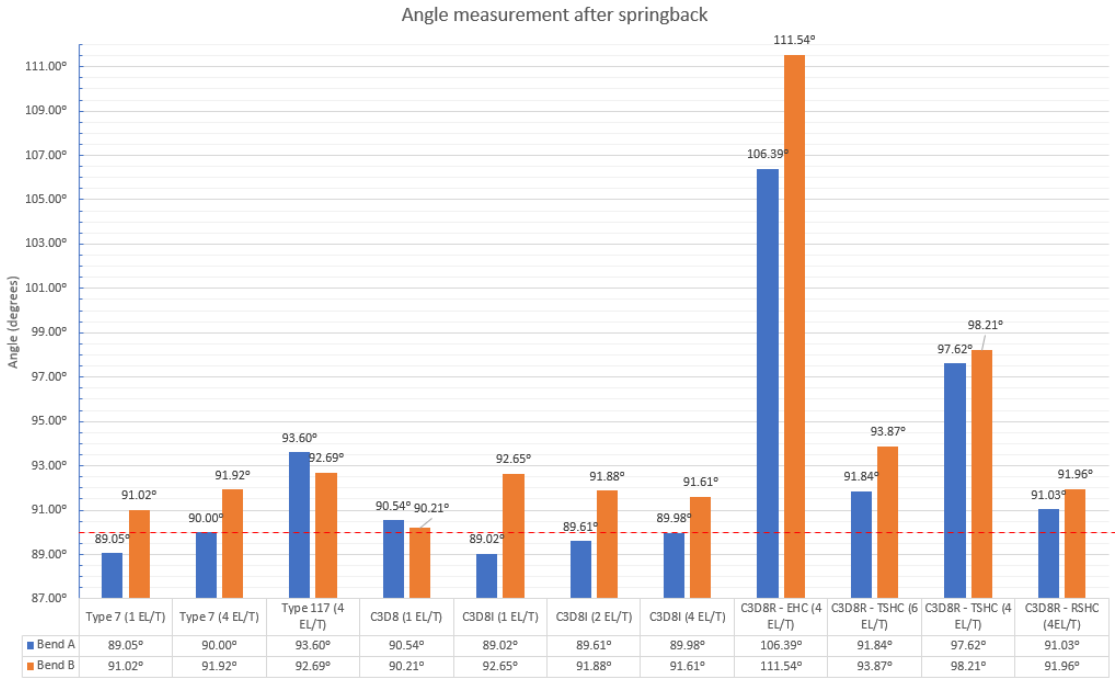

Figure 6.34: Plot of the angle measurements taken for each simulation after springback. The red line indicates the theoretical angle that the profile should have at this stage (90º).

After analysing table 6.3 and charts 6.33 and 6.34, several conclusions can be drawn:

- The final geometry of the profile is well represented by the results obtained by profiles modelled with the C3D8 and C3D8I elements.

- The C3D8R element with the relaxed stiffness hourglass control also yielded results that are approximate to the theoretical ones.
- The C3D8R element with the total stiffness hourglass control overestimated the both bending angles; however, a refinement of the mesh had a positive influence in the representation of the final angle values.
- Finally, the C3D8R element with the enhanced hourglass control wildly overestimated the angle values, yielding an unsatisfactory forming.

The sheet thickness after forming is also a subject of study. It allows for a better insight into the material movement around the bending areas. A lack of thinning in the bending areas can indicate an overly stiff element; on the other hand an excessive thinning can indicate the presence of defects or even material failure.

The subsequent figures illustrate the sheet metal thickness across the midsection of the roll formed profile.

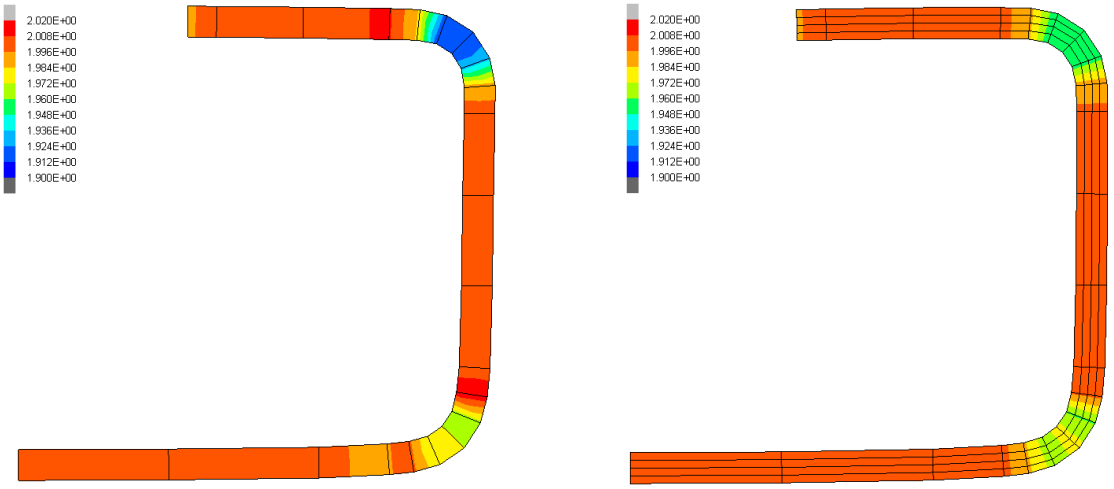

(a) One layer of elements.

(b) Four layers of elements.

Figure 6.35: Cross section of a roll formed C-Channel profile modelled in a mesh composed of type 7 elements, with (a) one layer of elements and (b) four layers of elements over its thickness and simulated in COPRA® FEA RF. The contour plot illustrates the sheet thickness of the roll formed C-channel, at the end of the simulation, in [mm].

By analysing figures 6.35a and 6.35b, section extracted from the simulations using MSC Marc's element type 7, leads to the conclusion that the mesh refinement leads to a less abrupt transition between the sections of the sheet metal that do not suffer from thinning effects (such as the web and the central part of the flanges) and the bending areas where the thinning phenomenon is more noticeable. Bend A (as described in figure 6.32) suffers a thinning of close to 1mm in figure 6.35a, as opposed to figure 6.35b where the sheet thickness suffers from a reduction of approximately 0.5mm. A similar behaviour is to be expected when refining the mesh of the sheet metal modelled with the C3D8I element.

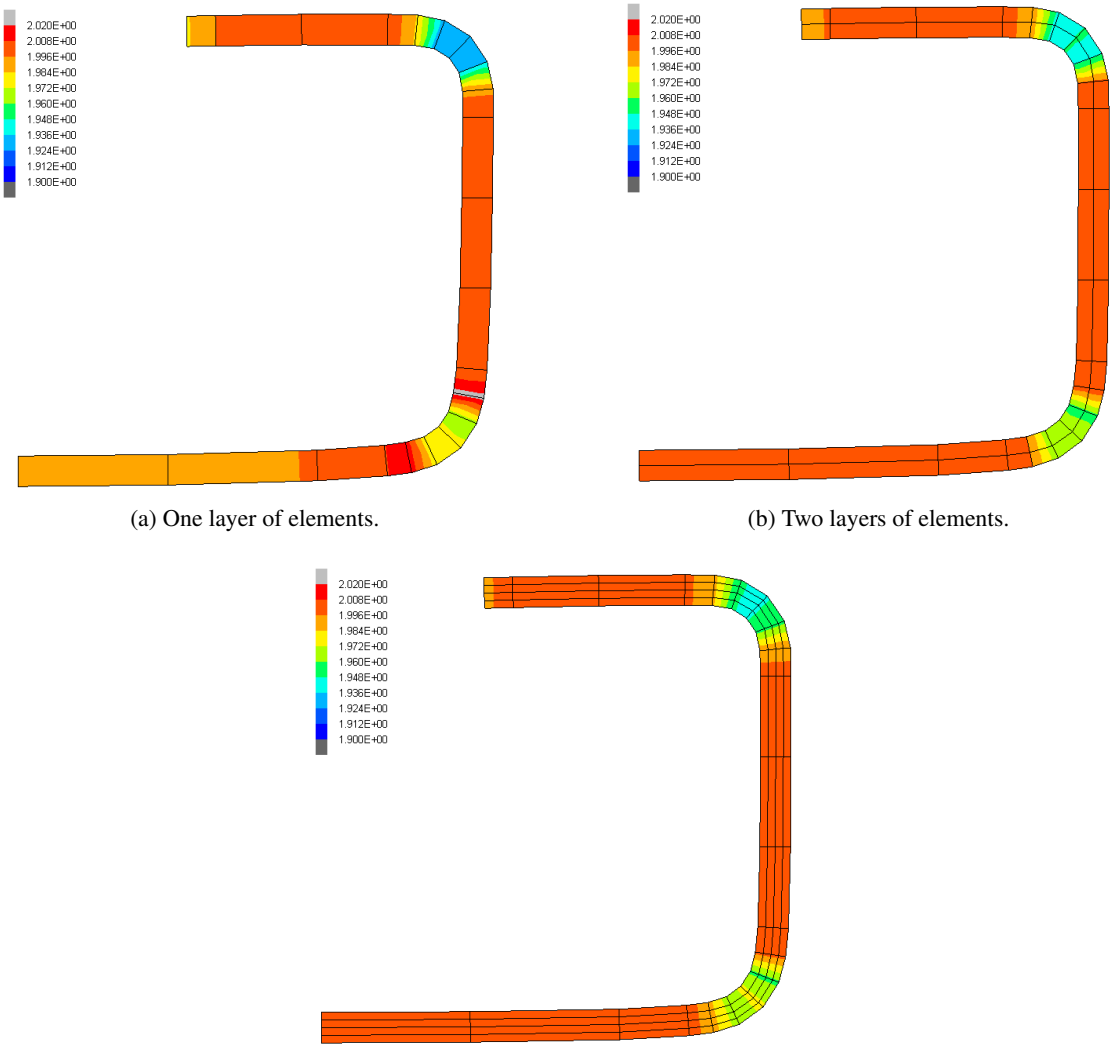

(a) One layer of elements.

(b) Two layers of elements.

(c) Four layers of elements.

Figure 6.36: Cross section of a roll formed C-Channel profile modelled in a mesh composed of C3D8I elements, with (a) one layer of elements, (b) two layers of elements and (c) four layers of elements over its thickness and simulated in Abaqus/Explicit. The contour plot illustrates the sheet thickness of the roll formed C-channel, at the end of the simulation, in [mm].

The aforementioned behaviour of sheet metal thinning mitigation in bend A is verified, by analysing figures 6.36a to 6.36c. Indeed, as predicted, the thinning effect in bend A is reduced when adding more layers of elements to the thickness of the sheet metal.

Another interesting phenomenon that can be pointed out by analysing figure 6.36a, is that the material in the web area suffers from a slight thinning effect. According to the theory in section 2 and to the figures 6.35a and 6.35b, this phenomenon should not occur, leading to the conclusion that one single layer of C3D8I elements might have some difficulties representing the material behaviour in a accurate way, when simulating roll forming processes in Abaqus/Explicit.

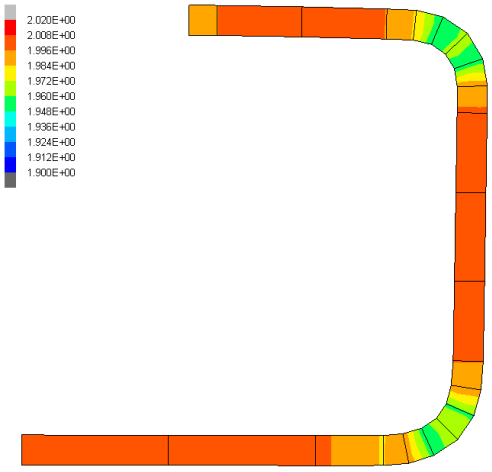

Figure 6.37: Cross section of a roll formed C-Channel profile modelled in a mesh composed of C3D8 elements, with one layer of elements over its thickness and simulated in Abaqus/Explicit. The contour plot illustrates the sheet thickness of the roll formed C-channel, at the end of the simulation, in [mm].

Figure 6.37 illustrates the cross-section obtained after simulating a roll forming process modelling the sheet metal with one layer of C3D8 elements. When comparing 6.37 with figures 6.35a and 6.36a, it is noticeable that the values of sheet thickness in the bending areas are higher in the former. Even though the representation of the sheet metal thickness is somewhat in accordance to figure 6.35b, the higher sheet metal thickness values are most likely due to the stiffness of the element rather than due to a correct representation of the variable.

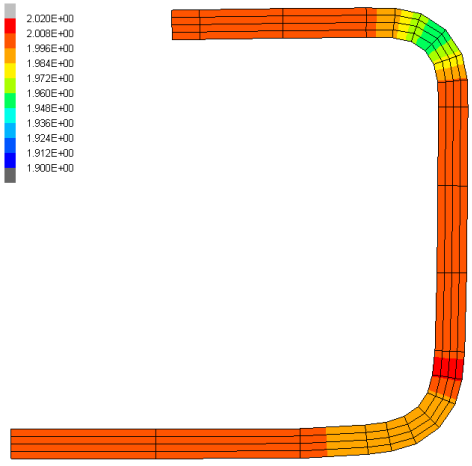

Figure 6.38: Cross section of a roll formed C-Channel profile modelled in a mesh composed of C3D8R elements, using the relaxed stiffness hourglass control, with four layers of elements over its thickness and simulated in Abaqus/Explicit. The contour plot illustrates the sheet thickness of the roll formed C-channel, at the end of the simulation, in [mm].

By analysing figure 6.38, it can be concluded that, despite the final correct geometry of the profile, the values of sheet thickness were overestimated. The correlation between these values

and the underestimated strain values in plot 6.23: lower values of strain lead to less material deformation, hence the lack of thinning in the sheet metal bending areas.

It is then interesting to analyse the behaviour of the sheet metal modelled with the C3D8R element using the total stiffness hourglass control and the influence of the mesh refinement through its thickness.

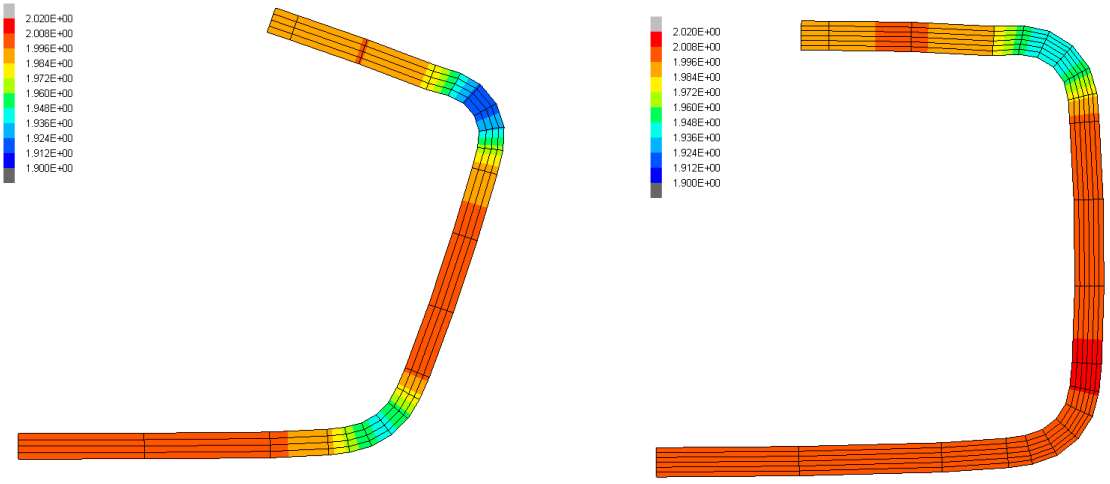

(a) Four layers of elements.

(b) Six layers of elements.

Figure 6.39: Cross section of a roll formed C-Channel profile modelled in a mesh composed of C3D8R elements, using the total stiffness hourglass control, with (a) four layers of elements and (b) six layers of elements over its thickness and simulated in Abaqus/Explicit. The contour plot illustrates the sheet thickness of the roll formed C-channel, at the end of the simulation, in [mm].

By observing figures 6.39a and 6.39b one can draw several conclusions:

- The refinement of the mesh composed of C3D8R elements using the total stiffness hourglass control mitigates the misrepresentation of the geometry seen in figure 6.39a. However, the geometry still falls short to the one illustrated by figures 6.35a and 6.35b.

- The sheet thickness value in bend A tends to the values seen in figure 6.35b.

- the sheet thickness value in bend B is grossly misrepresented; similarly to the situation seen in figure 6.38, there is no apparent thinning in the bending area in question.

- The thinning throughout the upper flange is a phenomenon that also does not occur in figures 6.35a and 6.35b.

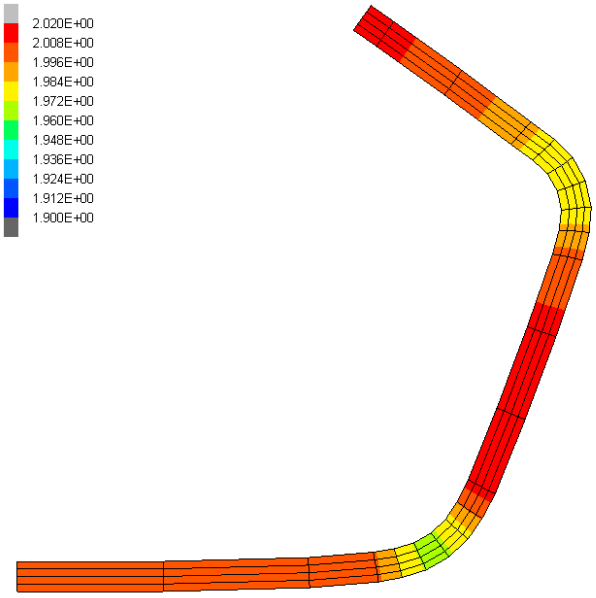

Figure 6.40: Cross section of a roll formed C-Channel profile modelled in a mesh composed of C3D8R elements, using the enhanced hourglass control, with four layers of elements over its thickness and simulated in Abaqus/Explicit. The contour plot illustrates the sheet thickness of the roll formed C-channel, at the end of the simulation, in [mm].

Finally, figure 6.40 illustrates the cross section obtained after simulating a roll forming process using the enhanced hourglass mode control. This hourglass mode control is unfit to represent roll forming in a reliable way. The element under EHC becomes too pliant, suffering from highly overestimated strain values (as seen in figure 6.23). Furthermore, figure 6.40 illustrates heavy thickening in the strip edge and in the lower flange, indicating a high deformation of the material in the forming direction; this assumption is corroborated by figure 6.29.

6.4 Contact Analysis

As mentioned several times beforehand, the contact is an essential factor of a roll forming process but also an extremely discontinuous process, contributing to the non-linearity of this sort of simulation. As such, the contact forces of the models simulated with the C3D8I element and Type 7 element – simulated in Abaqus/Explicit and COPRA® FEA RF, respectively – will be analysed in two stations.

The two stations to be analysed in both COPRA® FEA RF and in Abaqus are illustrated according to what to figures 6.41a and 6.41b. The goal is to analyse the contact force distribution and magnitude in those two stations, focusing on the contact between the inner surface of the second bend area and the upper rolls, as well as on the contact between the bottom rolls and the web/outer surface of the bending zone.

Since the contact was modelled using a node-to-surface algorithm, the refinement of the mesh through the thickness of the sheet metal does not have an influence in the contact status.

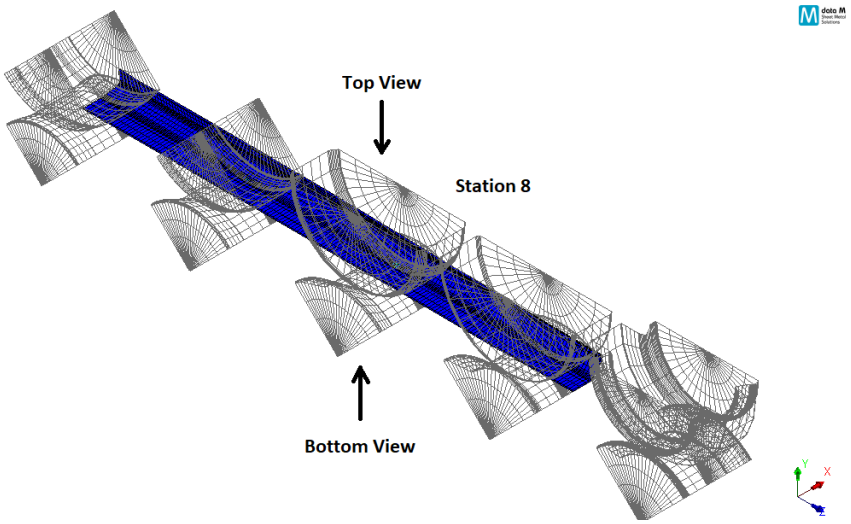

(a) Station 8.

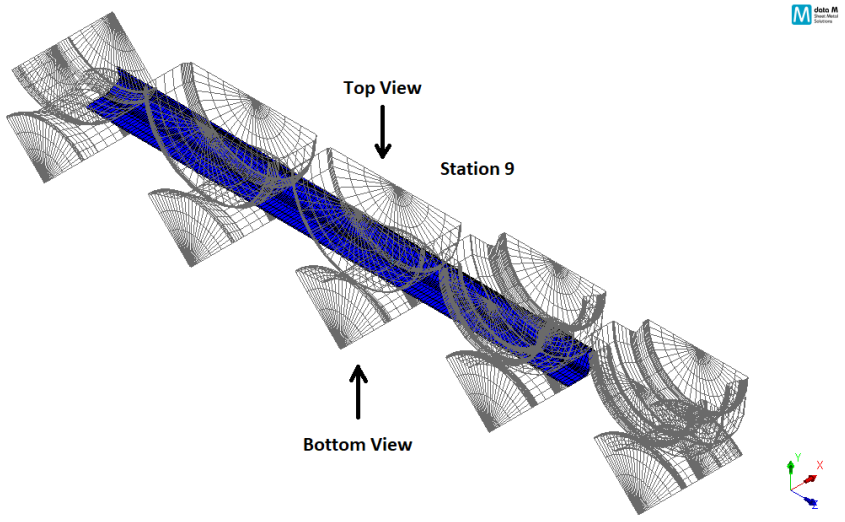

(b) Station 9.

Figure 6.41: Station 8 (a) and station 9 (b), where the contact forces are to be analysed and the views selected for that purpose.

The first contact situation to be analysed is the state of the simulation of a roll forming process at station 8, using a sheet metal modelled with C3D8I elements. This contact situation will be put side by side and compared to the contact situation when modelling the sheet metal with MSC Marc's element type 7 and simulating the process in COPRA® FEA RF.

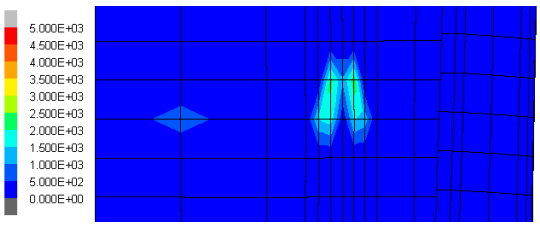

(a) Top view of station 8, after the simulation carried out in Abaqus/Explicit.

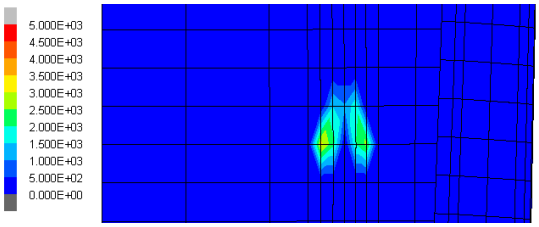

(b) Top view of station 8, after the simulation carried out in COPRA® FEA RF.

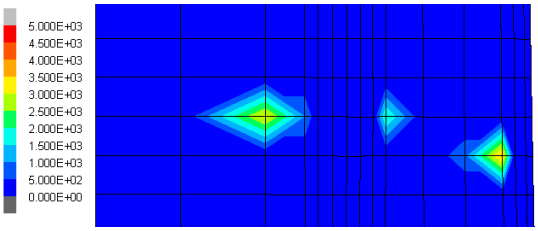

(c) Bottom view of station 8, after the simulation carried out in Abaqus/Explicit.

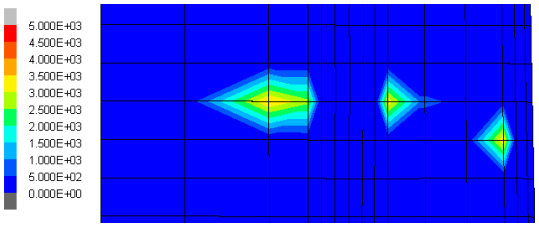

(d) Bottom view of station 8, after the simulation carried out in COPRA® FEA RF.

Figure 6.42: Different views of station 8, according to the description in figure 6.41a, and the contact force exerted by the rolls on the sheet metal. The upper row illustrates the top view of the sheet metal modelled with (a) C3D8I elements in Abaqus/Explicit and (b) type 7 elements in COPRA® FEA RF; the lower row illustrates the bottom view of the sheet metal modelled with (c) C3D8I elements in Abaqus/Explicit and (d) type 7 elements in COPRA® FEA RF. The contact force is in [N].

By analysing figures 6.42a to 6.42d one can draw several conclusions:

- The contact force distribution is similar for both cases; in figures 6.42a and 6.42b the top roll in station 8 exerts force over six nodes in the bending zone while in figures 6.42c and 6.42d the bottom roll exerts force over five nodes in the web, in three distinct regions. However, in figure 6.42a one point in the web is in contact with the top roll while in figure 6.42b it does not occur. This is effect is most likely due to the oscillatory nature inherent to explicit simulations.

- The magnitude of the contact force is roughly the same in both cases; however, the force exerted by the rolls in the simulation carried with COPRA® FEA RF is slightly higher, especially when observing the contact between the top roll and the bending zone.

The same analysis as the one carried out for station 8 is taken place for station 9 as well. Figures 6.43a to 6.43d illustrate the sheet metal in the same section of the sheet metal as figures 6.42a to 6.42d.

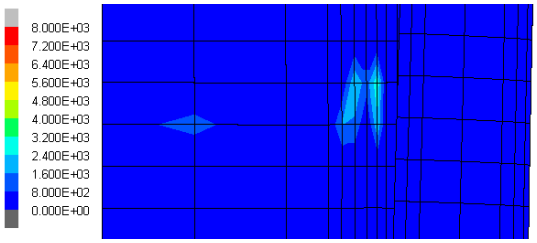

(a) Top view of station 9, after the simulation carried out in Abaqus/Explicit.

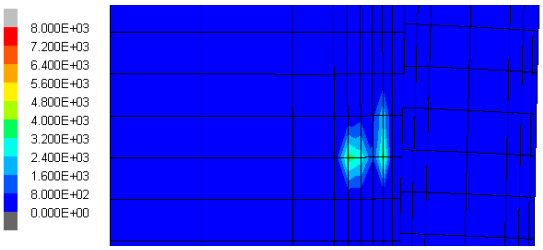

(b) Top view of station 9, after the simulation carried out in COPRA® FEA RF.

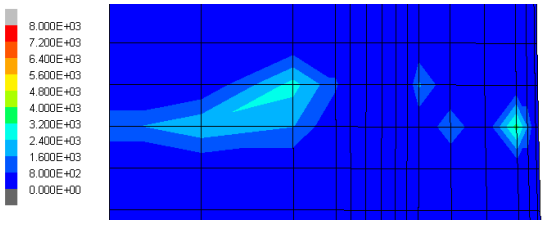

(c) Bottom view of station 9, after the simulation carried out in Abaqus/Explicit.

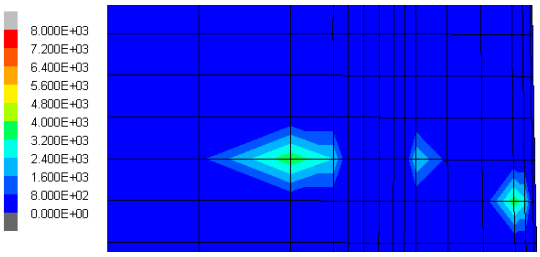

(d) Bottom view of station 9, after the simulation carried out in COPRA® FEA RF.

Figure 6.43: Different views of station 9, according to the description in figure 6.41b, and the contact force exerted by the rolls on the sheet metal. The upper row illustrates the top view of the sheet metal modelled with (a) C3D8I elements in Abaqus/Explicit and (b) type 7 elements in COPRA® FEA RF; the lower row illustrates the bottom view of the sheet metal modelled with (c) C3D8I elements in Abaqus/Explicit and (d) type 7 elements in COPRA® FEA RF. The contact force is in [N].

To the contrary of what was verified for station 8, the contact status in station 9, illustrated by figures 6.43a to 6.43d, presents some differences between the two distinct simulations.

- In figure 6.43a the erratic node outside of the bending zone that was in contact with the top roll in station 8 is still in contact in station 9. The vibration inherent to the explicit simulation might not be enough to explain the fact that the same node is in contact with the top roll at a different increment. Therefore, the probable hypothesis is that the contact enforcement in Abaqus/Explicit has a looser gap tolerance than the COPRA® FEA RF, leading to an erratic overclosure in that particular node.

- The contact distribution illustrated by figure 6.43c is totally distinct from the one illustrated in 6.43d. While the contact distribution in the results obtained in COPRA® FEA RF were kept consistent in both stations (five nodes in contact with the forming rolls), the results obtained in Abaqus/Explicit show that the contact with the rolls took place in eight nodes in four different areas. Once again, the lack of stability of the sheet metal is most likely the main responsible for the erratic contact distribution.

6.5 Computation Time

The last assessment parameter in this chapter is the computation time, or CPU time. This is an important parameter as it is a good indicator of the capability of an FEA package to quickly and effectively deal with highly non-linear problems such as roll forming. However, the studied C-channel model is quite simple; the results in table 6.4 cannot be extrapolated into more complex models.

Table 6.4: Computational time for the simulations carried out in Abaqus, in seconds. The simulation carried out using Abaqus/Implicit kept crashing shortly after reaching station 9.

Element	Solver	Number of Elements	CPU Time (s)
C3D8	Explicit	3423	6398
C3D8R	Explicit (TSHC)	13692	26713
	Explicit (EHC)	13692	27781
	Explicit (RSHC)	13692	30090
	Explicit (TSHC)	20538	45154
C3D8I	Explicit	3423	6877
	Implicit	3423	87010 (at Station 10)
	Explicit	6846	15143
	Explicit	13692	47449
Element 7	Implicit	3423	8196
	Implicit	13692	36158
Element 117	Implicit	13692	60144

It can be concluded that for simple models, Abaqus/Explicit fares particularly well in terms of CPU time; by comparing the simulations carried out using the same element (C3D8I, with one layer of elements across the thickness of the sheet metal) but resorting to different solver, it becomes clear that Abaqus/Implicit is not capable of handling the non-linearity inherent to roll forming simulations.

It is interesting to point out that for a mesh consisting in one layer of solid fully integrated elements, Abaqus/Explicit ran a faster simulation than COPRA® FEA RF; however, as the amount of elements increases and consequently, their size, the simulation using Abaqus/Explicit becomes considerably slower. This allows for the conclusion that further mesh refinement would highlight two major drawbacks for Abaqus/Explicit:

- Further mesh refinement without mass/time scaling would exponentially increase the CPU time of the simulation (refer to chapter 3).
- Further mesh refinement with mass/time scaling would deteriorate the quality of the results, as the kinematic effects would affect their accuracy.

The reduced integration element, despite the fast simulation time considering the amount of elements, yielded unsatisfactory results for the most part, which means that for this particular model the C3D8R is not a viable solution. However, the application of this element in a suitable model could be promising to deliver results faster than by resorting to the C3D8I element.

The values in table 6.4 are plotted in the subsequent chart, for a more expedite visualisation.

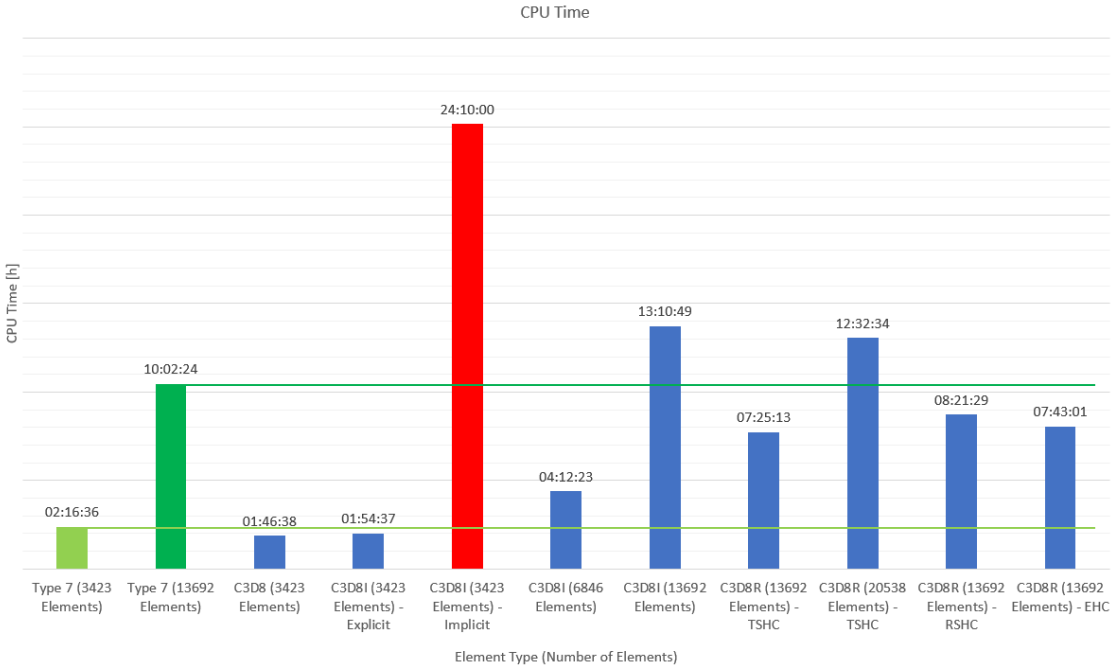

Figure 6.44: CPU time for each simulation. The CPU time is given in [h].

Chapter 7

Conclusions and Future Work

7.1 Conclusions

Throughout this dissertation, many parameters were studied in order to ascertain if the Abaqus solvers can be used to accurately represent roll forming processes. Several criteria were established in order to compare the quality and speed of the simulations carried out with Abaqus, with the ones carried out with COPRA® FEA RF, as it is the industrial standard FEA package when it comes to simulating roll forming processes.

It is important to point out that this dissertation is the foundation to a more in-depth research; the studied C-Channel model was simple and the presence of holes or indentations in the sheet metal were not considered for analysis. Furthermore, friction and roll rotation were also left out of this study.

Abaqus/Explicit allows for roll forming simulations to be accelerated, saving time in order to reach results. Resorting to the C3D8I element, satisfactory results were obtained in terms of stress and strain distribution when compared to the results obtained with COPRA® FEA RF.

In terms of longitudinal strain, when compared to COPRA® FEA RF, the C3D8I element simulated in Abaqus/Explicit yielded extremely similar results. When considering four layers of elements over the thickness of the sheet metal, the relative difference in the maximum value of longitudinal strain is 1,06%, while it stands at 22,6% for the minimum value (table 6.1). None of the other considered elements reached results that were as close as the aforementioned ones.

The same scenario is verified when analysing the equivalent stress; the maximum value of equivalent stress registered for the Abaqus/Explicit simulation using the C3D8I element (figure 6.26) and the simulation carried out in COPRA® FEA RF (figure 6.24b) are quite similar. The registered values were 994,6 MPa for the former and 982,8 MPa for the latter, as seen in table 6.2. As illustrated by chart 6.31, no other equivalent stress values come as close to the reference values as the ones obtained when resorting to the C3D8I element.

Finally, a part from the C3D8 element, the C3D8I element is the one that better represents the geometry when comparing to COPRA® FEA RF. The reason why the C3D8 element is not

considered as viable result, is because the stress and strain values, as predicted in chapter 4, differ too much from the reference one.

It is relevant to point out that even though the models in Abaqus were optimised to obtain satisfactory results, the same models were simulated in COPRA® FEA RF using the default settings and thus, incurring in with no optimisation whatsoever. Despite the satisfactory results using the C3D8I elements, there are several drawbacks to this FEA package that were exposed throughout this dissertation:

- The kinematic effects inherent to an explicit simulation slightly deteriorate the quality of the results, resulting in a subtle curvature to the web. This problem could be mitigated through refining the mesh in the web area and by reducing the time scaling factor.
- The refinement of the mesh affects the minimum stable increment time thus increasing the total simulation time.
- By increasing the complexity of the profile or by adding holes in the sheet metal would lead to a modification of the mesh – either by adding elements or by reducing the size of the smallest element in the mesh – resulting in a longer and unpractical total simulation time.
- Springback simulations had to be imported and restarted in Abaqus/Implicit. This scenario can increase the probability of errors induced by the user and adds up to the total simulation time, as the import and restart are not performed in the same module.
- The acceleration of explicit simulations is highly dependant on either trial and error or experience of the user, as monitoring the kinematic energy in quasi-static simulations is needed.

Therefore, even though the results were similar to the ones obtained using COPRA® FEA RF when applied to a simple roll forming model, the difficulties associated with simulating more complex roll forming processes hinder the feasibility of using Abaqus/Explicit as an FEA package dedicated to roll forming. However, for simpler simulations and resorting to the C3D8I element to model the sheet metal, Abaqus/Explicit consists in a legitimate solution to simulate roll forming processes.

On the other hand, the results yielded when using the C3D8R element were unsatisfactory, for the most part. Different hourglass mode controls were tested and only one, the relaxed stiffness hourglass control, yielded a correct final geometry of the profile. Nevertheless, the stress and strain values were underestimated when compared to the values obtained using the C3D8I element and when simulating with COPRA® FEA RF.

Finally, Abaqus/Implicit was also optimised and tested in roll forming simulations using the C3D8I element. However, convergence was not obtained, causing the simulations to crash; ultimately, after a considerable amount of optimisation, the further that the implicit simulation got was station 10 out of 13. The conclusion drawn is that under the settings defined for this particular model, the implicit solver was not capable of carrying out the entirety of the simulation. The convergence issues could be solved by further refining the meshes which would lead to an

impractical total simulation time. Another solution would be to loosen the convergence tolerance parameters which could lead to erroneous results. Nevertheless, this is a solution that requires Abaqus experience allied to a trial and error system of result validation.

To summarise, the usage of Abaqus as a viable FEA package for roll forming simulations inserted in an industrial context is complicated, due to the characteristics of both the solver and manufacturing process. As modelled, the simulations lacked sturdiness and there are too many parameters associated with explicit simulations that require a trial and error approach. Further studies on this subject are needed, in order to develop roll forming models that convey robustness to the simulations.

7.2 Future Work

The next steps to a more in-depth Abaqus assessment as an FEA package to simulate roll forming processes relate to the increase in model complexity.

- Adding holes or indentations to the sheet metal would allow an analysis to the increase in minimum stable increment time. Furthermore, it would allow to ascertain if the obtained results would still be in accordance to the results obtained in COPRA® FEA RF.
- Study the mesh sensitivity in depth to verify if the results improve in terms of quality (stress and strain distribution, final geometry of the profile) and to ascertain the impact in the total simulation time.
- Include friction and roll rotation to approximate the simulation to a real roll forming process.
- Studying mass scaling as it is a parameter that is determined in a trial and error basis. Understanding this feature and combining it with time scaling (as implemented throughout this dissertation) could contribute positively to the reduction of the total simulation time.
- Studying dynamic re-meshing in an effort to reduce the total simulation time while producing reliable results.
- Modelling the roll forming process using solid-shell elements, in order to overcome the drawbacks inherent to conventional shell elements.

References

[Abee and Sedlmaier, 2010] Abee, A. and Sedlmaier, A. (2010). Development of new 3d roll forming applications by means of numerical analysis as a part of a quality control methodology. *CBM Metal Matters, no. 18: 21–24*.

[Abvabi, 2014] Abvabi, A. (2014). *Effect of Residual Stresses in Roll Forming Process of Metal Sheets*. PhD thesis, Deakin University.

[Augarde and Deeks, 2008] Augarde, C. E. and Deeks, A. J. (2008). The use of Timoshenko's exact solution for a cantilever beam in adaptive analysis. *Finite Elements in Analysis and Design*.

[Baeker, 2018] Baeker, M. (2018). How to get meaningful and correct results from your finite element model. Unpublished, Technische Universität Braunschweig, Germany.

[Bhattacharyya et al., 1984] Bhattacharyya, D., Smith, P., Yee, C., and Collins, I. (1984). The prediction of deformation length in cold roll-forming. *Journal of Mechanical Working Technology*.

[Bieber, 2020] Bieber, S. (2020). Adaptive, verformungsabhängige finite-elemente-formulierungen zur stabilen und lockingfreien analyse von problemen mit großen deformationen. Undergoing research project.

[Bonab and Mazdak, 2014] Bonab, M. M. and Mazdak, S. (2014). Numerical study of the effect of anisotropy on the longitudinal strain in cold roll-forming process of symmetric channel section. *Advances in Environmental Biology*.

[Boulbes, 2010] Boulbes, R. J. (2010). *Troubleshooting Finite-Element Modelling with Abaqus*. Springer.

[Bui and Ponthot, 2008] Bui, Q. V. and Ponthot, J. P. (2008). Numerical simulation of cold roll-forming processes. *Journal of Materials Processing Technology*.

[Courant et al., 1928] Courant, R., Friedrichs, K., and Lewy, H. (1928). Über die partiellen differenzengleichungen der mathematischen physik. *Mathematische Annalen*.

[CustomPartNet, 2009] CustomPartNet (2009). https://www.custompartnet.com/wu/sheet-metal-forming. [Online; accessed August-2020].

[data M Sheet Metal Solutions GmbH, 2014] data M Sheet Metal Solutions GmbH (2014). *What you need to know about COPRA®*. data M Sheet Metal Solutions GmbH.

[data M Software India, 2020] data M Software India (2020). https://www.datamindia.com/. [Online; accessed 22-July-2020].

[dataM Sheet Metal Solutions, 2020] dataM Sheet Metal Solutions (2020). http://www.datam.de/en/products-solutions/simulation-with-fea/copraR-fea-rf/. [Online; accessed 2-June-2020].

[Dean, 2020] Dean, J. (2020). The direct stiffness method and the global stiffness matrix. Presentation for the Department of Material Science and Metallurgy University of Cambridge, England. [Online; accessed April-2020].

[Fagan, 1992] Fagan, M. (1992). *Finite Element Analysis*. Longman Group.

[Fang et al., 2015] Fang, G., Gao, W., and Zhang, X. (2015). Finite element simulation and experiment verification of rolling forming for the truck wheel rim. *International Journal of Precision Engineering and Manufacturing, 16*.

[Figueiredo, 2016] Figueiredo, P. B. (2016). Roll forming - a study on machine deflection by means of experimental analysis and numerical developments. Master's thesis, Faculdade de Engenharia da Universidade do Porto.

[G. Papazafeiropoulos, 2017] G. Papazafeiropoulos, M. Muñiz-Calvente, E. M.-P. (2017). Abaqus2Matlab: a suitable tool for finite element post-processing. *Advances in Engineering Software*, pages 9–16.

[Gavin, 2018] Gavin, H. P. (2018). Numerical integration in structural dynamics. Unpublished, Department of Civil & Environmental Engineering, Duke University, USA.

[Granta Design Limited, 2019] Granta Design Limited (2019). *CES Edupack 2019*.

[Gülçeken et al., 2007] Gülçeken, E., Abee, A., Sedlmaier, A., and Livatyali, H. (2007). Finite element simulation of flexible roll forming: A case study on variable width U-channel. In *4th International Conference and Exhibition on Design and Production of MACHINES and DIES/MOLDS*.

[Halmos, 2006] Halmos, G. T. (2006). *Roll Forming Handbook*. Taylor & Francis, Tenth edition.

[Harewood and McHugh, 2006] Harewood, F. and McHugh, P. (2006). Comparison of the implicit and explicit finite element methods using crystal plasticity. *Computational Materials Science*.

[Hellborg, 2007] Hellborg, S. (2007). Finite Element Simulation of Roll Forming. Master's thesis, Linköping University.

[Hibbitt, 1999] Hibbitt, K. . S. (1999). *Answers to common question in Abaqus*. Simulia™-Dassault Systèmes®.

[Huang, 2005] Huang, P. (2005). The New Age for Abaqus. Interview with Mark Goldstein, CEO of Abaqus for seven years. URL: http://www.eworksglobal.com/reports_127794587201093750.htm, accessed in 20/07/2020.

[Jiao et al., 2013] Jiao, J., Rolfe, B., Mendiguren, J., Galdos, L., and Weiss, M. (2013). The effect of process parameters on web-warping in the flexible roll forming of UHSS. *The 9th International Conference and Workshop on Numerical Simulation of 3D Sheet Metal Forming Processes*.

[Jung, 1998] Jung, D. (1998). Study of dynamic explicit analysis in sheet metal forming processes using faster punch velocity and mass scaling scheme. *Journal of Materials Engineering and Performance*.

[Jung, 2017] Jung, D. W. (2017). A new engineering technique in roller design to prevent thinning of sheet in roll forming process. *Applied Mechanics and Materials*, 873:42–47.

[Laney, 1998] Laney, C. (1998). *Computational Gasdynamics*. Cambridge University Press.

[Liang et al., 2019] Liang, J., Chen, C., Liang, C., Li, Y., Chen, G., Li, X., and Wang, A. (2019). One-time roll-forming technology for high-strength steel profiles with "A" section. *Advances in Materials Science and Engineering*.

[Lindgren, 2005] Lindgren, M. (2005). Finite element model of roll forming of a u-channel profile. *Advanced Technology of Plasticity*.

[Lindgren, 2007] Lindgren, M. (2007). Experimental investigations of the roll load and roll torque when high strength steel is roll formed. *Journal of Materials Processing Technology*, 191.

[Lindgren, 2009] Lindgren, M. (2009). *Experimental and Computational Investigation of the Roll Forming Process*. PhD thesis, Luleå University of Technology.

[Mashayekhi, 2015] Mashayekhi, M. (2015). Comparison of implicit and explicit procedures. MS Powerpoint Presentation, Isfahan University of Technology, Departement of Mechanical Engineering. [Online; accessed March-2020].

[McClure and Li, 1995] McClure, C. K. and Li, H. (1995). Roll forming simulation using finite element analysis. *Manufacturing Review*, pages 114–119.

[MSC Software, 2019] MSC Software (2019). *MSC Marc User Manual*. MSC Software.

[Najafabadi et al., 2019] Najafabadi, H., Naeini, H., Safdarian, R., Kasaei, M. M., Akbari, D., and Abbaszadeh, B. (2019). Effect of forming parameters on edge wrinkling in cold roll forming of wide profiles. *The International Journal of Advanced Manufacturing Technology*, 101.

[Natal, 2017] Natal, R. J. (2017). Sebenta: Mecânica das estruturas. Lecture Notes for the course "Structural Mechanics" Department of Mechanical and Industrial Management Engineering, Faculty of engineering of the University of Porto.

[Neto, 2014] Neto, D. (2014). *Numerical Simulation of Frictional Contact Problems using Nagata Patches in Surface Smoothing*. PhD thesis, University of Coimbra.

[Neto et al., 2016] Neto, D., Oliveira, M., Menezes, L., and Alves, J. (2016). A contact smoothing method for arbitrary surface meshes using nagata patches. *Computer Methods in Applied Mechanics and Engineering*, 299:283 – 315.

[Ni et al., 1991] Ni, C., Gatny, D., and Rahman, A. (1991). Application of finite element analysis to the curving or sweeping of roll formed sections for vehicle body structures. In *SAE Technical Paper*. SAE International.

[Nour-Omid and Wriggers, 1987] Nour-Omid, B. and Wriggers, P. (1987). A note on the optimum choice for penalty parameters. *Communications in Applied Numerical Methods*, 3(6):581–585.

[Pacheco, 2019] Pacheco, J. B. (2019). Presentation on Sheet Metal Bending for the course "Manufacturing Processes", Faculty of Engineering, University of Porto.

[Panton et al., 1996] Panton, S., Duncan, J., and Zhu, S. (1996). Longitudinal and shear strain development in cold roll forming. *Journal of Materials Processing Technology*.

[Paralikas et al., 2008] Paralikas, J., Salonitis, K., and Chryssolouris, G. (2008). Investigation of the effects of main roll-forming process parameters on quality for a V-section profile from AHSS. *The International Journal of Advanced Manufacturing Technology*, 44:223–237.

[Rebelo et al., 1992] Rebelo, N., Nagtegaal, J., and Taylor, L. (1992). Comparison of implicit and explicit finite element methods in the simulation of metal forming processes. *Abaqus Users Conference*.

[Roller King Enterprise Co., 2020] Roller King Enterprise Co., L. (2020). https://rollerking.en.taiwantrade.com/product/stud-and-track-roll-forming-lines-roll-forming-machine-2007731.html. [Online; accessed 22-July-2020].

[Roylance, 1996] Roylance, D. (1996). *Mechanics of Materials*. Wiley.

[Safdarian and Naeini, 2014] Safdarian, R. and Naeini, H. M. (2014). The effects of forming parameters on the cold roll forming of channel section. *Thin-Walled Structures*.

[Seabra, 2004] Seabra, J. (2004). Dinâmica do ponto material e do corpo rígido. Department of Mechanical and Industrial Management Engineering, Faculty of engineering of the University of Porto.

[Sedlmaier and Dietl, 2018] Sedlmaier, A. and Dietl, T. (2018). 3d roll forming center for automotive applications. In *17th International Conference on Metal Forming, Metal Forming 2018*.

[Sener and Yurci, 2016] Sener, B. and Yurci, M. E. (2016). Comparison of quasi-static constitutive equations and modeling of flow curves for austenitic 304 and ferritic 430 stainless steels. *Special Issue of the 6th International Congress & Exhibition (APMAS2016)*.

[Simulia, 2005a] Simulia (2005a). Abaqus/explicit: Advanced topics - quasi-static analyses. MS Powerpoint Presentation, ABAQUS/Explicit: Advanced Topics, 2005. [Online; accessed March-2020].

[Simulia, 2005b] Simulia (2005b). Overview of abaqus/explicit. MS Powerpoint Presentation, ABAQUS/Explicit: Advanced Topics, 2005. [Online; accessed March-2020].

[Simulia, 2019] Simulia (2019). *Abaqus Documentation*. Simulia™- Dassault Systèmes®.

[Talebi-Ghadikolaee et al., 2020] Talebi-Ghadikolaee, H., Naeini, H. M., Mirnia, M., Mirzai, M., Alexandrov, S., and Zeinali, M. (2020). Modelling of ductile damage evolution in roll forming of u-channel sections. *Journal of Materials Processing Technology*.

[Tehrani et al., 2006] Tehrani, M. S., Hartley, P., Naeini, H. M., and Khademizadeh, H. (2006). Localised edge buckling in cold roll-forming of symmetric channel section. *Thin-Walled Structures*, 44(2):184 – 196.

[Timoshenko and Goodier, 1934] Timoshenko, S. and Goodier, J. (1934). *Theory of Elasticity*. McGraw-Hill.

[Voestalpine, 2019a] Voestalpine (2019a). https://www.voestalpine.com/profilafroid/en/Products-Services/Custom-roll-forming. [Online; accessed April-2020].

[Voestalpine, 2019b] Voestalpine (2019b). https://www.voestalpine.com/profilafroid/en/Roll-forming-technology/The-cold-roll-forming-technology. [Online; accessed July-2020].

[Willmann, 2020] Willmann, T. (2020). Verbesserte blechumformsimulation durch 3d-werkstoffmodelle und erweiterte schalenformulierungen. Technical report, Fraunhofer Institute for Mechanics of Materials (IWM), Freiburg.

[Willmann and Bischoff, 2019] Willmann, T. and Bischoff, M. (2019). Shell models with enhanced kinematics for finite elements in sheet metal forming simulations. In *12th European LS-DYNA Conference*.

[Woo et al., 2019] Woo, Y., Han, S., and Oh, I. (2019). Shape defects in the flexible roll forming of automotive parts. *International Journal of Automotive Technology, 20*.

[Yin Ji-long, 2005] Yin Ji-long, Luo Ying-bing, L. D.-y. (2005). Simulation of roll forming with dynamic explicit finite element method. In *AIP Conference Proceedings 778*.